Department of Mathematics and Statistics

Proximal Monitoring in Landscape Environments

Shuqi Ng

This dissertation is presented for the Degree of
Doctor of Philosophy
of
Curtin University

December 2017

DECLARATION

To the best of my knowledge and belief, this thesis contains no material previously published by any other person except where due acknowledgement has been made.

This thesis contains no material which has been accepted for the award of any other degree or diploma in any university.

Shuqi Ng

March 2017

ABSTRACT

With the implementation of the initiatives in reducing emissions from deforestation and forest degradation (REDD), the accurate determination of the spatio-temporal variation of carbon stocks is crucial. Woody vegetation is one of the more noteworthy carbon storage pools. However, ever-changing forest inventory makes it difficult for countries to accurately measure woody biomass and by extension, predict carbon stocks. Although the most accurate mensuration of biomass is to harvest a tree, the method is destructive and obstructs the REDD initiative. Non-destructive methods use dendrometric measurements that have been obtained from non-contact, remote sensing technologies to estimate biomass derived from allometric models.

The commodity stereo-camera is an alternate consideration to remote sensing technologies currently used such as terrestrial laser scanning (TLS), which requires specialized equipment and some expertise in using the equipment. Improving technologies and software has enabled the photogrammetric measurements of objects to be reasonably accurate comparative to TLS. As a more mobile and cost-effective equipment, it also addresses some of the issues in using laser technology. In photogrammetric measurement, the application of spatial scale to the model is critical for accurate distance and volume estimates (Miller (2015)). The objective of this project is to develop a photogrammetric method that validates the use of a consumer-grade stereo-camera to obtain tree dendrometric measurements from landscape environments. These dendrometric measurements can be used for monitoring changes in woody vegetation and predicting biomass through allometric equations. The ability of the commodity camera to produce reasonably accurate dendrometric measurements were tested in three field case studies for two different groups of study trees in three different environments.

The first field case study conducted in Kojonup, Western Australia, tested the ability of the commodity stereo-camera to estimate tree metrics. We photographed and measured 47 paddock trees with a diameter tape and hypsometer to obtain ground truth values with which to evaluate against estimates obtained from the stereo-camera and aerial photogrammetric data. Against the hypsometer data, the stereo-camera generally overestimates tree height which ranges from 10% - 47%. Mean height difference is 1.961m while the average tree height is 14.75m and

16.99m for the hypsometer and stereo-camera respectively. Height estimates from aerial photogrammetric data is underestimated and attributed to the time difference in which the data was collected. This observation also occurred in the comparison between canopy diameters from the hypsometer and aerial photogrammetric data. The stereo-camera can accurately measure stem diameters for single-stemmed trees. The errors between the stereo-camera and tape diameter can range up to 0.33m, where the average stem diameter is 1m.

The second case study conducted in Geraldton, Western Australia tested the ability of the stereo-camera to measure the height and stem diameter of young trees from which biomass can be estimated via allometric models. From a restoration plantation, 10 trees and shrubs were photographed, measured with traditional methods and felled for ground truth validation. When cross-examining tree height between the methods, a scale ratio is used as comparison given that the average tree height is 3.8m. The differences between the estimates and scale ratio is 0.267m and 0.506m for the stereo-camera and traditional method respectively. There are limitations in identifying and measuring stem diameter from the sample due to the high density of basal stems at breast height which increases the occlusion effect. As a result, the biomass estimation obtained from several generic allometric models displayed contradicting results between the traditional and stereo-camera method.

The third case study conducted in Williamsdale, Australian Capital Territory, tested the ability of the stereo-camera to measure the height and stem diameter of mature paddock trees from which biomass can be estimated via allometric models. Although 19 trees were photographed, only 14 trees measured with traditional methods and felled could be compared for ground truth validation. The stereo-camera tends to underestimate tree height, with a mean error of approximately 7%. The average error for stem diameter at breast height is 8.7%. Errors between stem diameter estimates at 10cm and 50cm from the ground are much larger at 11% and 9.2%. Biomass estimates from the stereo-camera displayed a smaller difference against the harvest data.

Results show that stereo-photogrammetry using a consumer-grade digital stereo-camera is capable of producing dendrometric measurements that are as accurate as or even more so than traditional dendrometry techniques in certain environmental landscapes. Parameters that affect the accuracy of the dendrometric measurements, and in extension, aboveground biomass include camera calibration parameters, the

complexity of the background scene, complexity of the tree structure (i.e. high density of stem count at 1.3m measurement height), lighting and weather. Tree metrics of mature trees with distinguishable stems are the most accurate, which further improves biomass estimates. Conversely, shrubs or trees displaying a high density of stems at breast height cannot be accurately measured or predict biomass. There is still a lot of work that have to be done to accurately separate branches for identification and measurement in multi-stemmed shrubs or trees.

ACKNOWLEDGEMENTS

First, I would like to extend my sincere gratitude to my supervisor, Prof. Louis Caccetta. His help has been invaluable throughout this period. From introducing me to the Industrial Doctoral Training Centre program, to procurement of funding, to project guidance, analysis and thesis write-up. He has always been available and ready to assist, and I am grateful for all his efforts.

I would also like to thank my co-supervisors and industry partners Dr. Peter Caccetta and Dr. Xiaoliang Wu from the CSIRO's Mathematical and Information Sciences group. Dr. Peter Caccetta made me think about various possibilities in stereo-photogrammetric applications, and find a direction in my thesis. His constructive criticisms and ideas were invaluable through every stage of this thesis. I really appreciate him introducing several industrial partners to me which made my case-studies possible. My sincere thanks to Dr. Xiaoliang Wu for his guidance in the field of Photogrammetry when I first began the research project. I am also grateful for his help in using the equipment for the study and the different software programs necessary for the stereo-image processing.

Sincere thanks to Dr. David Belton, Dr. Petra Helmholz, and Dr. Joseph Awange for their help and guidance in the field of Photogrammetry. Also, sincere thanks to Tony Traylen, Gonzalo Mata, Geoff McArthur, Dr. David Belton, Dr. Keryn Paul and John Larmour for their help and support in conducting the field work for my case studies.

I am indebted to Curtin University for granting me the scholarship to undertake my doctorate, as well as CSIRO for partially funding my scholarship. Without the funding, this study would not have been possible.

Finally, I would like to thank my family and friends for supporting me throughout my thesis.

CONTENTS

LIST OF ABBREVIATIONS AND ACRONYMS

AGB	Above-ground Biomass
ALS	Aerial Laser Scanning
BGB	Below-ground Biomass
CCD	Charge-coupled Device
CD	Canopy Diameter
CP	Control Points
D	Equivalent Diameter at Breast Height
DBH	Diameter at Breast Height
DSLR	Digital Single-lens Reflex
DSM	Digital Surface Model
DOM	Digital Ortho-image Model
EO	Exterior Orientation
GEM	Ground Elevation Model
GPS	Global Positioning System
GSD	Ground Sampling Distance
HMLS	Handheld Mobile Laser Scanning
IO	Interior Orientation
MLS	Mobile Laser Scanning
NIR	Near Infrared
RO	Relative Orientation
RGB	Red, Green, Blue
RMSE	Root Mean Square Error
SIFT	Scale Invariant Feature Transform
TLS	Terrestrial Laser Scanning

Chapter 1

Introduction

In response to the phenomena of deforestation and global warming, the United Nations Framework Convention on Climate Change (UNFCCC) 1992, the Montreal Process 1994 and the Kyoto Protocol 1997 (Brack and Richards (2002), Brand (1998), Cannell (1999), Dixon (1997), Joshua (1998), and Maclaren (1996)) have been introduced to enhance national and/or international action on mitigating climate change. The policy approaches and positive incentives on issues relating to reducing emissions from deforestation and forest degradation in developing countries, and the role of conservation, sustainable management of forests and enhancement of forest carbon stocks in developing countries (UNFCCC (2008)) are collectively known as REDD (Reducing Emissions from Deforestation and Forest Degradation). In order to implement REDD, the determination of the spatio-temporal variation of carbon stocks (also known as carbon accounting) is extremely crucial.

One of the noteworthy carbon storage pools is woody vegetation. Forests and urban trees are one of the most well studied organic carbon pools given the uncertainty in the magnitude of carbon uptake by global forests and distribution of carbon stocks in forest ecosystems (Houghton (2005)). Trees use carbon dioxide (CO_2) in the photosynthesis process and store it, thereby locking away a large proportion of the world's carbon within their tissue and acting as a carbon sink. Past research has established that woody vegetation biomass consists of approximately 50% carbon (Brown and Lugo (1982), Malhi et al (2004), and West (2009)) and this

percentage does not vary much between species or different parts of the tree (West (2009)). Countries intending to mitigate climate change through forestry must provide verified reports (including the uncertainty) on national forest carbon stocks and subsequent contribution to the global carbon cycle and effects on climate change (Berger et al (2014)). Given that forest inventory is constantly changing due to natural or human-caused events such as cyclonic activity, forest fires, insect swarms and deforestation, this accuracy is hard to achieve unless frequent and continuous monitoring of forest resources is conducted. Furthermore, the objectives outlined in REDD are also cause for changing forest inventories. For example, government initiatives towards carbon trading in Australia have seen a rapid increase in forest plantations on a broad industrial scale as well as smaller plantings on farms (Specht and West (2003)). The incentive for increasing carbon stock offset through those plantings is financial compensation, which is also subjective to the accuracy of biomass mensuration.

Thus, a key challenge for carbon accounting lies in the need for biomass quantification. The reliable estimation of forest biomass is obtainable through forest mensuration, but there are uncertainties in this method which will give rise to inaccurate assessments of carbon emissions and deforestation rates (Petrokofsky (2012)). To reliably account for carbon stock is to improve the accuracy and reduce the uncertainties in quantifying tree biomass and measuring tree metrics. The methods to estimate the biomass and carbon sequestration by plant ecosystems are currently being investigated by many countries so as to report on the state of their national forests (National Forest Inventory (1998)).

The most direct method is to measure the carbon content from a sample of trees and extrapolate the total carbon stock across the plantation, together with a 95% confidence limit. Usually, biomass sequestered carbon is measured in the laboratory instead of in the field. However, previous research has shown that carbon content can be converted from the biomass of the sampled trees, by assuming that carbon makes up a certain percentage of biomass (Anon (2002), Gifford (2000), Lambert and Turner (2000), and Maclaren (1996)).

True mensuration of biomass involves felling trees, excavating their root systems and drying and weighing the biomass. The process is destructive, difficult and expensive. For large-scale inventory operations or monitoring of plant growth, this mensuration method is not practical or viable. Therefore, empirical equations and

allometric models have been developed by research groups to estimate the biomass of large vegetative structures with easy to measure characteristics such as tree stem diameter (Specht and West (2003), Snowdon et al (2002), Makungwa et al (2013), and Houghton (2005)). Based on field measurements of standard tree metrics, regression models have also been developed for different tree species (Houghton (2005), and Zianis et al (2005)). Yet, there will be some degree of error when applying species-specific models to any tree of a certain species. According to a study by Repola (2008), the biomass of an individual tree is affected by the region or conditions in which it grew. This indicates that for a particular tree species, its growth rate and size is dependent on the environmental conditions of its growth which subsequently affects its biomass and dendrometric measurements. As a result, allometric equations developed for a particular tree species may not be applicable to an identical tree grown in another region and environment. Therefore, it is concluded that for a given tree species in a particular plot, their biomass is more closely correlated to other trees within the same plot than with the same species in another location. Hence, for forest inventory which is dependent on height, stem diameter, stem taper and volume, the need for accurate tree mensuration is extremely important.

1.1 Forest Mensuration

A number of applications within the fields of ecology, commercial and urban forestry stresses on the importance in obtaining accurate tree metrics (Clark et al (2000), Henning and Radtke (2006), Liang et al (2014b), Moskal and Zheng (2012), and Saarinen et al (2014)). Spatial dimensions of trees can be used for urban planning purposes or assessing ecosystem services such as effects on land stability, fire spread risk and biodiversity assessment (Miller (2015)). The role of urban trees in mitigating urban pollution has also been heavily researched. Nowak et al (2006) estimated that trees in Chicago removed an annual amount of 888 tons of air pollution, which is valued at $6.4 million based on national median externality costs.

Forest mensuration is the keystone in the forestry industry by providing quantifiable information about forest resources in order to make reasonable decisions on the use and management of forest resources. It is the determination of dimensions, form, weight, growth, volume and age of trees, individually or collectively, and of

the dimensions of their products (Husch et al (2003)). Technical aspects of tree and forest stand measurements include:

- Measurement of tree and stand variables such as diameter, height, basal area, bark parameters and volume of standing and felled trees.
- Foliage quantity and live crown measurement.
- Biomass and biomass components estimation of individual trees and stands.
- Diameter, basal area, height and volume growth estimation of single trees and forest stands.
- Assessing damages to and the quality of individual trees and forest stands.
- Mensuration in the broader sense deals with estimation of volume and growth of large forest tracts for regional and national forest inventories.

Since the 18th century, foresters began to improve the customary ocular methods for estimating standing timber (van Laar and Akça (2007)). In 1791, xylometric methods were developed by Hennert (van Laar and Akça (2007)) to determine the volume of tree sections by measuring the amount of displaced water from the timber. He also introduced the concept of sampling as a means to assess the volume of entire stands. Later, Cotta (van Laar and Akça (2007)) introduced the calliper in 1804. Soon after, a rapid development in forest mensuration methods was witnessed. Traditional dendrometry is not without deficiencies. It is time and labour intensive for commercial and urban forest inventories (Fernandez-Sarria et al (2013)). The measurement of tree size and architecture is prone to error which further introduces systematic error into commercial, biophysical and ecological characteristics. This has encouraged the development for better and more reliable mensuration instruments.

With advancing technology, remote sensing technologies for forest resources have been developed. For cost effective large-scale analysis, remote sensing techniques such as aerial laser scanning (ALS), terrestrial laser scanning (TLS) and digital stereo imaging are most ideal (West (2009)). However, the costs associated with these methods are impractical when individual-tree scale studies are implemented. Therefore, there is a need for a low-cost, time efficient method suitable for individual-tree studies. Multi-view stereo-photogrammetry is a method that is capable for estimating tree metrics. A study into this methodology and its application into measuring tree metrics against traditional dendrometry will form the basis of this thesis.

1.2 CSIRO's Proximal Monitor Project

This research was conducted as part of the Proximal Monitor project by CSIRO's Mathematical and Information Sciences (CMIS) group to develop methods for fine-scale quantitative monitoring of urban and peri-urban environments on a terrestrial level. The project aims to use close-range stereo photogrammetry techniques to monitor environmental indicators such as tree structure, canopy height, foliage distribution and biomass estimates in urban and general landscape environments at fine scale level (resolutions up to 10mm). The research complements the Urban Monitor (Caccetta et al (2016)) project by introducing additional information of an environment from another viewpoint and dimension. Some of the research challenges (adapted from a personal communication with Wu (2008)) are:

- Developing a close-range stereo photogrammetric procedure in a proximal monitoring environment. The procedure contains several technical issues to be solved i.e. arbitrary terrestrial stereo image orientation and network adjustment, image matching and point cloud generation, volume calculation, retrieving 3D structure from point cloud, and optimising procedures for imaging, processing and analysing data.
- Image segmentation and feature extraction from stereo-images.
- Generating information for site monitoring.
- Liaison with other researchers in the fields of biomass estimate, tree growth models, monitoring landscape changes etc. to consolidate the information together.
- Point registration between multiple sensors i.e. optical, LiDAR (Light Detection and Ranging), spectrometers.

The objective of this research is to develop and validate a photogrammetric method for dendrometric measurements as an alternative cost and time-efficient non-destructive forestry sampling method. As a highly mobile instrument, a camera is suitable for capturing data at different positions and locations in a short time. This thesis contributes to the area of forestry monitoring and management in providing an alternative source of non-destructive measurement method. The proposed methodology also contributes to carbon inventory in estimating biomass using dendrometric measurements from digital stereo-images. As a non-contact

dendrometry method, it is preferred over destructive sampling when taking into account the conservation of forest stocks. This thesis is more focused on the geometric aspects of the photogrammetric method of obtaining tree measurements from stereo-imagery. We also place emphasis on the low time and equipment requirements on site.

1.3 Thesis outline

We present the thesis in six chapters. Chapter 1 is an introductory chapter and provides the background information that drives the objectives of this research. In the literature review in Chapter 2, we review previous studies that applied remote sensing methods into forestry inventory and biomass estimation models. Chapter 3 covers the fundamental principles of photogrammetry required for our algorithms. The chapter also includes the experimental protocols that we implemented during our studies. Chapter 4 is structured into two parts. In the first part, we develop a methodology for object measurement based from an object measurement model proposed by Mustafah et al (2012) and Hsu and Wang (2016). We test the model using the photogrammetric procedures described in Chapter 3 against true measurement values of random objects. The second part introduces a control panel into the methodology and tests how well our object measurements fare against actual object dimensions when we vary the principal distance between the subject and the sensor.

Chapter 5 introduces three case studies that were selected to quantify the applicability of a stereoscopic sensor in actual field surveys. We chose the case studies to test the performance of the stereo-camera in different environmental landscapes and with different tree structures. The study sites and tree species are described and the problems associated with acquiring data and assessing accuracy are discussed with the results. The potential of using stereo-camera measured dendrometrics in estimating tree aboveground biomass is also explored in the two case studies presented in the second and third sections. Chapter 6 summarises the results and general conclusions of this research. It also outlines the achievements of this project and suggests recommendations for future work.

Our results have shown that the accuracy of dendrometric estimates achieved by the stereo-camera is comparable to the traditional method for measuring mature trees

with well-defined trunks in a sparsely populated environment. The dendrometric measurements from the stereo-camera can also be used to estimate the biomass of the tree using general allometric models. This estimate is shown to be closer to the true weight as compared to estimates from traditional dendrometric measurements.

Chapter 2

Literature Review

The following literature review provides an introduction in the relevant methods and technology used for forest inventory and carbon stock accounting. They also act as a guide to identify the methodologies used by other researchers and their thresholds for success to which we compare our methodology and technology against. In particular, we focus on optical dendrometry and photogrammetric techniques with a brief overview on laser scanning methods.

2.1 Non-destructive Sampling Methods

The prediction of standing tree volume and mass traditionally involves destructive measurement methods which cannot be used in fragile forest ecosystems (Parker and Matney (1998)). The basis for non-destructive field biomass estimation is the measurement of stem diameters in a non-destructive manner given the advances in developed telescopic and laser dendrometer instruments in the latter part of the 20th century. Forestry inventories that include volume estimation in preharvest measurements or of modelling growth in forest management place a high importance in dendrometric measurements such as diameter measurements from multiple heights, as they affect the accuracy of volume or biomass estimates derived from allometric models. Other exploitable tree characteristics such as biomass, leaf area, stem quality or wood density improve the qualitative aspects of forestry applications

but can be hard to measure effectively. Measurement of individual stems using traditional methods can be time consuming when shrub and tree species involved are multi-stemmed or have branches close to the ground (Paul et al (2014)). This can result in excessive time spent in measuring a small number of specimens.

The first non-contact measuring device started with hand-held optical dendrometers in the early 20th century of which modern day instruments used today have been based on this technology and platform (Drew and Downes (2009)). The development of field measuring devices has become increasingly intensive in recent years, with attempts to develop and test new efficient and easier to use devices for forest measurements (Carr (1992 and 1996), Williams et al (1999), Kalliovirta et al (2005), Parker and Matney (1998), Varjo et al (2006), and Vastaranta et al (2008)). Variable forest environments make dendrometric measurements a challenge for all measuring devices, and the development of easy-to-use field measurement has been an ongoing process. Kalliovirta et al (2005) states that field measuring devices of the future must be precise, quick, user friendly, water and shockproof with a reasonable price tag and also enable efficient measurement of all basic tree characteristics. Clark et al (2000) summarises the non-contact methods proposed over the past 100 years for stem diameter at breast height (DBH) measurements. The benefits from using a new instrument or method instead of traditional field methods is determined by considering the following factors: accuracy, productivity, cost requirements and practical restrictions on the method (Clark et al (2000), and Kalliovirta et al (2005)). It is within the last few decades that laser scanners and digital cameras have made such remarkable improvements in creating 3D point clouds as a useful source of data for object measurement.

Even though hand-held devices continue to be used in field mensuration, there has been an increasing reliance on the automatic extraction of forest metrics from modern digital datasets driven by the new application discoveries with remote sensing technologies. With further advances in both research and technology, there is the possibility for forest mensuration to move towards full automation (West (2009)).

2.1.1 Traditional methods

According to Clark et al (2000) and Hopkinson et al (2004), traditional dendrometry is inherently flawed and prone to errors, even though the simplicity and

standardisation of the method has led it to be widely adopted in field applications. Factors such as the location and condition of the environmental landscape can affect the outcome of a dendrometry study (Clark et al (2000), and Li and Weiskittel (2012)). In traditional dendrometry studies, tree height and stem diameter are considered more important among the dendrometric measurements used in forest management.

Tree height generally presents a challenge to many surveyors to accurately measure this metric. In forestry, it is defined as the vertical distance from ground level to the highest point on the tree (which is usually referred as the tip of the tree). Although West (2009) states that the height for leaning trees is defined in forestry as the height to the highest point rather than its stem length, Bragg (2007) and Schreuder et al (1993) perceive the height to be the length of the tree axis from its base to its tip. There are several methods to measure tree height. The direct method involves holding a vertical measuring pole directly alongside the tree stem. A set of pole segments can be fitted together to effectively measure tree heights to approximately 15m before they become too unwieldy or heavy to hold. Good sighting of the tree tip would give a measurement accuracy of 0.1m, however the potential measurement error is greater in the presence of taller trees and windy conditions that makes sighting a challenging task (West (2009)).

Another method is the trigonometric method. Presently, hypsometers are commonly used (Liang et al (2014b), and West (2009)) as they combine clinometers and laser rangefinders that use geometric and trigonometric functions to estimate tree height. Not all hypsometers use the same trigonometric method in estimating tree height. Some use the sine method while others use the tangent method (Bragg (2007), Husch et al (2003), and Larjavaara and Muller-Landau (2013)). The sine method is argued to be more accurate than the tangent method (Bragg (2007), Husch et al (2003), and Larjavaara and Muller-Landau (2013)), even though the latter is used more by professional forestry researchers. Compared to the sine method, the tangent method has the risk of over-measuring since it is only accurate under perfect conditions where the tree lies on a flat surface, has a perfectly vertical stem and its highest point is centered over the bole (Bragg (2007)) as seen in Figure 2.1.1(a).

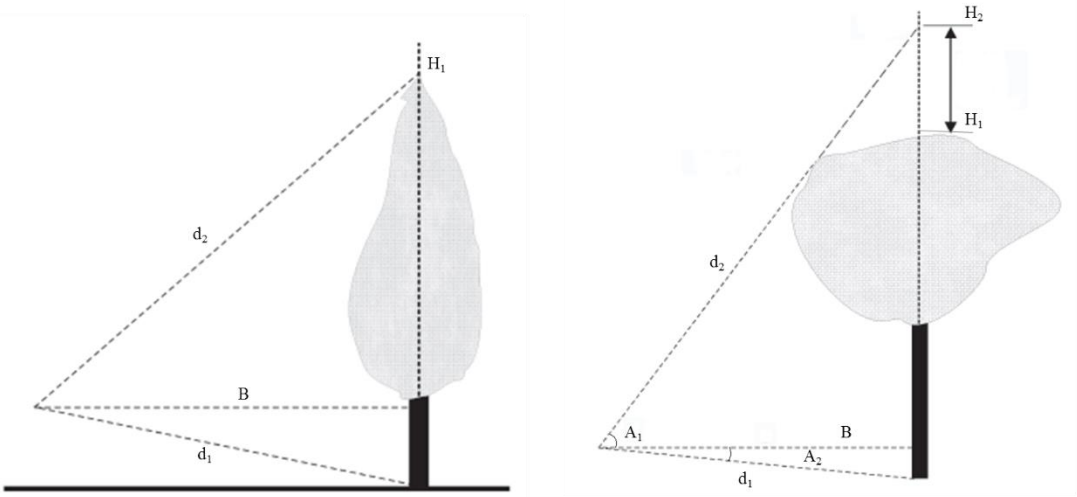

(a) Idealised tree height measurement under perfect conditions

(b) Overestimation bias from tangent method

Figure 2.1.1: (a) represents the situation and type of tree where the tangent method works perfectly. (b) represents the typical tree condition that results in overestimation bias from the tangent method.

In reality, such ideal conditions rarely exists for the tangent method to work perfectly. A large proportion of trees lean, have bends on angles in their upper boles, are found on sloping grounds, have asymmetric crown and shape or a wide spreading crown with no obvious apex (Bragg (2007)). Figure 2.1.1(b) illustrates an example where the vertical height (H_2) relies on the angle A_1 and horizontal distance B, resulting in an overestimation bias from a non-existent crown apex (H_2) while the true apex (H_1) lies below. Falconer (1931) pointed out that with the tangent method, the error is due, not to the actual chainage of the distance, but in the location of the point to which the distance is measured.

To summarise, both methods are still subject to error given the underlying assumptions that all angles and distances have been accurately measured and that the observer has correctly identified the tip of the tree (West (2009)). Errors also occur when these assumptions do not consider ground slope, the direction of the tree lean or crown shape (Bragg (2007), and Husch et al (2003)). In close-canopy forests or forests with dense undergrowth, the identification of the tree base and tip can be extremely challenging due to occlusion.

The geometric method involves positioning a 3 – 5m stick vertically at the base of the tree and having the observer stand a distance away from the tree holding a graduated ruler perpendicular to his outstretched arm (West (2009)). The observer

then has to maintain the ruler such that his line of sight for the base and tip of the ruler coincides with the base and tip of the tree and read three measurements from the ruler: the length of the ruler, the length of the ruler representing the distance from the horizontal line of sight to the tree base or tree tip. From these three measurements, the tree height can be approximated. The advantages to this method are that the distance between the observer to the tree and the ground slope angle need not be measured, and also the equipment used is simple and cheap. The difficulty of this method is in the observer's ability to hold the ruler steady and keep in view all that needs to be sighted at the same time. With this method and under the most optimal conditions, the accuracy of the tree height measurement should be within 0.5m (West (2009)).

Stem diameters are usually measured with callipers or a diameter tape, depending on the thickness of the stem. In most literature, the commonly measured stem diameter is measured at 1.3m above ground, denoted as diameter at breast height or DBH. The measurement is also subjected to a number of error sources (Clark et al (2000), and West (2009)). Height differences between field technicians indicate that the height of the stem diameter measurement is between 1.3m – 1.4m and cause some variation in DBH measurement. The placement of the tape above or below the recorded height, or at an axis not perpendicular to the tree can also affect DBH measurement (Elzinga et al (2005)). Using a tape diameter affects approximation of the stem diameter which is derived from the circumference of the tree bole especially for non-circular tree boles.

Optical dendrometers such as the Tele-Relaskop (Bitterlich (1978)) and Criterion model 400 (Laser Technology Inc. (1992)) have been used and tested in industrial and research applications in measuring tree height and diameters (Bitterlich (1984), Carr (1992), Heske and Parker (1983), and Parker and Matney (1998)). Parker and Matney (1998) conducted a rigorous study in examining the accuracy of dendrometer measurements from standing trees and the prediction of tree volume from stem profile equations against felled-tree data. The measurement error between the Tele-Relaskop and Criterion model 400 is not significant. The mean differences in DBH and total height is 0.12cm and 15cm respectively. Although the Criterion 400 produced the smallest mean differences in standing tree measurements and profile equation predictions of merchantable height, the Tele-Relaskop has the most

consistent tree measurement and profile prediction trends (Parker and Matney (1998))

Stem taper is depicted as a function of height and stem diameter and is used to estimate stem volume. There are modern tools such as xylometry and remote sensing that are capable of calculating stem volume more precisely, yet they are not always practical or appropriate for field mensuration of standing trees. Felling trees in particular disrupt the monitoring of tree growth (Clark et al (2000), and Liang et al (2014b)). Thus traditional dendrometry is still relied upon for ground truth validation (Berger et al (2014), and West (2009)) and have been used to develop allometric models explaining stem volume and biomass. Section 2.3 will look into some allometric models that have been developed through tree felling in forestry studies.

2.1.2 Terrestrial laser scanning

In the past few years, terrestrial laser scanning (TLS) has been regarded as a fast, precise, efficient and contactless option to collect accurate field data. Terrestrial laser scanners were developed mainly for acquisition purposes, driven by applications such as documenting facility arrangements, acquiring representations of natural and man-made architecture and surveying road surfaces under high traffic volume. The purpose of the applied field also determines the type of terrestrial laser scanner that is appropriate for the study. They can be classified based on two measurement strategies: kinetic and static (Staiger and Wunderlich (2007)), and the measurement range: close range (30m), mid-range (up to 800m) and long-range (>1000m). The range of precision is also considered in relation to the applications (Zogg (2008)). Typically, the system is mounted on a tripod with a pan and tilt rotator on top. It uses light pulses to record the distance from the light source to the subject to derive the 3D position of the subject within the scanner field of view by collecting 3D data clouds of several million data points in a few minutes. The range images produced from the laser scanner enables the quantification of plot level attributes such as the spatial distribution of canopy elements, and the exploration of linkages between forest structure and function that cannot be achieved with traditional field measurements (Lovell et al (2003)).

Regarding developments of terrestrial laser scanners for forestry practices, Hopkinson et al (2004) achieved relatively accurate results from measured stem

location, tree height and density with TLS data. Mean height was generally underestimated by LiDAR by approximately 1.5m, while there was no systematic tendency to under- or over-estimate stem diameter. Timber volume estimates were within 7% of manually derived estimates. Kalliovirta et al (2005) used a laser-relascope to measure tree diameter, height and location with standard errors of 8.2mm, 49cm and 32cm respectively. Despite its accuracy, the method was observer-dependent in which the majority of fieldwork time was spent on measuring the diameter. In a comparison study, Vastaranta et al (2008) focuses on the accuracy of measuring stem diameters using 4 methods: TLS, laser-camera, laser-relascope and traditional steel calipers. They concluded that the stem diameter measured by the new laser-based methods is as accurate as it had been measured with the steel calipers. Dassot et al (2011) demonstrated the potential of TLS for assessing wood volume in leaf-off conditions and used simple geometric fitting to model the woody structure up to branches of 7cm.

While TLS appear to produce fairly accurate estimates of tree height, diameter and volume, there are still a fair number of disadvantages that makes it unfeasible for certain research groups. The most pressing issue would be the cost of the system: entry-level systems range from $30,000 to $100,000 (Liang et al (2014b)) and high-end systems can cost up to $500,000. Self-assembled systems or 2D LiDAR sensors are cheaper but nevertheless costs in the upper thousands. It should be noted that several scans are at times necessary to offset problems caused by shadowing with the utility of a single scan image during the collection of TLS data. This will add to the operational costs when conducting repeated surveys. Other factors include the portability of the system, variability of forest structure that causes occlusion of objects and surfaces, and the distance from the laser sensor which affects point density and accuracy. The accessibility of using TLS equipment is more limited than traditional dendrometry. The systems used in research studies generally weigh around 10 – 20kg (Dassot et al (2011), Liang et al (2014b), and Maas et al (2008)) and additional supportive equipment such as a tripod, pan-tilt unit, generator and field computer can add to the bulk of the required field equipment. The utility of TLS also decreases in forests with high tree density from occlusion in the upper canopy and undergrowth that prevents the penetration of TLS laser pulses. This is supported by a 40% total tree identification by Strahler et al (2008) of which 33% were

partially or fully occluded. Multiple scans from different positions are recommended when conducting a plot-scale analysis to address the occlusion problem.

2.1.3 Handheld Mobile Laser Scanner

The research cited in the previous section has shown that TLS can be used to record and measure forest structure. However, broader acceptance of TLS as a valid alternative to manual survey methods requires efficient and affordable hardware (Newnham et al (2015)). Some examples of low-weight (<5kg) and low-cost (<$20,000) instruments have been recently reported in the literature (Kelbe et al (2012)) to produce estimates of stem diameters and form in complex environments such as tropical forests, mangroves and salt marshes (Holopainen et al (2013), Jaakkola et al (2010), Liang et al (2014a, 2014b), and Schaaf et al (2014)). However, the attainment of maximum scanning range, angular resolution and positional accuracy has resulted in some trade-off in the performance of the instrument. The efficiency and value of merging scans recorded at multiple locations would be increased if there exist a method that is more efficient both in the field and during data processing (Newnham et al (2015)).

Handheld mobile laser scanners (HMLS) offer a solution to the problem of creating ground-based point clouds with the necessary geospatial extent whilst maintaining accuracy (Holopainen et al (2013)) and minimizing time and cost. The occlusion effect in TLS data that limits its use in forest inventory can be addressed by the complementary effect of HMLS. Its potential have been explored by Ryding et al (2015) and Bauwens et al (2016) in providing point clouds of similar precision and accuracy to those currently being produced through TLS applications. Prior to their studies, mobile laser scanners (MLS) were introduced in tree measurement starting in early 2010 (Jaakkola et al (2010), and Rutzinger et al (2010)). These first studies focused on sparse urban trees scanned from a MLS mounted on a car. The limitations of using MLS however included low GNSS (Global Navigation Satellite System) detection under forest cover, mobility and practicality issues with using a mobile platform in forest ecosystems. The Finnish Geodetic Institute addressed this problem with a backpack mounted personal laser scanner (PLS) (Kukko et al (2012)), however a lack of proper satellite visibility during the field measurements

led to less accurate platform positions and thereby undermining the heading angle estimates (Liang et al (2014a)).

The focus subsequently shifted to HMLS instruments such as the FARO Focus 3D and ZEB1 that were initially designed for use in architecture, civil engineering and robotics projects. The FARO Focus is small (24×20×10cm) with a relatively light weight of 5.2kg as compared to the larger TLS instruments (Bauwens et al (2016)). This HMLS instrument is a phase-based lidar with a working range of up to 120m and a maximum point collection of 9.76×10^5 per second (Bauwens et al (2016), and Ryding et al (2015)), resulting in a short scanning time (approximately 3 minutes without photographs). Object space XYZ coordinates and a reflectance value is given for each point return, and RGB values are also provided when the internal colour camera is used. The ranging error is up to ±2mm at 10m according to the manufacturer. FARO registration and survey spheres are used to provide tie points to join scans from multiple set-ups.

The ZEB1 consists of a 2D laser scanner and low-cost inertial measurement unit (IMU) that is mounted on top of a spring; itself mounted on a hand grip (Bauwens et al (2016)) designed to have the resonant frequency of the average human gait (Ryding et al (2015)). The scanner is a time-of-flight laser with a rate of 43,200 points per second and a field of view of 270˚ horizontally and approximately 120˚ vertically. The hand-held part of the scanner is linked to a backpack data logger that processes the IMU and laser data to calculate the position and orientation of the scanner head. Total carry weight is approximately 4.4kg. As the user carries the instrument through the environment, a 3D field is being created from the data captured from the back and forth rocking motion of the scanner head. With each additional data added, the algorithm uses a linearised model to minimize the error in the IMU measurements along with minimizing the correspondences between the 3D point cloud data for the respective time segment (Ryding (2015)). The manufacturer's stated measurement error is ±30mm at a range of 0.1m to 10m in a closed environment and 50mm in bright light environments. In open environments, data capture can be difficult due to foliage motion from weather conditions.

From the cited literature, the HMLS method is a faster laser scanning platform compared to multi-scan TLS and yields better results for a number of tree parameters (DBH and tree detection). Given that HMLS is a recent addition to forest surveying methodologies, there are still many limitations in the usability of the method to be

addressed. The ZEB1 has a limited scanning range of 15–20m, resulting in poorly described forest canopy for trees which exceed the scanning range. Scanning and surveying time is also associated with the hardware capabilities. Ryding et al (2015) states that the resolution of the point cloud to allow acceptable feature extraction may also be an issue when using the ZEB1 approach.

2.1.4 Close-range photogrammetry

Photogrammetry is a mathematical representation of the geometrical relations between physical objects in 3D space derived from their images recorded with a 2D medium. The photogrammetric method has been routinely used in aerial photography, cartography, remote sensing and architectural surveying, with a strong focus in 3D reconstruction (Luhmann (2006), Schenk (1999, 2005)). Traditionally, handheld or ground based cameras have not been commonly used for tree mensuration but digital cameras are considered as a potential field instrument to quickly capture information that can be stored and used indefinitely. With the advancement in technology, higher resolution digital cameras can now be obtained at an increasingly lower cost and have re-opened the possibility of utilizing the camera for mensuration purposes (Chandler et al (2005), Forsman et al (2016), Kytö et al (2011), Liang et al (2014b), Menna et al (2013), Morgenroth and Gomez (2014))Previous studies (Brown (1971), Fraser (1980, 1982), Fryer and Brown (1986), Luhmann et al (2006, 2016), Luong and Faugeras (1992)) before the emergence of the digital camera used analogue cameras where the resolution of the resultant measurement is largely dependent on three factors:

- Image magnification.
- The precision of the device used to measure the image.
- The user's ability to distinguish the endpoints of measurement.

Problems arising from this usage included time delays from film developments, improper exposure, orientation problems and complicated calculations. Digital cameras negate some of these problems as the images can be transferred immediately to a computer for processing. The resolution of digital imagery is dependent on the size and arrangement of the charge-coupled device (CCD) elements and the algorithms that have been developed to facilitate photogrammetric measurements. The mobility of a hand-held camera is also suitable for rapid acquisition of data and

does not require the user to have any expertise in operating the system, unlike the TLS method. The data collector only requires a set of guidelines about the image data criteria instead of a time-consuming training period in using a handheld camera or any image capturing device. User-friendly software packages like iWitness removes some of the technicalities in image processing and does not require much training to use.

It is undeniable that photogrammetry will eventually go mainstream. The demand for 3D creation software and products is continuously growing and consumers have a readily available data collection tool in their mobile phones. The ability to obtain 3D products or object measurement for photogrammetry is not limited by socio-economic and logistically factors, unlike laser scanning which requires bulky, expensive equipment and calibration for creating a point cloud. Creating 3D geometric models through photogrammetric means is also achievable by means of using a mathematical model from multiple 2D images to recreate geometric surfaces of objects (Luhmann et al (2006), and Schenk (2005)). Recently developed software such as Agisoft Photoscan Pro, uses Scale Invariant Feature Transform (SIFT), Structure from Motion (SfM) and Multi-view Stereo (MVS) to create 3D models. Other programs include PhotoModeler: an older platform that uses close-range photography for the photo-sets and SURE: a software solution for multi-view stereo by deriving dense point clouds from a given set of images and its orientation. Current dense stereo matching solutions are able to create point clouds of comparable density to TLS techniques (Hullo et al (2009)). Open source codes and programs for analysing and processing images can now be readily found online and the democratization of computing power in the cloud makes it possible to perform a photogrammetric process on a large number of photographs and reconstruct a digital 3D model.

In a study recreating a 3D model of a cultural monument, Bayram et al (2015) compared the products generated from TLS, conventional photogrammetric and automatic image matching-based approaches. Data collection time was shorter for the photogrammetric method at 2 hours while the TLS survey took 7 hours to complete. The differences between TLS and photogrammetric methods have been found to be very close. They observed several difficulties in processing TLS data, point cloud noise elimination being the most time consuming part. It was concluded that the image-based approach is a good alternative to TLS and has an added

advantage of the ability to superimpose the generated point cloud onto its original photographs to improve interpretation quality that may not be possible with TLS techniques.

According to West (2009), the average time taken for a TLS scan is approximately two hours. The time period can be quicker or slower depending of the scale of the target area. However, when data recollection is necessary in the face of inadequate data, the additional time spent on the recollection can be quite costly. The use of a TLS system is also limited by the level of training of the operator. Taking this into account, the time spent on collecting and processing TLS data is considerably longer than photogrammetric data. Therefore, compared to TLS methods, camera-based methods offer potentially less expensive hardware, increased mobility and reduced time on-site (Forsman et al (2016)) and yet produces reasonably accurate information comparative to the TLS method.

2.2 Image-based Dendrometry

Photogrammetric measurements of trees are a developing field (Forsman et al (2016)). The measurement of trees using the photogrammetric method involves aerial-based or terrestrial-based photogrammetry. Before the development of digital cameras, individual tree heights and mean stand heights were estimated by photogrammetric measurements of stereo pairs using classical aerial photographs (Balenović et al (2015)). Tree height is determined by placing stereo markers of the instrument on the top of the tree and ground next to the tree and the elevation difference between the two markers is then calculated as the height. The disadvantages of this process is the limited potential of identifying the bottom of a tree in a densely canopied forest (Paine and Kiser (2012)) and the practical application of the method given the amount of manual processing required (Balenović et al (2010), and Paine and Kiser (2012)). One of the pioneers in terrestrial forestry photogrammetry was Weber (1902), where he used a camera that have been orientated parallel to the stem axis to obtain tree dendrometric characteristics from a conversion scale into the plane of the photograph. Crosby et al (1983), Gaffrey et al (2001), and Prodan (1965) further improved this principle when they applied the same principle into their research. Crosby et al (1983) used a handheld camera to photograph pine trees and extract their diameter and height

information. Their study produced relatively accurate estimates of tree diameters with errors of less than 2% for trees with diameters less than 50cm. There has been little research conducted in applying stereo-camera techniques for dendrometric measurements while the majority of photogrammetric tree measurement studies are based on single camera techniques (Brownlie et al (2007), Clark et al (2000), Crosby et al (1983), Dean (2003), Gaffrey et al (2001), Kim et al (2005), Liang et al (2014b), Miller (2015), Montès et al (2000), and Wackrow (2008)).

There have been several studies where photogrammetry is applied to calculate wood volume of an individual tree captured in images. Dean (2003) uses a calibrated reference framework with a single photograph of an individual tree and calculated the volume data from the image through a multiplicative taper factor for the stem. Wood volumes were underestimated by an average of 0.5% for stems and 4% for branches. On the other hand, the deficit areas from non-circular cross-sections of the buttress resulted in the overestimation of stem volumes as high as 10% on average.

Montès et al (2000) developed a method based on deriving the aboveground biomass of a tree from its estimated volume using an ordinary photograph of a tree. The primary software is Microsoft Excel which the user uses for data entry, results storing and data processing through Excel macros. Biomass of various components of the tree is subsequently estimated based on the computerised evaluation of the tree bio-volume. The steps involve:

- Obtaining two photographs from an orthogonal viewing angle, physical samples of the different components and dendrometric measurements for each tree subject.
- Calculating the scale of the photograph.
- Determining the volume, bulk density and biomass of each different component.
- Validating the results.

Mensuration with respect to the gridlines becomes problematic when there is tilt in the tree or its branches i.e. the measurement does not represent the true stem diameter at that point. Another ambiguity in stem mensuration arises from the difficulty in classifying the parts of trees as the trunk or branch. The mensuration Excel code is dependent on the appropriate representation of the trunk or branch and can introduce bias if not properly classified. The results show that the method is

relatively reliable with a mean error percentage varying between 2.5% - 7.5% per tree (Montès et al (2000)). Biomass estimations for young trees are not as accurate, but could be improved by using a tree morphology classification. The main limitation of the method is that it can only be used in open forests. A complete tree outline is required on the image as the representative density directly influences the accuracy of the method.

Forsman et al (2016) set up a 5-camera rig in which the camera positions were arranged such that no three-camera subset was collinear. The rig was designed such that once calibrated, it removed the need for a scale bar given that the known length of the rig baseline established the scale of the scene. A point cloud was generated from each viewpoint using rig-based matching of detected SIFT keypoints and then merged to identify and estimate stem diameters. The method had a 76% detection rate in plots with clearly visible stems, of which stem diameters could be estimated from 40% of the detected stems with an RMSE of 2.8 – 9.5cm. Although the results are inferior to TLS-based methods, the methodology has low commission errors and on-site time. There is also the potential for improved results by increasing the station image schemas and reducing the angular separation of the cameras.

Morgenroth and Gomez (2014) reconstructed individual trees from a set of photos taken all around the tree with a digital camera. PhotoScan Professional was used to produce the 3D point cloud models of the trees, from which the heights and stem diameters were estimated. Tree height and stem diameter estimates had errors of 2.59% and 3.7% or about 10cm and 3cm respectively. The results are quite accurate and are comparable to LiDAR techniques.

2.3 Allometric aboveground biomass

Initial techniques for biomass estimation consist of felling and weighing a number of representative plots or individuals (Brown et al (1989), Chave et al (2004, 2005), Hunter et al (2013), Husch et al (1982), Mate et al (2014), Nogueira et al (2014), Ter-Mikaelian and Korzukhin (1997), Muukkonen (2007), Zainis et al (2005)). These techniques however raised economic and scientific problems i.e. time, cost, repeatability, and conservation of endangered species and ecosystems, which fuelled the need for non-destructive methods (Montès (2009)). There are two commonly

used approaches for estimating biomass density of the tree biomass. The first directly estimates biomass density through biomass regression equations and the other method converts wood volume estimates to biomass density using biomass expansion factors (Brown (1997)). For forest ecosystems, a majority of the non-destructive methods developed for aboveground biomass (AGB) estimation focuses primarily on temperate (Husch et al (1982), Ter-Mikaelian and Korzukhin (1997), Muukkonen (2007), and Zainis et al (2005)) and tropical (Brown et al (1989), Chave et al (2004, 2005), Hunter et al (2013), Mate et al (2014), and Nogueira et al (2014)) forests.

A study in reducing emissions from degradation and deforestation by United Nations (UN-REDD) (Poultouchidou (2013)) found that a majority of allometric models uses one predictor variable to estimate aboveground biomass (AGB). These predictor variables such as diameter at breast height (DBH), height (H), wood specific density (ρ) and basal area are related to AGB through different interpretations of allometric models as found in various studies on individual AGB. DBH is the most used predictor variable for biomass estimation, accounting for 87% of all single parameter allometric models that have been proposed (276 equations), whereas crown diameter (CD) and tree height (H) place 3rd and 4th as the preferred predictor variable. According to Chave et al (2005), the most important variables for predicting AGB in decreasing order are DBH, ρ, H and forest type. Gregoire et al (1989) cites that errors associated with DBH measurements are generally less than 3%, making it a statistically appropriate choice as the parameter with the least measurement error. Comparatively, the height measurements for mature trees tend to fall within 10-15% of the true height (Brown et al (1995)). Since the procedure to obtain height measurements is both time-consuming and costly, forest inventories do not undertake rigorous tree height measurements.

Allometric models with two or more predictor variables have also been developed. Of the allometric equations that have been developed, 75% are dependent on DBH and H, whereas 13% are dependent on DBH and CD. While there are practical and statistical reasons for using DBH alone to predict AGB, there are some (Husch et al (2003), Montagu et al (2005), Schmitt and Grigal (1981), and Williams et al (2005)) who agree that the inclusion of height as a second order polynomial does improve the performance of the general allometric model. Madgwick and Satoo (1975) argue that tree height has little effect in a diameter-based allometric equation.

Tree height is also often dismissed in carbon-accounting programs because of the difficulty in measuring tree height accurately in closed-canopy forests (Hunter et al (2013), and Larjavaara and Muller-Landau (2013)). The evidence supporting tree height as a secondary predictor variable is equivocal due to serious controversies in the global change community from neutral, positive and negative results in allometric model studies (Baccini et al (2012), Harris et al (2012), and Specht and West (2003)). Given that the allometric models estimating AGB is of the form AGB = f(D, H, ρ), errors in trunk diameter, height or density measurement all result in AGB estimation errors (Chave et al (2004)).

In general, the literature fits several models to the data from which model fit is assessed using multiple and/or adjusted R^2 with some inclusion of error estimates between observed and predicted values. The models that have been developed are also compared to empirical data of the same individuals using linear or non-linear regression techniques.

Uncertainties associated with AGB estimates (Chave et al (2004), and Petrokofsky et al (2012)) are

- Sampling uncertainty (associated with sample size and sampling design).
- Inaccurate measurements of predictor variables including instrument, technician and calibration errors.
- Use of unsuitable allometric models.
- Poor representativeness of the sampling network.

Petrokofsky et al (2012) states that the average sample size of 10 – 30 trees per species in most biomass papers are too few for biomass estimation for large countries in the tropics. In contrast, a number small scale biomass measurement campaigns in Europe has resulted in compiling a large set of data to derive generic models. By region, allometric equations are summarised for North America by Chojnacky et al (2014), South America by Nogueira et al (2014), Europe by Zianis et al (2005), Southeast Asia by Yuen et al (2016) and Australia by Montagu et al (2005), O'Grady et al (2000), Paul et al (2014), Specht and West (2003), Werner and Murphy (2001), and Williams et al (2005). A few papers have been published on allometries derived from destructively sampling trees in Africa (Ebuy et al (2011), and Sawadogo et al (2010). However, they are insufficient to represent the rich biodiversity of the country.

Not only is height for individual trees difficult to measure, there is a high predisposition for errors to occur. Larjavaara and Muller-Landau (2013) compared the results from estimating tree height using the sine and tangent method conducted by 5 technicians with different levels of experience and skills. Although the sine method was recommended for tree height estimation, it is also susceptible to underestimation errors from instrumentation, forest structure and time spent per tree. Measurements with the tangent method had little systematic error but high random error and systematic differences among technicians.

The effect of uncertainty in tree height measurement on biomass estimation was demonstrated by Vieira et al (2008). When using the model of Chave et al (2005) on a 13m tree with 20cm DBH and keeping DBH constant, a 7% increase in height input caused an equivalent increase in the estimated AGB. On the other hand, Scatena et al's (1989) model gave a 5% increase in the estimate AGB. The quality of tree height estimation from ALS and TLS also decreases from factors such as elevation differences, branching frequency and stand density. Inherent occlusion effects and increasing point spacing results in uncertainty in differentiating tree tops from the tree canopy.

When reviewing biomass estimation literature, there are cases where the allometric equations cited in some studies have been compiled from other literature. Equations derived from trees growing in a different climate or developed for a different species were applied to trees that were of a different species or environment. The use of general allometric equations for species within a similar genus is predominant in past biomass studies when species specific allometric equations have yet to be determined. This observation was presented by McHale et al (2009) in Table 2.3.1 below. It shows the different allometric equations used or cited by various researchers when predicting the biomass for a specific tree species.

Table 2.3.1: Sources of allometric equations used in urban biomass studies (sourced from McHale et al (2009)).

Species	Source Species	DBH Range (cm)	Source
Bur Oak, *Quercus macrocarpa*	Red Oak	13–129	Brenneman et al. 1978, Ter-Mikaelian and Korzukhin 1997
	Bur Oak	3–40	Perala and Alban 1994
	Oak	14–163	Bunce 1968
Silver Maple, *Acer saccharinum*	Sugar Maple	6–168	Young et al. 1980, Ter-Mikaelian and Korzukhin 1997
	London Plane	15–74	Pillsbury et al. 1998
	Silver Maple	5–46	Alemdag 1984
Green Ash, *Fraxinus pennsylvanica*	White Ash	13–129	Brenneman et al. 1978, Ter-Mikaelian and Korzukhin 1997
	Green Ash	15–84	Pillsbury et al. 1998
	Green Ash	3–79	Schlaegel 1984
	Ash	9–104	Bunce 1968
Honeylocust, *Gleditsia triacanthos*	General	10–85	Harris et al. 1973, Jenkins et al. 2004
	General	>94	Hahn 1984
	Green Ash	15–84	Pillsbury et al. 1998
Little Leaf Linden, *Tilia cordata*	American Basswood	13–129	Brenneman et al. 1978, Ter-Mikaelian and Korzukhin 1997
	American Basswood	5–56	Alemdag 1984
Populus sargentii	Cottonwood	6–32	Standish et al. 1985
	Cottonwood	>94	Hahn 1984
American Elm, *Ulmus americana*	American Elm	5–30	Perala and Alban 1994, Ter-Mikaelian and Korzukhin 1997
	General	10–85	Harris et al. 1973, Jenkins et al. 2004
	Elm	>94	Hahn 1984
	American Elm	5–56	Alemdag 1984
Hackberry, *Celtis occidentalis*	Hackberry	>94	Hahn 1984
Siberian Elm, *Ulmus pumila*	General	10–85	Harris et al. 1973, Jenkins et al. 2004
	Sawleaf Zelkova	6–34	Pillsbury et al. 1998
	American Elm	5–30	Perala and Alban 1994, Ter-Mikaelian and Korzukhin 1997
	Elm	>94	Hahn 1984
	American Elm	5–56	Alemdag 1984
Kentucky Coffee Tree, *Gymnocladus dioicus*	General	10–85	Harris et al. 1973, Jenkins et al. 2004
	General	>94	Hahn 1984
Norway Maple, *Acer platanoides*	Sugar Maple	6–168	Young et al. 1980, Ter-Mikaelian and Korzukhin 1997
	Sugar Maple	3–66	Bickelhaupt et al. 1973, Tritton and Hornbeck 1982

Current allometric equations are almost entirely based on Southeast Asian, European and North and South American measurements according to Petrokofsky et

al (2012). As mentioned before, the allometric model database is insufficient to represent the rich diversity in woody vegetation of the world. It is of great importance to build up databases similar to the aforementioned countries in other parts of the world. This therefore allows for accurate AGB estimation from the appropriate allometric models.

Chapter 3

Methodology

The photogrammetric process can be used in any application where a measuring object can be photographically recorded and evaluated (Wackrow (2008)). A review of the relevant research literature and technologies on photogrammetry is provided in Chapter 2. In this chapter, I will give a brief overview of stereo-photogrammetry, before explaining the main principles behind photogrammetry, including the mathematical models used, and fundamentals of camera calibration. I will also include the method of camera calibration for the stereoscopic sensors used in my case studies (Chapters 4 and 5), as well as the experimental protocol in estimating object dimensions from the stereo-images.

3.1 Stereo-vision in Digital Cameras

A boom in stereoscopic research since the 1980s has led to researchers turning towards stereoscopic 3D solutions in fields related to neurosurgical operations, psychological research, endoscopy and computer aided design (Vlad (2013)). Today, the applications are far more numerous, including television, game consoles, simulation systems, data visualisation and many others. The realisation of integrating stereoscopic technology into our daily lives is slowly materialising with the rapid expansion of software tools and packages designed to facilitate photogrammetry.

Some 3D sensing sensors that uses active projections such as the Kinect, Xtion and FinePix 3D, have been developed around 3D software implementations from their predecessors, paired digital cameras (Masuda et al (2011), Menna et al (2013), and Takahashi and Matsuoka (2010)). However, regardless of the numerous improvements, the techniques necessary for the manipulation of stereoscopic images are still complex and there remains technical limitations of stereoscopic technology. The difficulty of exploitation is attributed to the tight interconnections among the various components of a stereoscopic system, which requires a precise control of all the parameters at every step of the processing network (Vlad (2014)). Stereo-vision can be simulated by means of using two camera sensors to record stereo-images. The sensors are placed at different positions on a horizontal plane in imitation of two viewing angles of the eyes. In binocular vision, the separation between the left and right eye allows for two distinct angles of view and representing slightly different perceptions of the world. These differences help to create depth once both images have been combined by a neuronal process.

Two types of configurations exist for stereoscopy. The first is a parallel configuration in which the optical axes of the two cameras are positioned on the horizontal plane facing a parallel direction. The other is the toed-in configuration in which the camera axes are converging. In most research, the parallel configuration is preferred given that less geometrical distortions are introduced and will be easier to correct for. IJsselsteijn (2000) suggests avoiding the toed-in configuration because the underlying keystone distortion can be very difficult to correct for. The parallel configuration can be simulated by using two digital cameras mounted on a horizontal bar with known baseline between the two sensors (Mustafah et al (2012)) or attaching a single camera on a moving track (Hsu and Wang (2015)).

3.2 Camera Calibration

As with all camera sensors, calibration must be performed for both cameras. Early works for close-range photogrammetry by Brown (1971), Faig (1975), Fraser (1980, 1982, 1997) and Fryer and Brown (1986) created the foundation principles of close-range photogrammetry that remain in use to this day. The invention of computers has resulted in the transition from processing analogue images to processing digital images (computer vision). Now, the integration of camera calibration in computer

vision (CV) has been successfully developed by CV researchers such as Tsai (1986), Lenz and Tsai (1988), Luong and Faugeras (1992) and Zhang (2000), making the process more efficient and reliable. However, there still exist cases where calibration becomes a more difficult task (Luhmann (2016)):

- Camera geometry is unstable during image acquisition.
- The number of acquired images is insufficient for the number required for self-calibration.
- Bundle adjustment through self-calibration cannot be processed due to weak intersection angles or insufficient orthogonal camera rolls about the optical axis.
- There is insufficient keypoints in the image object for calibration.

The process of camera calibration is necessary to the application of modern consumer-grade digital cameras for close-range photogrammetric measurement. It involves determining the intrinsic (Interior Orientation) and extrinsic (Relative and Exterior Orientation) parameters of a camera to identify the changes in the geometry of image formation in the camera from the geometry of a central perspective projection. This allows us to correct images to be used in applications such as surface fitting and modelling, 3D object reconstruction, and object measurement.

Close-range photogrammetry can be categorized into terrestrial photogrammetry and aerial photogrammetry. The approach to calibrating cameras for terrestrial use is different from the aerial photogrammetric process although the theoretical principles are the same. Calibration for terrestrial close-range photogrammetry is distinguishable from aerial camera calibration by the following characteristics (Luhmann (2016)):

- High-accuracy requirements in object space equivalent to 0.1 or less pixel accuracy in image space.
- Single and multi-sensor imaging configurations.
- Absence of control points and camera station constraints.
- Multi-station convergent imaging.

We will briefly describe the underlying principles of photogrammetry in the subsequent sections.

3.2.1 Interior Orientation

The purpose of interior orientation (IO) is to establish an accurate relationship between the pixel coordinate system and image coordinate system. This is necessitated by the high-accuracy requirements for close-range photogrammetric applications as stated in Section 3.2.2. Development of digital cameras have removed some modelling considerations such as out-of-plane distortion. This distortion is commonly found in analogue cameras where the film is not perfectly flat in the camera casing. However, 'unflatness' in thin CCD wafers can also occur from 'crinkling' despite strict manufacturing requirements. This can cause systematic image coordinate errors which also limit high photogrammetric accuracies (Cronk (2008)). These systematic errors can be compensated for by the 8-term physical model developed by Brown (1971). The model addresses the factors that cause deviations from the theoretically exact model; changes in image location (spatial position of the perspective center and the focal length) and changes in image quality (radial and decentering distortions, affinity and shear).

3.2.1.1 Focal length

The focal length is defined as the distance between the perspective centre of the lens and the principal point of an image (see Figure 3.2.1). The term focal length and principal distance can be used synonymously when the camera lens are focused at infinity. Focal length is represented by the symbol "c" in the following text.

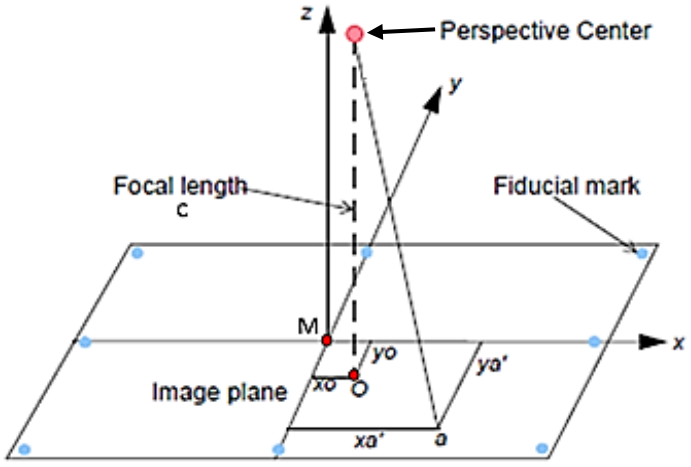

Figure 3.2.1: Internal geometry of a camera.

3.2.1.2 Principal point offset

The principal point is defined as the intersection of the perpendicular line through the perspective centre of the image plane. It is represented by the point "O" in Figure 3.2.1. The principal point does not always line up with the physical centre of the image acquired by the CCD (point M). The principal point offset which is the difference between point M and point O (x_0 , y_0) can cause deviations in the origin point for distortion measurement, thereby contributing to photogrammetric measurement errors. Therefore, it is important to recover (x_0 , y_0) whenever possible. For an image point "*a"* (x_a , y_a), the corrected image point (x , y) from principal point offset is represented by Equation (3.2.1):

$$\begin{aligned} \boldsymbol{x} &= \boldsymbol{x_a} - \boldsymbol{x_0} \\ \boldsymbol{y} &= \boldsymbol{y_a} - \boldsymbol{y_0} \end{aligned} \tag{3.2.1}$$

3.2.1.3 Radial lens distortion

A radially distorted image is one which has been displaced radially either closer to or farther from the principal point. Radial lens distortion is symmetric and varies with focal length (Cronk (2008)). It is more pronounced at shorter focal lengths (Fraser (1997)) and usually 10 times more significant than the decentring distortion in cameras with good quality lens (Luhmann et al (2006)). A mathematical derivation of the effect of radial lens distortion on close-range stereo-photogrammetry is presented and discussed by Fryer and Mitchell (1987). They included an analysis showing the amount of x-parallax introduced by the distortion across a stereo-model, and the remaining amount that is uncompensated for during relative orientation. It is these uncompensated systematic errors that cause a flat object to appear curved. The effects of radial distortion is viewed as a barrel or pincushion distortion as illustrated in Figure 3.2.2.

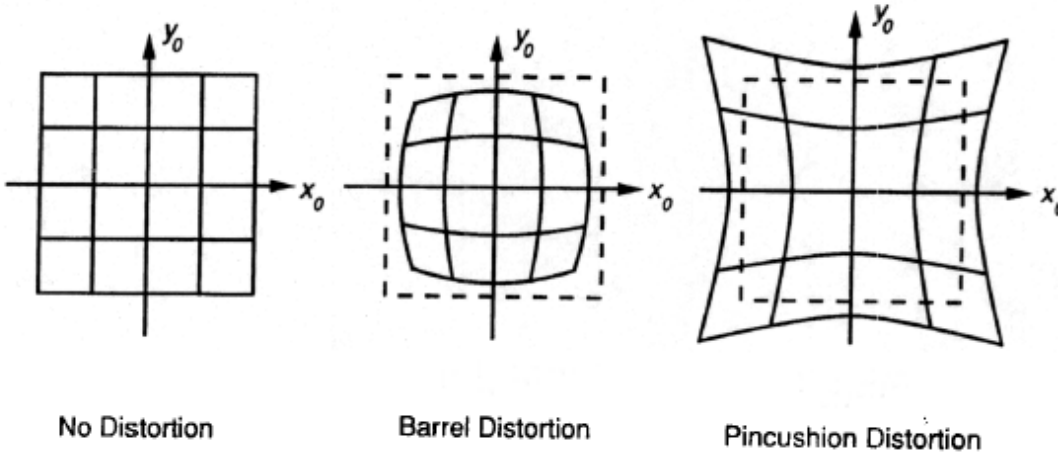

Figure 3.2.2: Effects of radial distortion; barrel (distorted outwards from principal point) and pincushion (distortion towards the principal point).

The mathematical representation of radial distortion can be expressed in its pure or Gaussian form as a series of odd powered terms, derived from the Seidel aberrations. The magnitude of the radial distortion (Δr) can be expressed by:

$$\Delta \boldsymbol{r} = \boldsymbol{k_1 r^3 + k_2 r^5 + k_3 r^7}$$
$$\boldsymbol{r} = \sqrt{\boldsymbol{x^2 + y^2}} \qquad (3.2.2)$$

where k_1, k_2, k_3 are the coefficients of radial distortion corresponding to infinity focus and x, y are determined from Equation (3.2.1). As the distortion parameters are numerically correlated with image scale or principal distance, a linear part of the distortion is separated to avoid these correlations. The corrections to image coordinates (Δx_{rad} and Δy_{rad}) for radial distortion are then:

$$\Delta \boldsymbol{x_{rad}} = \frac{\boldsymbol{x}}{\boldsymbol{r}} \Delta \boldsymbol{r}$$
$$\Delta \boldsymbol{y_{rad}} = \frac{\boldsymbol{y}}{\boldsymbol{r}} \Delta \boldsymbol{r} \qquad (3.2.3)$$

3.2.1.4 Decentring distortion

Departures from collinearity occur due to vertical displacement or rotation of a lens element from a perfect alignment along the camera's optical axis (Brown (1966), and Atkinson (1996)) as illustrated in Figure 3.2.3.

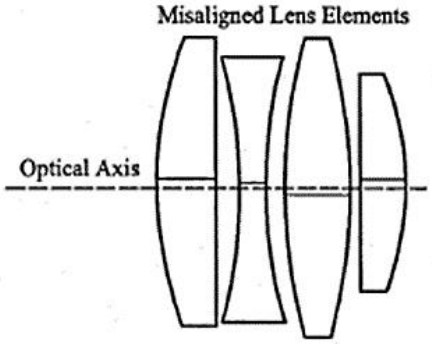

Figure 3.2.3: Exaggerated decentring distortion caused by misaligned lens elements (Cronk 2008).

The decentring distortion can be compensated for by the following function (Brown (1971)):

$$\Delta x_{dec} = p_1(r^2 + 2x^2) + 2p_2xy$$
$$\Delta y_{dec} = p_2(r^2 + 2y^2) + 2p_1xy \quad (3.2.4)$$

where Δx_{dec} and Δy_{dec} are the decentring distortions in x-axis and y-axis, and r is the radial distance (see Equation (3.2.2)). The coefficients for the decentring distortion p_1 and p_2 express the effect of the decentring of optical elements within the lens assembly while x and y are determined from Equation (3.2.1). Although the decentring distortion has been called as tangential distortion by some (Luhmann et al (2006), and Schenk (1999, 2005)), the actual distortion comprises of both tangential and asymmetric radial effects. A profile function $p(r)$ can be used to determine the maximum magnitudes of both effects, and is approximated by:

$$p(r) = \sqrt{p_1^2 + p_2^2} \cdot r^2 \quad (3.2.5)$$

where the maximum tangential effect is given by this function. Coupled with a radial effect that is 3 times as large, the resulting distorted image is illustrated in Figure 3.2.4.

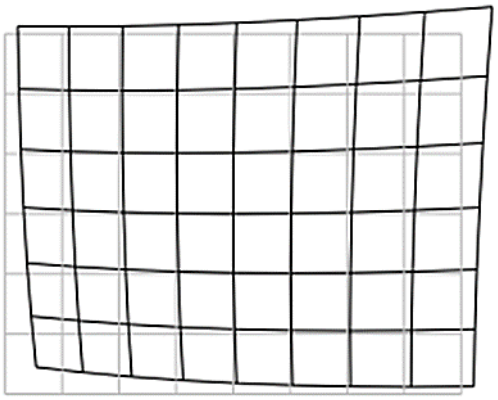

Figure 3.2.4: Decentring distortion from tangential and asymmetric radial effects.

Decentring distortion is generally smaller than radial lens distortion by several magnitudes and thus only determined for high accuracy applications. Low costs lens should be calibrated for decentring distortion as significant decentring distortion can be present.

3.2.1.5 Affinity, Shear and Total Correction

In addition to radial lens and decentring distortion, photogrammetrists often try to model additional departures from the ideal central perspective projection. The 8-parameter model by Brown (1971) is often expanded to a 10-parameter model to account for any image-invariant affine distortion (Luhmann et al (2016)). The additional 2 parameters, affinity and shear are used to describe deviations of the image coordinate system with respect to orthogonality and uniform scale of the coordinate axes (Luhmann et al (2006)). Affinity describes the effect of a differential scale between the horizontal and vertical axes (Lichti (2006)), whereas shear describes the non-orthogonality of the pixels (Fraser et al (1995), and Patias and Streilein (1996)). These characteristics can appear when the digital imaging sensor has light sensitive elements that are not on a regular grid or are rectangular rather than square. Affinity and shear can be corrected by the following function:

$$\Delta \boldsymbol{x_{aff}} = \boldsymbol{b_1 x} + \boldsymbol{b_2 y}$$
$$\Delta \boldsymbol{y_{aff}} = \boldsymbol{0} \tag{3.2.6}$$

where Δx_{aff} is the in-plane distortion correction applied to the x image coordinate, and b_1 and b_2 are the affinity and shear terms. Usually, the correction for affinity and shear needs to be applied to either the ordinates or abscissae of the image co-ordinates, but not both. As seen in Equation (3.2.6), the correction is only applied to the x image coordinate but not the y coordinate. Alternatively, a similar correction could be applied to the y coordinate, while the correction to the x-coordinate would be 0.

The total correction for the imaging errors of most typical photogrammetric imaging systems can be summarised by Equation (3.2.7).

$$\Delta \boldsymbol{x} = \Delta \boldsymbol{x_{rad}} + \Delta \boldsymbol{x_{dec}} + \Delta \boldsymbol{x_{aff}}$$
$$\Delta \boldsymbol{y} = \Delta \boldsymbol{y_{rad}} + \Delta \boldsymbol{y_{dec}} + \Delta \boldsymbol{y_{aff}} \tag{3.2.7}$$

The total error in the image point (Δx, Δy) is the summation of all radial, decentring and affinity distortion errors calculated from Equations (3.2.3), (3.2.4) and (3.2.6). The error is then 'corrected' for each point on the image and a calibrated image is generated.

3.2.2 Relative Orientation

Relative orientation (RO) is the reconstruction of the same perspective relative situation between a stereo-pair of photographs when they are taken. This is a fundamental photogrammetric procedure in the orientation of a stereo image pair process when control points are not available. The procedure involves determining five unknowns in the base components and the three rotation angles; b_y, b_z, omega (ω_R), phi (φ_R), kappa (κ_R)) of the right image as the RO is formed at the perspective center of the left image with its orientation coincident with the three major axes of the left image coordinate system (we fixed the parameter values of the left image at zero). The right image is then relative oriented such that its orientation parameters are in the left image coordinate system. The parameters of the exterior orientation with respect to the model coordinate system is then defined as:

$$x_L = 0 \qquad y_L = 0 \qquad z_L = 0$$
$$\omega_L = 0 \qquad \varphi_L = 0 \qquad \kappa_L = 0 \tag{3.2.8}$$

$$x_R = b_x \qquad y_R = b_y \qquad z_R = b_z$$
$$\omega_R = \omega \qquad \varphi_R = \varphi \qquad \kappa_R = \kappa \tag{3.2.9}$$

The local 3D model coordinate system XYZ is located in the perspective centre of the left image and oriented parallel to its image coordinate system. Therefore, the parameters of the exterior orientation of the left image with respect to the model coordinate system is given in Equation (3.2.8). As the right image is oriented in the model system, there are 3 translations and rotations in the image presented by b_x, b_y, b_z, ω, φ, κ. The components b_x, b_y, b_z define the base vector between the perspective centers of the left and right images. b_x is the horizontal distance between the left and right camera's center of projection, also known as the baseline. The remaining 2 translations b_y, b_z and 3 rotations ω, φ, κ are unknown and have to be solved. There are several techniques available in determining RO which have been based on the collinearity or coplanarity models (Luhmann et al (2006), Mikhail et al (2001), and Schenk (1999)) or projective geometry methods from solving essential and fundamental matrices (Cronk (2008), Faugeras et al (1992), and Longuet-Higgins (1981)). The coplanarity model is generally used in photogrammetry for orienting stereo pairs and is an extension of the collinearity equations. We first look at the collinearity model and then show the connection between the two.

3.2.2.1 Collinearity Model

The collinearity condition expresses the basic relationship in which an object point, the perspective center of the image and its corresponding image point all lie on the same line (Schenk (1999), Luhmann et al (2006)). It characterizes the perspective projection of each image and is of the form:

$$\begin{bmatrix} x_a - x_0 \\ y_a - y_0 \\ -c \end{bmatrix} = \lambda R \begin{bmatrix} X - X_c \\ Y - Y_c \\ Z - Z_c \end{bmatrix} \tag{3.2.10}$$

where

- x_a, y_a are image point coordinates, x_0, y_0 are the coordinates of the principal point and c is the focal length of the camera.
- λ is a scale factor and R is 3×3 rotation matrix formed from the three rotation angles ω, φ, κ describing the rotation of the image coordinate system with respect to the object coordinate system.
- X, Y, Z describe the position of the perspective centre in the primary 3D coordinate system and X_C, Y_C, Z_C are the coordinates of an object point in the 3D coordinate system.

We expand Equation (3.2.10) to derive the following equations:

$$\begin{aligned} \boldsymbol{x_a - x_0} &= \boldsymbol{\lambda[r_{11}(X - X_c) + r_{12}(Y - Y_c) + r_{13}(Z - Z_c)]} \\ \boldsymbol{y_a - y_0} &= \boldsymbol{\lambda[r_{21}(X - X_c) + r_{22}(Y - Y_c) + r_{23}(Z - Z_c)]} \\ \boldsymbol{-c} &= \boldsymbol{\lambda[r_{31}(X - X_c) + r_{32}(Y - Y_c) + r_{33}(Z - Z_c)]} \end{aligned} \qquad (3.2.11)$$

where r_{ij} are the (i, j) elements of the rotation matrix R.

$$R = \begin{bmatrix} \cos\phi\cos\kappa & \cos\omega\sin\kappa + \sin\omega\sin\phi\cos\kappa & \sin\omega\sin\kappa - \cos\omega\sin\phi\cos\kappa \\ -\cos\phi\sin\kappa & \cos\omega\cos\kappa - \sin\omega\sin\phi\sin\kappa & \sin\omega\cos\kappa + \cos\omega\sin\phi\sin\kappa \\ \sin\phi & -\sin\omega\cos\phi & \cos\omega\cos\phi \end{bmatrix}$$

where the angle ω is the pitch (vertical angle) of the optical axis, angle φ is the yaw (horizontal angle) of the optical axis, and angle κ is the roll or twist about the optical axis. Angular orientation is specified by three independent sequential rotations of the orthogonal axes in 3D space (see Figure 3.2.5): rotation ω about the x-axis, rotation φ about the new y-axis, and rotation κ about the new z-axis.

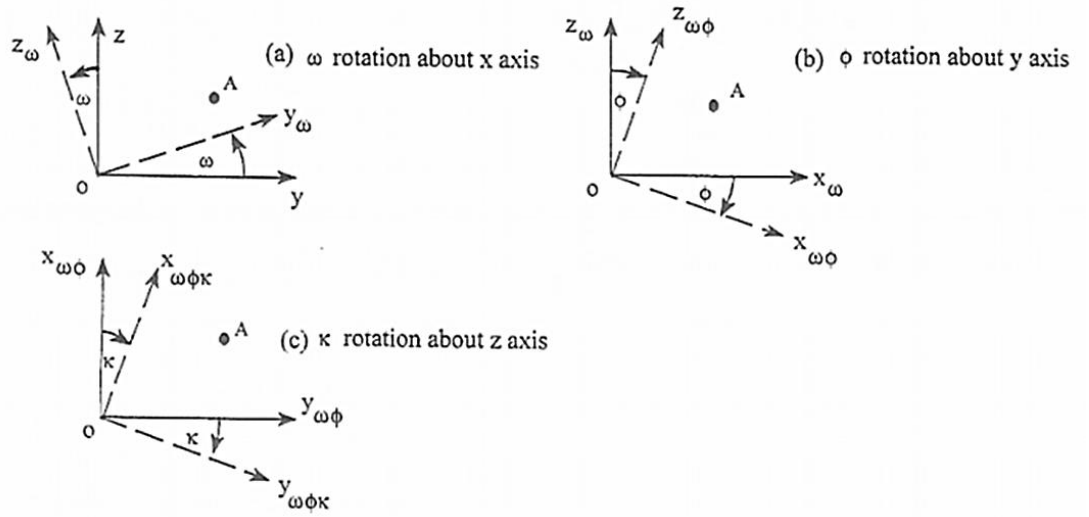

Figure 3.2.5: Sequential rotations of the axes in three dimensional space (Cooper and Robson, 2001).

Rearranging Equation (3.2.11) gives the collinearity equations:

$$x_a = x_0 - c\left[\frac{r_{11}(X - X_c) + r_{12}(Y - Y_c) + r_{13}(Z - Z_c)}{r_{31}(X - X_c) + r_{32}(Y - Y_c) + r_{33}(Z - Z_c)}\right]$$
$$y_a = y_0 - c\left[\frac{r_{21}(X - X_c) + r_{22}(Y - Y_c) + r_{23}(Z - Z_c)}{r_{31}(X - X_c) + r_{32}(Y - Y_c) + r_{33}(Z - Z_c)}\right] \quad (3.2.12)$$

The collinearity equations in (3.2.12) allows the RO to be solved with the condition that some initial object space point is provided to compute the five unknown parameters from the twelve orientation parameters (seven are declared as constants). At least five control pints in two images are required for this computation.

Although the advantage of the collinearity model lies in its generality and simultaneous computation of orientation parameters and object points (Schenk (1999)), it is limited in its usefulness when control points or EO devices are not readily available (Cronk (2008)). The coplanarity model, which is an extension of the collinearity equations in stereo pairs, is a more applicable approach to RO and is widely used amongst photogrammetrists for stereo restitution as it does not require any existing object space coordinates for computation.

3.2.2.2 Coplanarity Model

The coplanarity condition states that for a given point in 3D space (*X, Y, Z*), the points lies on a common plane with the perspective centres PC_1 and PC_2 of two images and their corresponding image points (x_1, y_1) and (x_2, y_2). An epipolar plane is defined by the vectors: the baseline b between PC_1 and PC_2 and the image rages r_1 and r_2 projected from PC_1 and PC_2 to the object point (*X, Y, Z*) as shown in Figure 3.2.6. The coplanarity condition is satisfied when the scalar triple product of the three vectors equal zero i.e. $r_1 \cdot (b \times r_2) = 0$.

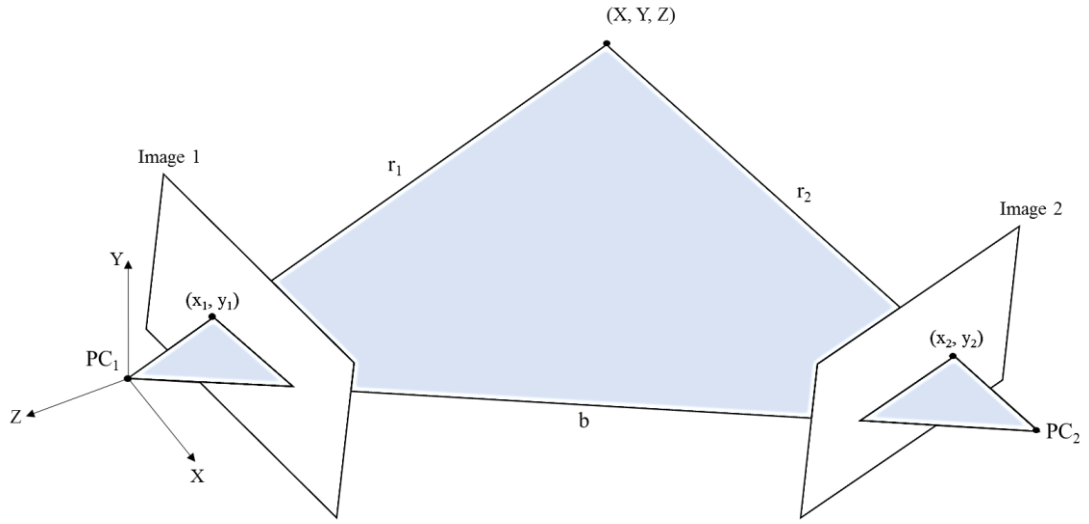

Figure 3.2.6: The coplanarity condition in a stereo image pair.

We can express the coplanarity condition as the determinant of a 3×3 matrix (Mikhail et al (2001)) built from the vectors b (b_x, b_y, b_z), r_1 ($\bar{x}_1$, $\bar{y}_1$, $\bar{z}_1$) and r_2 ($\bar{x}_2$, $\bar{y}_2$, $\bar{z}_2$). It is of the form:

$$\begin{vmatrix} \boldsymbol{b_{Xx}} & \boldsymbol{b_y} & \boldsymbol{b_z} \\ \boldsymbol{\bar{x}_1} & \boldsymbol{\bar{y}_1} & \boldsymbol{\bar{z}_1} \\ \boldsymbol{\bar{x}_2} & \boldsymbol{\bar{y}_2} & \boldsymbol{\bar{z}_2} \end{vmatrix} = \mathbf{0} \qquad (3.2.13)$$

For a given image pair, we can solve the unknown parameters from the coplanarity model with a minimum of 5 conjugate points. Mikhail et al (2001) defines this as dependent RO:

$$[x_1 \quad y_1 \quad -c]\begin{bmatrix} 0 & b_z & -b_y \\ -b_z & 0 & b_x \\ b_y & -b_x & 0 \end{bmatrix} R^T \begin{bmatrix} x_2 \\ y_2 \\ -c \end{bmatrix} = 0 \qquad (3.2.14)$$

where (x_1, y_1) and (x_2, y_2) are conjugate image point coordinates, c is the focal length, (b_x, b_y, b_z) are baseline translations in the x, y, z-axes, and R is the rotation matrix expressing the orientation of Image 2 with respect to Image 1 (Cronk (2008)). Since scale is not recoverable from RO and our stereo images are captured side-by-side, we can assign an arbitrary value to the baseline component b_x. For the stereo-camera FujiFilm FinePix REAL 3D W3, the arbitrary value for b_x is 75 and 500 (units in mm) for the pseudo stereo-cameras Canon Mark II (see camera specifications in Table 3.1).

Another method for solving RO of two images is to linearize the coplanarity equation in terms of the five unknowns (b_y, b_z, ω_R, φ_R, κ_R) before using an iterative least-squares method to solve for said unknowns. Initial approximations of the five unknowns and a set of point correspondences between the image pair is required. Mikhail et al (2001) gives an in-depth description of the method and its equations.

3.2.3 Automatic Orientation with Interest Points

We use an in-house software to determine relative orientation for stereo-images. To extract points of interest, a search is conducted through areas with high variance for points with distinct features. An interest point in the left image is then selected as the base point. A search window in the right image is computed, producing several interest point candidates with high correlation. The point yielding the highest correlation factor is usually considered the conjugate point to the template's center. In some cases, the y-component for selecting the conjugate point is also considered (Tang and Heipke (1996)). The exterior orientation is a crucial factor in determining the location of the search window. The uncertainties of these parameters also determine the size of the search window. Given that the orientation of the stereopair is uncertain, an initial approximation of the orientation is made. A simplified version of the search window can be expressed by the following equations:

$$x_s = x - bx$$
$$y_s = y \qquad (3.2.15)$$

where (x, y) are the coordinates of the interest point in one image and (x_s, y_s) the coordinates of the search window center. The uncertainty in the model surface and orientation parameters determines the size of the window in the x- and y-direction respectively. A hierarchical approach limits the number of matching candidates by targeting points that have been accepted as conjugate points on a previous level of the image pyramid.

3.3 Stereoscopic sensors

When considering the types of sensors to use, digital single-lens reflex (DSLR) cameras are regarded to give better results than consumer grade digital cameras. They are generally equipped with lenses of higher quality, have higher resolutions, and provide more controls for image capture (Chandler et al (2005)). Higher resolutions are associated with a higher number of megapixels. This equates to more information that can be obtained from the image of a DSLR camera. That is not to say that consumer-grade commodity cameras are inferior to DSLR cameras in any meaningful applications. Current automatic camera calibration methods are sufficiently robust to improve the photogrammetric accuracies of cheap commodity cameras from 1:2000 to 1:50000+ which is on par with DSLRs (Cronk (2008)). This research takes both types of equipment into consideration by using a pair of DSLR Canon 5D Mark IIs and a consumer grade handheld stereo-camera FujiFilm FinePix REAL 3D W3.

3.4 Experimental Protocol

This section outlines the protocol of our experimental studies in later chapters. Table 3.4.1 summarises the technical specifications for the stereo cameras used in the experimental studies. Pixels sizes vary and many proprietary digital cameras do not provide this information beyond the standard resolution setting. The appropriate pixel size can be calculated from the camera settings by dividing the CCD sensor

width by the image width. Theoretically, pixels are assumed to be square; height should be equivalent to width (Cronk (2008)), but this is not always true. Whilst Canon's 5616×3744 resolution and FujiFilm's 3648×2736 resolution does yield a pixel size of 6.41×6.41µm and 1.69×1.69µm, the calculated pixel size for FujiFilm's alternate image ratio setting <16:9> of resolutions 3584×2016 and 1920×1080 is 1.72×2.29µm and 3.21×2.29µm respectively. These calculated values as well as the camera specifications obtained from their manufacturers' websites are presented in Table 3.4.1 below.

Table 3.4.1: Technical specifications for the FujiFilm FinePix REAL 3D W3 and Canon 5D Mark II.

Model	**FinePix REAL 3D W1**	**CANON 5D Mark II**
Effective pixels	10 Megapixel	21.1 Megapixel
Baseline	75mm	0.5m for stereo-pair
Focal length	6.3 – 18.9mm	35mm
Image ratio W:H	S: <16:9> L: <16:9> L: <4:3>	3:2
Sensor size	1/2.3 inch	
Sensor type	CCD	CMOS
Number of recorded pixels	1920×1080 pixels 3584×2016 pixels 3648×2736 pixels	5616×3744 pixels
Pixel size	3.21×4.28 µm 1.72×2.29 µm 1.69×1.69 µm	6.41×6.41 µm
Effective sensor size	6.16×4.62 mm	36×24 mm
Dimensions (W x H x D)	123.6×68×25.6 mm	152×113.5×75 mm
Weight	260g	850g

3.4.1 Canon 5D Mark II

The Canon 5D Mark II is a DSLR camera, used primarily by professional photographers, that is capable of imaging up to 21.1 megapixels. In combination with their internal stability, design, functionality and larger CCD sensor sizes that allow for wider-angle lenses makes it suitable for higher accuracy photogrammetric applications. Although most DSLR cameras have the classic format of 25.1×16.7mm for CCD size, the Canon 5D Mark II has a sensor size larger than a 35mm film frame with dimensions 36×24mm. As with many proprietary digital cameras, the size of the sensor element or pixel size is not given and must be estimated indirectly. Technical specifications are presented in Table 3.4.1.

3.4.1.1 Calibration

Camera calibration was conducted using the Australis software and a 2×1m calibration wall. An example is shown in Figure 3.4.1 below.

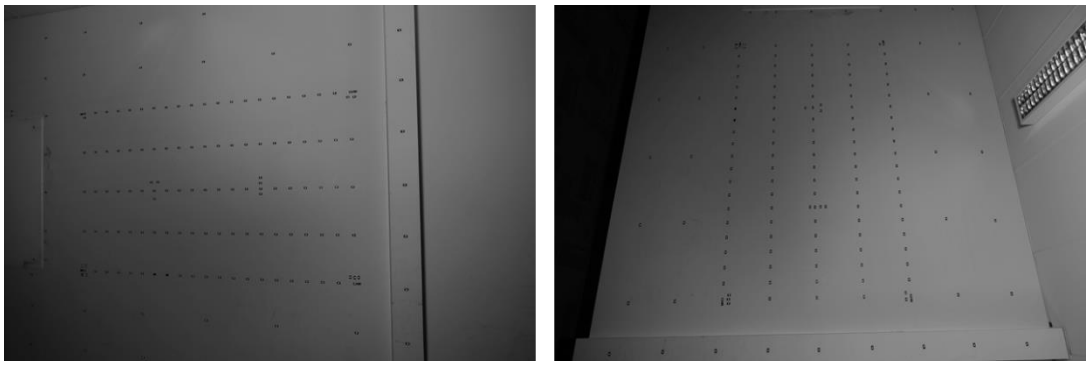

Figure 3.4.1: Calibration wall.

Several images have been captured using two Canon 5D Mark II cameras at orthogonal roll angles with at least three images in landscape and portrait orientation respectively to create a highly convergent imaging configuration. For example, the left image in Figure 3.4.1 has been acquired in landscape orientation while the right image is in portrait orientation. Having a diverse photogrammetric network configuration would ensure that the errors at each point will not align with each other and will instead behave differently. In addition, a minimum of four images are usually necessary for quality calibration given that high redundancy enables accuracy testing (Luhmann et al (2006), and Schenk (1999)).

The images were captured at <3648×2736> resolution. Third party software was used to extract JPEG images from both cameras. Calibration was conducted separately for the left and right camera with their respective images. For each camera, the corresponding acquired images are imported to a new project in Australis. Given that Australis is only able to process grayscale TIFF images, it automatically converts the raw images to the appropriate format during the importing process. Although Australis has a camera database to reference the target camera, we were not able to find the relevant camera in the database and had to manually enter the camera focal length and image pixel size.

For the calibration, we have measured 4 object space coordinates (I1, I2, I3, I4) marked in green. The four points are presented in Figure 3.4.2 below. They are used as a 3D data file in Australis to enable ‘resection driveback’. The process first establishes an approximate camera location through space resection. Each photograph is then orientated and approximate XYZ coordinates are determined for all or some of the target points in the image. Utilising these orientation information, the ‘driveback’ process is used to predict the image point location of the targets and automatically measure all the visible points.

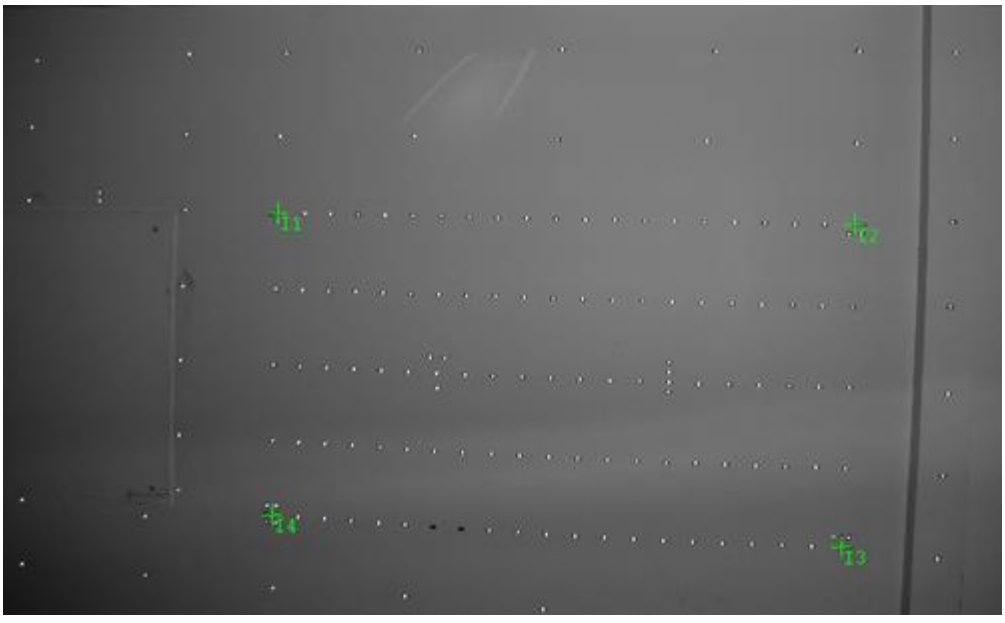

Figure 3.4.2: Object coordinates measured in image of calibration.

Initial resection was conducted for each image where the four object coordinates have been identified. This determines the initial exterior orientation of the camera

using intersection triangulation. Excluding the initial four object space coordinates that have been measured for the initial resection, we labelled another 109 observations in the images and conduct bundle adjustment. This allows us to find initial values for the interior orientation parameters and is necessary for redundancy in accuracy measurement (Schenk (1999)). An example of the labelled observations is presented in Figure 3.4.3.

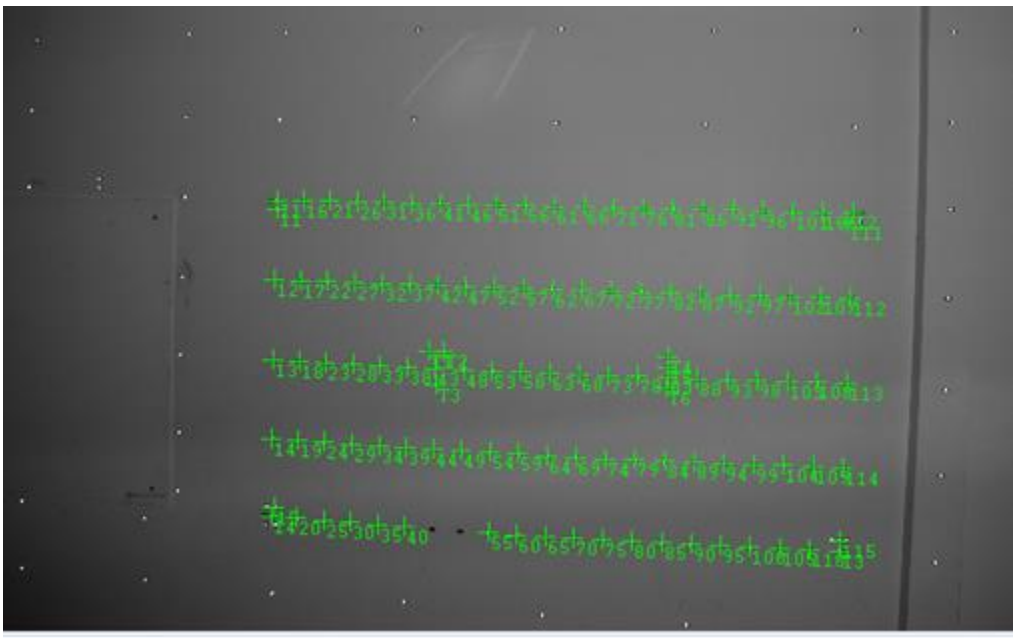

Figure 3.4.3: 109 observations labelled for image.

Bundle adjustment is applied a second time to achieve self-calibration. Insufficient roll diversity results in a weak self-calibration but is addressed by eliminating similar images from the dataset and introducing additional images with good roll diversity. The number of iteration runs was set to the maximum and the calibration output for both Canon cameras is summarised in Table 3.4.2.

Table 3.4.2: Camera calibration parameters correction values for Canon 5D Mark II left and right cameras at <3648×2736> resolution.

Left Camera	
c	24.50310
x_0	-0.35440
y_0	-0.11380
k_1	1.450E-05
k_2	1.980E-08
k_3	-5.965E-11
p_1	4.935E-05
p_2	1.172E-05
b_1	9.225E-07
b_2	4.218E-05

Right Camera	
c	24.44050
x_0	-0.42700
y_0	0.03290
k_1	1.602E-05
k_2	2.670E-08
k_3	-9.187E-11
p_1	5.156E-05
p_2	7.689E-06
b_1	-5.930E-07
b_2	-6.127E-05

3.4.1.2 Fieldwork and Image capture

Image acquisition starts with setting up the stereoscopic system for the Canon 5D Mark II cameras. To achieve stereoscopy, two Canon 5D Mark IIs are mounted on a bracket, spaced 0.5m apart and fixed on a tripod. Both cameras are positioned in a parallel configuration before they are connected to a mechanism that synchronizes image capture for both cameras at the same time. The synchronizer resolves the problem of dissimilar left and right images that can arise from the presence of wind and operator error in capturing both images.We then need to determine the most appropriate position from which the tree can be photographed.

The available light, the lean and/or sweep of the tree and visibility of the features up the stem should be taken into consideration (Brownlie et al. (2007)). The camera should not face towards the sun as doing so would result in overexposure and/or increased shadowing of the tree. The principal distance from the tree is determined by the fit of the target in the image's field of view. It is not recommended that the object target fits snugly within the boundaries of the field of view (see Figure 3.4.4a). The operator must consider that during the calibration process, the principal point offset will shift the image's centre and result in the exclusion of some interest points as illustrated in Figure 3.4.4b. It can be seen that the right end of the canopy has been excluded from the image after calibration. Therefore, it is necessary to leave a

margin of background in the field of view during image capture. A good example is shown in Figure 3.4.4c.

(a) (b) (c)

Figure 3.4.4: Example of a good image.

A reference frame or panel is placed next to each subject, ensuring that it aligns with the subject. Once the frame is in place, two or more landscape oriented stereo-images are captured. Next, another set of images were captured a few steps sideways from the previous capture spot. This procedure is repeated while circling the tree and usually results in approximately 20 – 50 photos per tree and takes about 15-30 minutes as time is spent moving the tripod and checking the fit of the tree within the camera's field of view at each location. With multiple images taken at different viewing angles, we can account for any tree detail that was occluded from previous images, in particular multi-stemmed trees. Clear to semi-clear skies provided the best conditions for photography as it gives good exposure and clarity in subject details. Overcast skies are not as ideal given that underexposure increases darkening of tree parts and reduces detail in branch and foliage.

3.4.1.3 Data Processing

JPEG image files of the raw data is extracted from each Canon 5D Mark II camera and converted to TIFF format. We use an in-house CSIRO program to correct for principal point offset and lens distortion for all images using the calibration parameter values derived in Section 3.4.1.1 (see Table 3.4.2). Another in-house CSIRO measurement program is used to manually identify and match interest points with high variance from the stereo-images.

Since the orientation of the stereo-pair is unknown, the procedure begins with initial approximations. A minimum of 10 interest points are identified from the stereo-pair and a robust fitting algorithm provided an initial estimation of the affine

transformation coefficients. Interest points are accepted if correlation is high (greater than 0.90) and rejected if they are too low (less than 0.80). Stereo-points that have a matching correlation value between 0.80 and 0.90 are accepted under the condition that a manual inspection shows the points to be identical. There are instances where the program matches a stereo-pair with a high correlation value of which the left image and right image point is not identical. The semi-automatic method allows us to measure an interest point from the left stereo-image (top left image in Figure 3.4.5) from which a similar conjugate point will be automatically measured in the right stereo-image (bottom left image in Figure 3.4.5) with the corresponding correlation value. Once a sufficient number of conjugate points have been locked as a base pair, we estimate the relative orientation (RO). If the residuals value of the relative orientation is high (greater than pixel size), we go back to the stereo-pair and add more conjugate points to improve the matching.

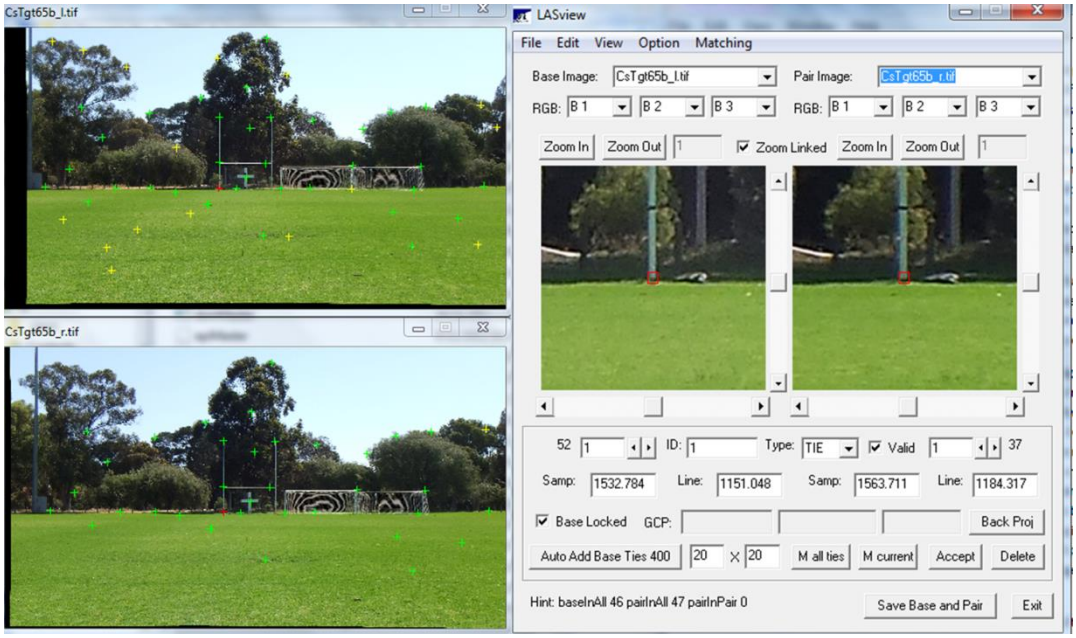

Figure 3.4.5: Point matching and relative orientation performed with CSIRO in-house program.

Epipolar images are generated from RO parameters and dendrometric measurements are measured from the epipolar images. The reference scale in the initial image acquisition allows us to translate image space coordinates into object space coordinates and determine the metric distance between two points (calculate height, width and stem diameters) using in-house CSIRO measurement programs.

Tree height is measured by calculating the vertical or diagonal (for leaning trees) distance between a point at the tree base to the highest identified point of the tree. Stem diameter is determined by transposing breast height at 1.3m into pixel values and extrapolating from the tree base point the image height at which stem diameter is to be measured. For non-vertical stems, diameter is measured by taking the perpendicular length of the stem in the direction of the stem growth.

3.4.2 FujiFilm FinePix REAL 3D W3

The FujiFilm FinePix REAL 3D W3 is a consumer grade digital camera designed to allow for stereo-vision (Masuda et al (2011), and Menna et al (2013)). The camera encases two Fujinon 3x optical zoom lenses in a die-cast frame and utilizes a synchronized Twin-Lens-CCD system to capture two images simultaneously.

(a) front *(b) back*

Figure 3.4.6: FujiFilm FinePix REAL 3D W3 camera (a) front and (b) back.

The baseline is 75mm and each CCD resolution is 10 megapixels as presented in Table 3.4.1. The typical aspect ratio of the image width to height is 4:3 for standard digital cameras or 3:2 for most DSLRs, but the FujiFilm FinePix REAL 3D W3 includes an additional image ratio 16:9 higher than the standard aspect ratio. The back includes an auto-stereoscopic display of lenticular type that allows for live view and the 2D and 3D visualization of the captured images (Vlad (2014)). The FujiFilm FinePix REAL 3D W3 is more user-friendly in terms of size, weight and portability relative to the Canon 5D Mark II cameras.

3.4.2.1 Calibration

Camera calibration was conducted using iWitness and the accompanying set of coded targets. A 3D distribution network was incorporated into the layout of the reference codes such that all points are not coplanar. An example is shown in Figure 3.4.7 below.

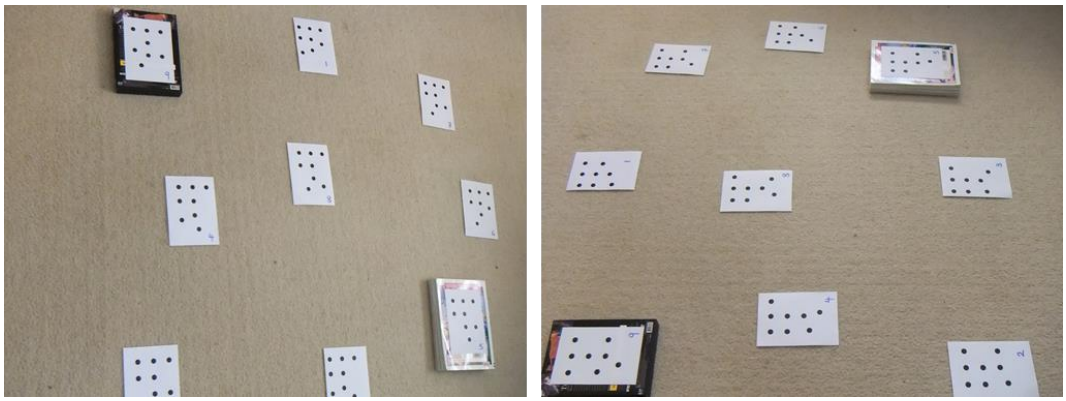

Figure 3.4.7: Calibration coded target distribution.

Several images have been captured using the FujiFilm FinePix REAL 3D W3 at orthogonal roll angles with at least three images in landscape and portrait orientation respectively. For example, the left image in Figure 3.4.7 has been acquired in landscape orientation while the right image is in portrait orientation. We captured the images on two resolution settings; <3648×2736> and <3584×2016>. Third party software is used to extract the left and right JPEG images from the MPO file and converted to TIFF format. Calibration was conducted separately for the left and right camera with their respective images. For each camera, the corresponding acquired images are imported to a Camera Calibrator project in iWitness from which the program automatically reads the camera type from the 'EXIF' file header. In most cases, it is not necessary for the operator to identify or manually enter the camera's details given that iWitness has an updated list of most digital cameras and their key metric design characteristics.

iWitness scans the input images and identifies the coded targets for calibration. Some adjustment is made to the settings. The pixel brightness threshold is selected at 10 at the minimum number of rays for each point is 4. The coded targets used in this calibration are black and white. Initial camera and lens distortion parameter (x_0 , y_0 , k_1 , k_2 , k_3 , p_1 , p_2 , b_1 , b_2) values are left at zero. When self-calibration is run in iWitness, Camera Calibrator will open and scan each image before performing the

automatic camera calibration and generating the analysed results. A summary of the calibration results for both settings are shown in Tables 3.4.3 and 3.4.4 below.

Table 3.4.3: Camera calibration parameters correction values for FujiFilm left and right cameras at <3648×2736> resolution.

Left Camera	
c	7.28666
x_0	-0.31691
y_0	-0.12643
k_1	2.289E-03
k_2	-6.458E-05
k_3	1.081E-06
p_1	9.290E-04
p_2	1.934E-04
b_1	1.163E-02
b_2	-9.469E-04

Right Camera	
c	7.27896
x_0	-0.11697
y_0	-0.07415
k_1	2.039E-03
k_2	-2.834E-05
k_3	1.360E-07
p_1	1.312E-03
p_2	-8.095E-05
b_1	1.165E-02
b_2	-1.719E-04

Table 3.4.4: Camera calibration parameters correction values for FujiFilm left and right cameras at <3584×2016> resolution.

Left Camera	
c	7.28260
x_0	-0.32270
y_0	-0.10780
k_1	2.073E-03
k_2	-4.771E-05
k_3	1.056E-06
p_1	9.957E-04
p_2	2.407E-04
b_1	1.159E-02
b_2	-9.601E-04

Right Camera	
c	7.28500
x_0	-0.11780
y_0	-0.07300
k_1	2.007E-03
k_2	-3.480E-05
k_3	8.655E-07
p_1	1.479E-03
p_2	-6.183E-05
b_1	1.127E-02
b_2	8.179E-05

3.4.2.2 Image Acquisition

Given that the camera is dual lens, there is no need to set up a stereoscopic system as explained in Section 3.4.1. The camera configuration explained in Section 3.4.2

indicated that stereo-image is captured simultaneously with the left and right lens. As with zoom cameras, focal length values can vary dramatically. However, our camera calibration seeks one value for the camera used in the survey. Therefore the zoom function is not used during the photographic session. The principal distance from the tree is determined by the fit of the target in the image's field of view. As mentioned in Section 3.4.1.2, it is not recommended that the object target fits snugly within the boundaries of the field of view but to leave some margin of background during image capture (see Figure 3.4.4c).

Parallel setting of both camera lens in the FujiFilm FinePix REAL 3D W3 camera indicated that image acquisition can only be obtained in landscape orientation for the tree to be within the overlapping area of the left and right camera. The operator should take extra care in image acquisition and leave a wider margin of background in the field of view. The display screen on the FujiFilm combines both left and right images to produce a 3D display of the image captured of which the tree appear to fit well within the image but neglects to display the actual raw left and right images.

The camera was set to automatic exposure mode which automatically calculates and adjusts exposure settings to match the mid-tone of the two images as closely as possible. ISO was set at 200 to prevent excessive noise from being captured. The aperture was sufficiently high to obtain a high depth of field and retain sharpness of imagery. Clear to semi-clear skies provided the best conditions for photography as it gives good exposure and clarity in subject details. However, one should take care not to face the sun when taking images as doing so would result in overexposure and/or increased shadowing of the tree. Overcast skies are not as ideal given that underexposure increases darkening of tree parts and reduces detail in branch and foliage.

We introduce a panel with marked points and known dimensions to obtain 3D object space coordinates in the image. The reference frame or panel is placed next to each subject, ensuring that it aligns with the subject. Once the frame is in place, two or more landscape oriented stereo-images are captured. Next, another set of images were captured a few steps sideways from the previous capture spot. This procedure is repeated while circling the tree and usually results in approximately 20 – 50 photos and takes about 5 – 10 minutes per tree. With multiple images taken at different viewing angles, we can account for any tree detail that was occluded from previous images, in particular multi-stemmed trees.

3.4.2.3 Data Processing

Image processing using the FujiFilm FinePix REAL 3D W3 is similar to the process explained in Section 3.4.1.3 with the exception of image extraction. From the MPO image file, third party software is used to extract JPEG left and right image files of the respective camera lens and converted to TIFF format. We use an in-house CSIRO program to correct for principal point offset and lens distortion for all images using the calibration parameter values derived in Section 3.4.2.1 (see Tables 3.4.3 and 3.4.4). Another in-house CSIRO measurement program is used to manually identify and match interest points with high variance from the stereo-images. Subsequent data processing steps are repeated (see Section 3.4.1.3) in the following order; RO determination, epipolar image generation and dendrometric measurement from the epipolar images.

Chapter 4

Applications in Simple Environments

The advancement of technology has enabled an increased use of stereo vision in applications such as 3D reconstruction, face recognition, object detection, recognition and mensuration (Hsu and Wang (2015), Muljowidodo et al (2009), Mustafah et al (2012), Yang et al (2002), and Yu et al (2003)). These applications have proven to be essential in various fields such as mobile autonomous systems and surveys conducted in engineering, forestry, mining and archaeology (Menna et al (2013), and Kytö et al (2011)).

Intensive studies focusing on obtaining object distances from an image have been undertaken and proposed in different ways. This area of research evolved from measuring distance based on a single sensor (Rahman et al (2009), Kim et al (2005), and Muljowidodo et al (2009)) to multiple vision sensors (Mustafah et al (2012), Hu et al (2011), Mahammed et al (2013), and Kytö et al (2011)).

In this chapter, we compare the performance of a consumer grade camera against the true measurements of small objects at close-range. In this context, we define close-range as metric distances up to 100m. The performance is evaluated in two cases, where the target objects are photographed from a short distance (<10m) in Section 4.1 and a large distance (>10m) in Section 4.2. We analyse the object measurements from the stereo-images in both cases and compare it against true measurements.

4.1 Object Mensuration at distances less than 10m

4.1.1 Materials and Methods

The experimental study took place in Curtin University in December 2014. A flow chart summarising the methodology used in this study is presented in Figure 4.2.1. In this section, we describe the procedures for data collection and processing.

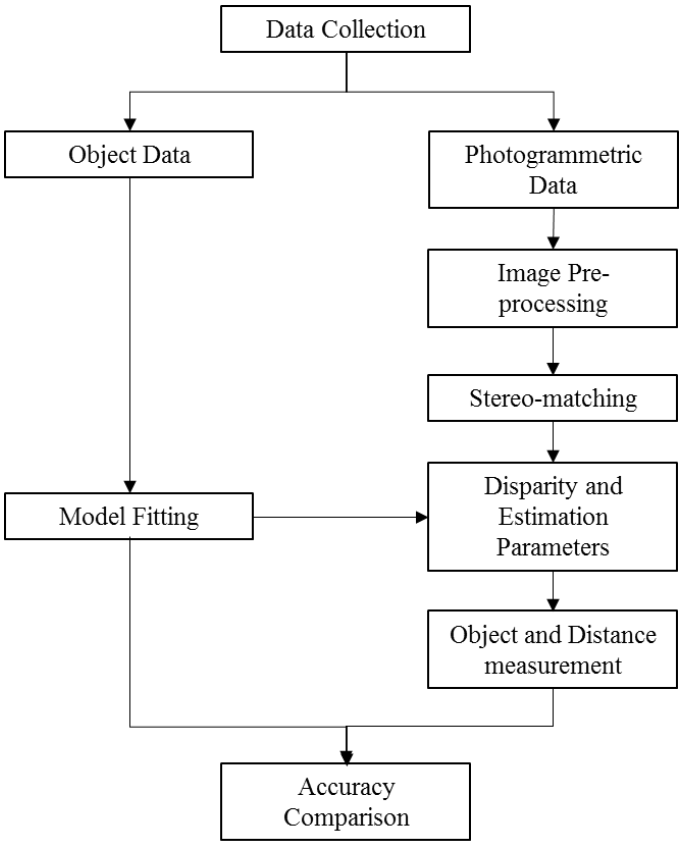

Figure 4.1.1: Flow chart of the process of data collection to object measurement and accuracy comparison.

4.1.1.1 Data collection

For the purpose of this experimental study, 5 random objects of various sizes were first measured for true heights and width in the later analysis. Stereo images were captured using a FujiFilm FinePix REAL 3D W3 camera and the principal distance between the stereo-camera and target object was measured and recorded accordingly.

The camera setting used in this study is 3584×2016 pixels resolution, therefore the corresponding pixel size is 1.72×2.29 µm.

4.1.1.2 Image pre-processing

The iWitness package was used in computing the calibration parameters by means of a free network photogrammetric bundle adjustment. From each MPO image file, the left and right JPEG files were extracted using the proprietary software and converted to TIFF format. The stereo-camera had been calibrated beforehand and the calibration parameters in Table 4.1.1 were used to correct the images for principal point offset and distortion.

Table 4.1.1: Calibration parameters for the stereo-camera.

FujiFilm FinePix			
Parameters	Left Camera	Right Camera	Units
c	7.287	7.279	mm
x_p	-0.317	-0.117	
y_p	-0.126	-0.074	
k_1	2.289E-03	2.039E-03	
k_2	-6.458E-05	-2.834E-05	
k_3	1.081E-06	1.360E-07	
p_1	9.290E-04	1.312E-03	
p_2	1.934E-04	-8.095E-05	
b_1	1.163E-02	1.165E-02	
b_2	-9.469E-04	-1.719E-04	
μ_x	0.00172	0.00172	mm/pixel
μ_y	0.00229	0.00229	mm/pixel

4.1.1.3 Stereo-matching

To reduce the complexity and inherent error in pixel matching, we first perform image rectification to make the epipolar lines of the two cameras horizontally aligned. We use an in-house CSIRO measurement program to match image points on

a stereo-pair of images for an initial assessment of the camera orientation. Each pair of stereo-points is accepted if the matching correlation is high (>0.9) and rejected if the correlation is less than 0.9. Once a set of stereo-points have been matched, RO is carried out. Residuals are checked for each RO stereo-pair. If the residual value is too high, we add more stereo-points to the initial set and check for any changes in the matching correlation for each pair of stereo-points. The data file generated from the RO is then used to generate the epipolar images in which the epipolar lines of 2 projected points are parallel and horizontally aligned along the new image planes. Disparity is subsequently measured from the epipolar images using the ERDAS ER Mapper software.

While Mustafah et al (2012) measured disparity as the pixel difference between the horizontal centroids of their object of interest (see Figure 4.1.2(a)), Hsu and Wang (2016) took the average of every matched feature distance from the SURF algorithm as the object disparity as shown in Figure 4.1.2(b). We believe that determining disparity from a single measure of object centroid difference contains some uncertainty and could potentially cause computational errors if incorrectly measured. Therefore, we apply Hsu and Wang's strategy in determining disparity from a stereo-pair of images by taking the average disparity value of every matched feature.

[The figure "Object disparity" (Mustafah et al (2012)) is unable to be reproduced here due to the reason that permission to reproduce the image from the following publication has not been obtained.]

[The figure "Object disparity" (Mustafah et al (2012)) can be instead be accessed via http://ieeexplore.ieee.org/stamp/stamp.jsp?arnumber=6271270]

[The figure "Calculating the matched feature distance as disparity" (Hsu and Wang (2016)) is unable to be reproduced here due to the reason that permission to reproduce the image from the following publication has not been obtained.]

[The figure "Calculating the matched feature distance as disparity" (Hsu and Wang (2016)) can be instead be accessed via

https://pdfs.semanticscholar.org/e12c/67ac4a8265928b983993e20ba2c0a44d7fd2.pdf]

4.1.1.4 Object distance measurement

Distance measurement from stereo images has theoretically been a simple model, where disparity between the stereo left and right images is inversely proportional to distance. The distance can be estimated from the following equation adapted from Mustafah et al (2012):

$$\boldsymbol{Distance} = \frac{\boldsymbol{bc}}{\boldsymbol{d\mu_p}} \tag{4.1.1}$$

where b is the baseline between the two cameras, c is the focal length, d is the disparity and μ_p is the pixel size.

4.1.1.5 Object measurement

Object measurement was established based on the model proposed in Mustafah et al (2012). Their research stated that per pixel width and height of an object is linear and inversely proportional to its disparity from various experimentations. This relationship was found by capturing various objects of known heights and widths in stereo-images, where the disparity between the stereo-images is measured. A variation of disparity values was obtained by changing the distance of the object. A scatterplot is subsequently plotted between the disparity against the parameters λ_w, λ_h which represents the relationship between object width and height per pixel. A linear regression equation is obtained from the scatterplot:

$$\boldsymbol{\lambda'_w = m_w d + c_w} \tag{4.1.2}$$

$$\boldsymbol{\lambda'_h = m_h d + c_h} \tag{4.1.3}$$

where m_w, m_h are the gradients, c_w, c_h are the intercepts and λ'_h, λ'_w are the predicted parameters of height and width per pixel from the regression model. These

parameters represent the scale factor of converting pixel height and width to an estimated real-time object height and width. The equations representing these conversions are described by Equations (4.1.4) and (4.1.5):

$$\boldsymbol{W = \lambda'_w w'} \tag{4.1.4}$$

$$\boldsymbol{H = \lambda'_h h'} \tag{4.1.5}$$

where w' and h' is the image object width and height in pixels.

4.1.2 Results

We present the results for object distance and size measurement from stereo-vision image capture, following the model described by Mustafah et al (2012) and Hsu and Wang (2014) in Sections 4.1.1.4 and 4.1.1.5.

4.1.2.1 Object Distance

The disparity values between each pair of stereo-image were plotted against distance as presented in Figure 4.1.3. Although, the data appears to fit better to a power or logarithmic function, we fit a linear regression line to the data that is in agreement with the inverse relationship between distance and disparity.

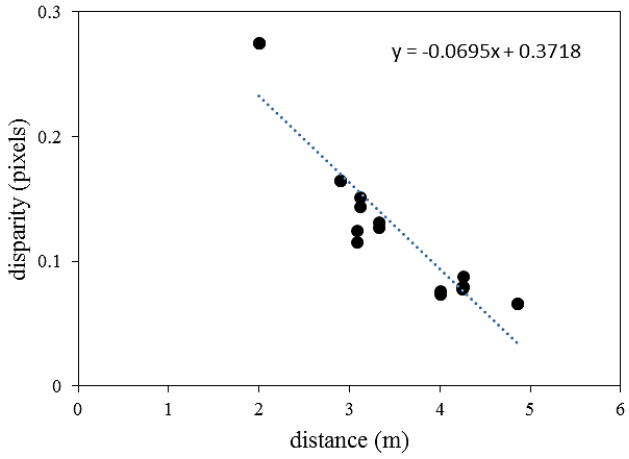

Figure 4.1.3: Inverse relationship between distance and disparity as explained by the linear regression equation.

Using Equation (4.1.1) adapted from Mustafah et al (2012) and Hsu and Wang (2016), we estimated the object distance and present the experimental results in Table 4.1.2. The results indicated that the distance measurement method proposed in Section 4.1.1.4 performed poorly. The most accurate measurement was where the actual distance was 2m and the calculated distance is underestimated at 1.985m. For actual distances greater than 2m, the predicted distance became exponentially larger. Measurement error fluctuated between 60% - 90% when the actual distance is within the 4m range, and 15% - 54% within the 3m range.

Table 4.1.2: Object distance measurements estimated from stereo-images and compared against actual distances.

Object ID	Actual Distance (m)	Estimated Distance (m)	Error (m)	Error (%)
1	3.117	3.618	0.501	16.062
	3.117	3.793	0.676	21.687
	4.258	6.223	1.965	46.155
	4.258	6.909	2.651	62.264
2	4.860	8.329	3.469	71.374
	4.860	8.335	3.475	71.504
3	3.087	4.401	1.314	42.551
	3.087	4.735	1.648	53.394
	4.002	7.453	3.451	86.232
	4.002	7.241	3.239	80.929
4	3.331	4.176	0.845	25.363
	3.331	4.314	0.983	29.525
	4.246	6.925	2.679	63.089
	4.246	7.075	2.829	66.625
5	2.000	1.985	-0.015	-0.764
	2.000	1.985	-0.015	-0.768
	2.900	3.312	0.412	14.219
	2.900	3.317	0.417	14.375

4.1.2.2 Object measurement

The relationship between λ_h, λ_w and disparity was shown by Mustafah et al. (2012) to be linear and inversely proportionate. However, we found that a logarithmic function

fit the data better in explaining the relationship between λ_h and λ_w against disparity. As mentioned in Section 4.1.1.1, λ_h and λ_w were calculated from initial object measurements and presented in a plot against disparity in Figure 4.1.4. A corresponding λ_h and λ_w is determined from the fitted logarithmic function and applied to Equations (4.1.4) and (4.1.5) to predict object height and width. We present the results in Table 4.1.3.

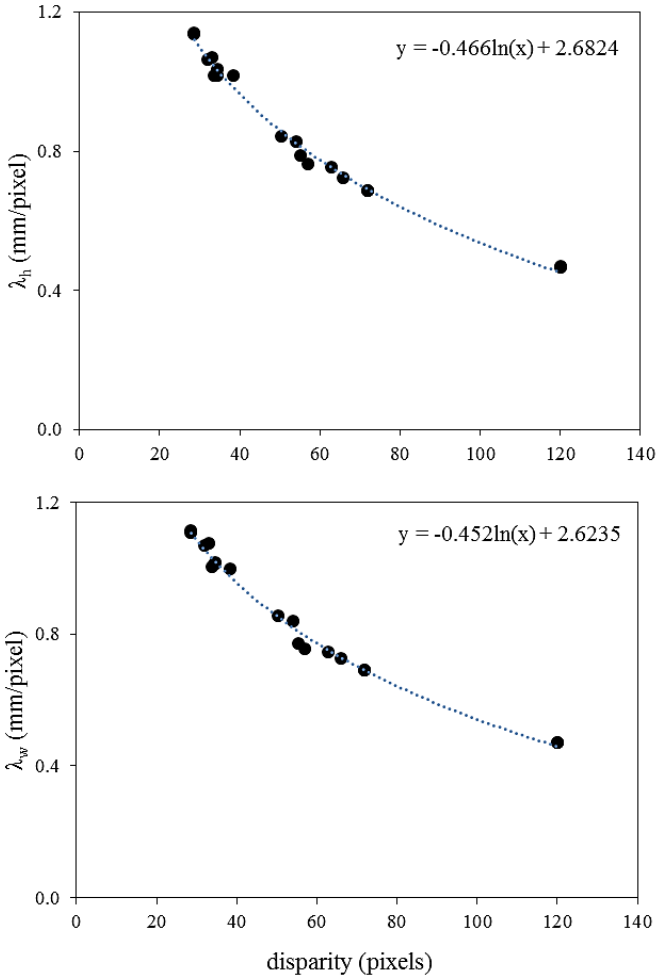

Figure 4.1.4: Plot of λ_h and λ_w against image disparity and fitted with a logarithmic equation.

Table 4.1.3: Object measurements estimated from stereo-images and compared against actual object measurements.

Object ID	Height			Width		
	Actual (mm)	Estimated (mm)	Error (mm)	Actual (mm)	Estimated (mm)	Error (mm)
1	1255.0	1266.35	11.35	2410.0	2419.24	9.24
		1252.41	-2.59		2423.72	13.72
		1211.62	-43.38		2357.13	-52.87
		1250.14	-4.86		2422.28	12.28
2	2074.0	2043.14	-30.86	889.0	888.02	-0.98
		2035.66	-38.34		883.68	-5.32
3	275.0	273.65	-1.35	518.0	504.18	-13.82
		279.48	4.48		515.44	-2.56
		276.41	1.41		511.64	-6.36
		270.72	-4.28		502.46	-15.54
4	1340.0	1401.60	61.60	497.0	522.62	25.62
		1381.72	41.72		521.49	24.49
		1359.99	19.99		502.88	5.88
		1375.95	35.95		512.02	15.02
5	800.0	771.16	-28.84	545.0	531.98	-13.02
		769.77	-30.23		532.08	-12.92
		802.85	2.85		544.77	-0.23
		802.80	2.80		544.80	-0.20

The object height and width results from the model appear to perform quite well with a precision of 6cm for height and 5cm for width. It should be noted that the model introduced is simply a reverse-engineered process that is inherently dependent on the initial true object measurements to find λ_h and λ_w. The parameters are also subjected to camera and setting specifications as they are the size represented by a pixel in object coordinate space.

4.1.3 Discussion

The model examined in this study requires a prior knowledge in target specific dimensions in order to estimate said target. In the application of the photogrammetric

method, its usefulness lies in the predictive capability to estimate unknown object dimensions. The methodology proposed by Mustafah et al (2012) calculates the parameters λ_h and λ_w based on true measurements of the object to estimate its size from the images. As such, there is no practicality in the proposed photogrammetric method and this disagrees with our objective of utilising stereo-vision to estimate unknown object dimensions. The application of spatial scale to the model is critical for accurate distance and volume estimates (Miller (2015)). At least two points in object space must be known. While Liang et al (2014b) suggests that a more efficient method is to use natural reference features in the stead of an external object, the reference target has to be well represented in the imagery for easy identification.

4.2 Object Mensuration at distances greater than 10m

The objective of this experimental study is to test the utility of stereo-camera object size and distance measurement against other methods such as a rangefinder over a larger range of depth.

4.2.1 Materials and Methods

The experimental study took place in the Edinburgh Oval of Curtin University in October 2015. A flow chart summarising the methodology used in this study is presented in Figure 4.2.1. In this section, we describe the procedures for data collection and processing.

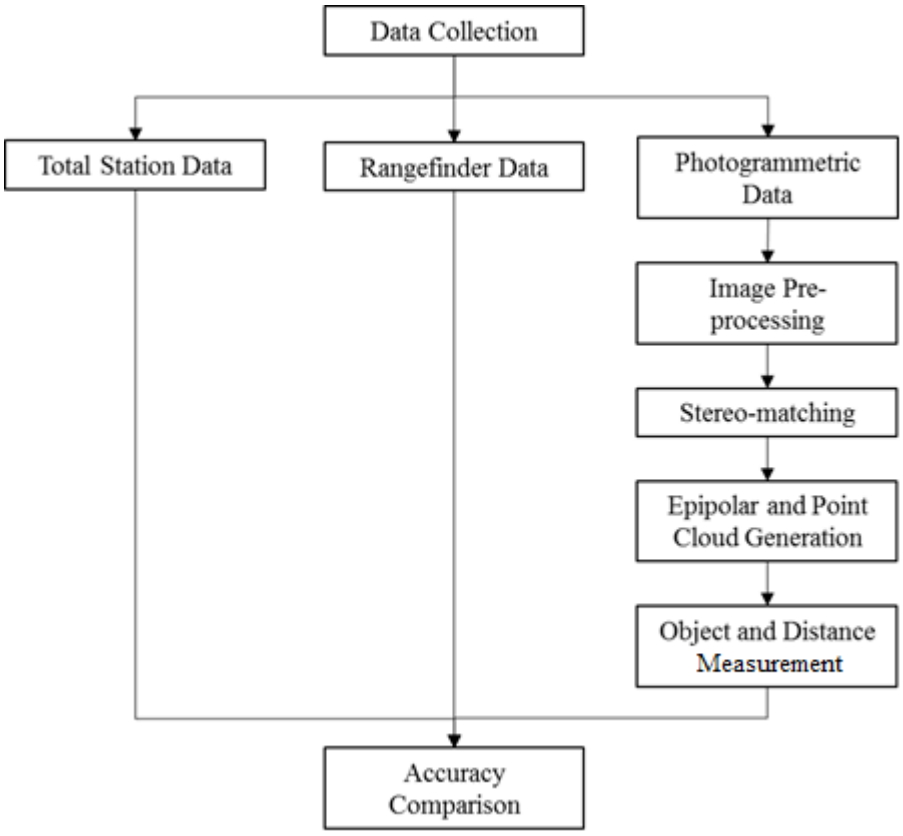

Figure 4.2.1: Flow chart of the process of data collection to object measurement and accuracy comparison.

4.2.1.1 Data collection

The target objects in this experimental study comprises of a rugby goalpost and a cross-shape construct. Two circular targets with a centroid point were fixed onto the vertical length of the cross to increase the amount of metric information for the analysis (see Figure 4.2.2). Since we are interested in how the stereo-camera performs against a rangefinder over a range of distances, it is therefore important that we can accurately measure the distance between the camera and the target. Both targets are set along the same plane where we assume that depth (y-axis) is zero. To achieve accuracy, a total station is used to measure out the perpendicular distance ranging from 10 – 100m in 5m increments from the target. Depth measure from the total station is accurate to 5mm. Each distance measurement were marked with pegs (19 pegs in total) and are key to depth comparison betweeen the stereo-camera and rangefinder methods.

The metric information for analysis is recorded in the following notation:

- GP1 and GP2 are lengths of 1m and 2m measured from the base GP0 and marked with tape along the left goalpost as presented in Figure 4.2.2. GP3 is determined as the vertical height from the base of the goalpost to the top of the horizontal bar. This was measured by the total station at 2.835m.
- GPW is the distance between the two goalposts or the length of the horizontal crossbar at 5.6m.
- CPH is the vertical length between the centroid points of each circular target represented by CPH_1 and CPH_2 in Figure 4.2.2 and was measured by tape at 1.615m.
- FCH and FCW are the vertical and horizontal lengths of the cross-shaped target, measured at 2.419m and 1.81m respectively.

Figure 4.2.2: Photogrammetric data captured at 10m.

The stereo images in this experimental study were captured with a consumer grade stereo FujiFilm FinePix REAL 3D W3 camera. The camera setting used in this study is 3584×2016 pixels resolution, and the corresponding pixel size is 1.72×2.29 µm. Two pairs of stereo-images were captured at each marker previously measured by the total station. At each marker position, GPS coordinates (longitude and latitude) were also recorded in a geotagged image as well as height metrics from the targets (GP1, GP2, GP3, CPH and FCH), depth distance, object base and top linear distance (d_1, d_2) and the incidence angle from the rangefinder.

Figure 4.2.3: Height and depth measurement using the 2-point height measurement method as shown by the external display of the rangefinder. The distance from the rangefinder to the base and top of the target is denoted by d_1 and d_2.

4.2.1.2 Stereo-matching and point cloud generation

Image pre-processing was performed as described in Section 4.1.1.2. We first perform RO to orient the cameras in 3D space. An in-house CSIRO measurement program was used to match image points on a stereo-pair of images for an initial assessment of the camera orientation. Each pair of stereo-points is accepted if the matching correlation is high (>0.9) and rejected if the correlation is low. Once a set of stereo-points have been matched, RO is carried out. Residuals were checked for each RO stereo-pair. If the residual value is too high, we add more stereo-points to the initial set and check for any changes in the matching correlation for each pair of stereo-points. The data file generated from the RO is then used to generate the epipolar images in which the epipolar lines of 2 projected points are parallel and horizontally aligned along the new image planes. Disparity is subsequently measured from the epipolar images using the ERDAS ER Mapper software. Another in-house software is used to match and generate 3D object space points and create a pointcloud illustrated by Figure 4.2.4.

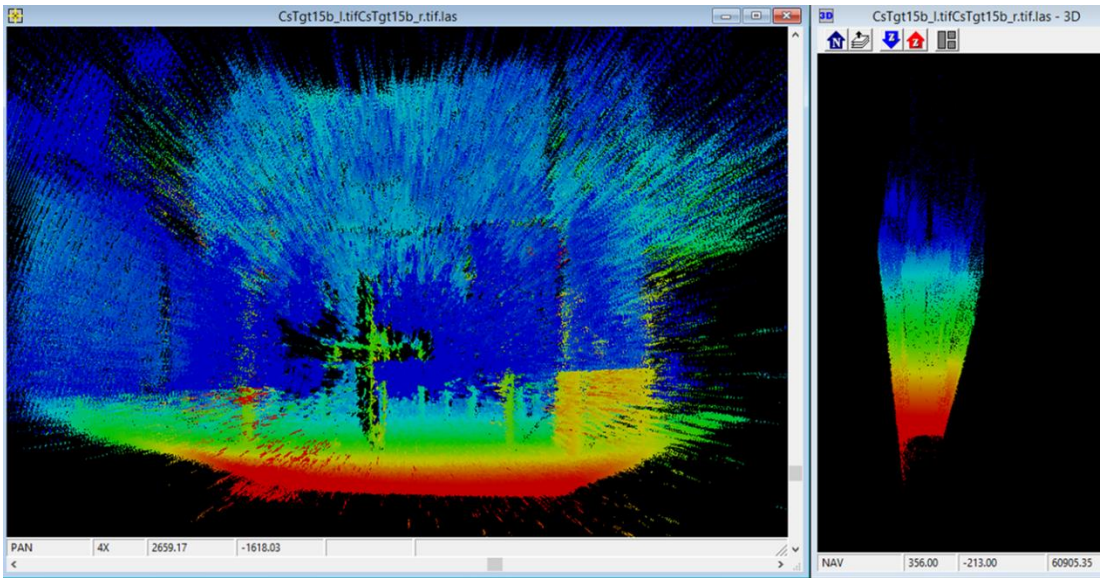

Figure 4.2.4: 3D point cloud from dataset.

4.2.2 Results

We present the object distance and size estimation from stereo-vision image capture, and compare our results with the actual widths and heights of the object interest in Section 4.2.1.1. We are unable to compare how well the stereo-image width measurements compare against the rangefinder method as it does not have the capability to measure horizontal lengths, and instead only analyses the vertical lengths of our targets.

From the left graph in Figure 4.2.5, we first compare the measured distances from the stereo-camera and rangefinder against the actual distance determined by the total station to 5mm accuracy. The Nikon Forestry 550 rangefinder is good in determining depth as observed by the strong agreement between actual distances and rangefinder prediction. There is very little differences between the methods unlike the stereo-camera method which is consistently underestimating depth. As the principal distance increases, the differences in depth estimation increases proportionately to the principal distance. Since the stereo-camera measured distance is determined from the generated point cloud (see Section 4.2.1.3) from initial pre-processed images and stereo-matching, we back calculate a theoretical set of object image heights (in pixels) from the pre-processed images and compare that dataset against our initial measurements.

The graph on the right in Figure 4.2.5 represents a plot of the predicted object image height against the measured object image height. We observe that the object image heights measured have been over-measured. This suggests that the image appears to distorted outwards, indicative of radial distortion (see Section 3.2.2.1.3). Initially, all pre-processing of the stereo-images were based on a single set of camera calibration. It is possible that our initial image correction was suitable for the principal distance from which it had been calibrated at, but is not sufficient to correct for all image distortion as the measuring distance increases, resulting in a disproportionate measurement of image pixel width and height from the remaining distortion. One solution to this problem is to calibrate the camera for its principal distance used in surveying work as suggested by some photogrammetry texts (Brown (1971), Hengl and Križan (1997), and Luhmann et al (2006, 2016)). However, in consideration of the diversity of target objects (trees) in our research and image processing flexibility, it may not be feasible to calibrate the camera for all principal distances and apply specific image correction parameters to their corresponding images. We can, on the other hand, use this experimental study as a basis for determining the level of estimation bias in object or distance mensuration with increasing principal distance from the initial calibrated camera parameters.

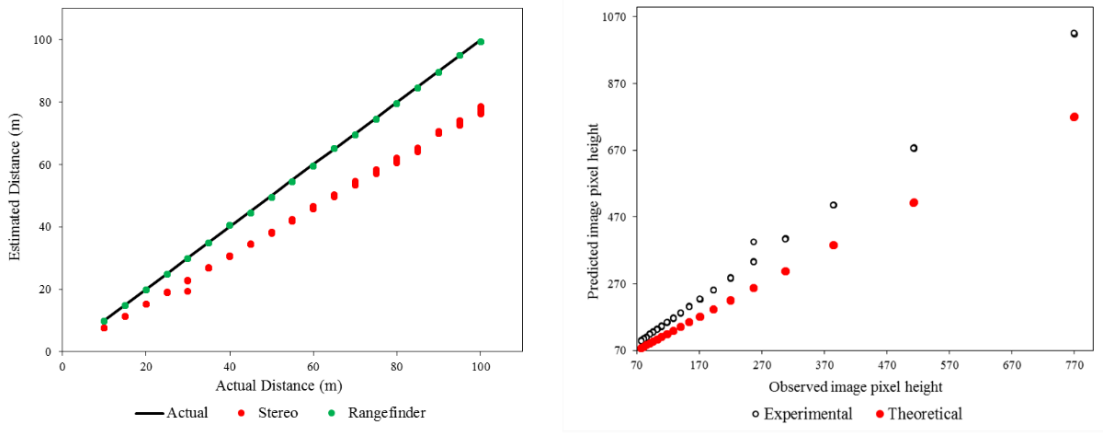

Figure 4.2.5: (left) Comparison of estimated distance against actual distance using the stereo-camera and rangefinder method, (right) Theoretical image object height against measured image object height.

Figure 4.2.6 represents the object width dataset (GPW and FCW) measured from stereo-images (red scatter points) and plotted against the actual object width.

Comparison with the rangefinder method was not conducted given that the rangefinder does not have the ability to measure horizontal lengths, and therefore no data was recorded for the analysis. We note that object width is generally underestimated using the stereo-camera method. The estimation errors are initially small for shorter distances but increases as the principal distance from the target increases. Mean error in the estimated width is 7.81cm (GPW) and 2.21cm (FCW) for stereo-images captured at less than 50m. The estimated width mean error tripled (21.8cm and 6.96cm) when we take the average of all width differences estimated from stereo-images captured after 50m. This phenomena is in agreement with our previous comparative analysis in distance measurement that the increasing error can be attributed to image distortion that have not been fully corrected for.

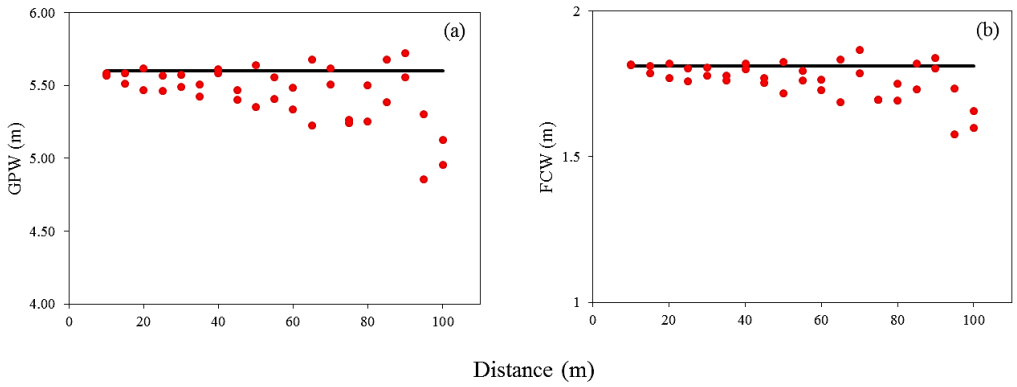

Figure 4.2.6: Comparison of estimated object width from stereo-camera against actual width over a range of distance.

Object height measurements from the stereo-camera method, rangefinder and actual height is presented in Figures 4.2.7. The graphs below represents the following measurements; (a) GP1 (b) GP2 (c) GP3 (d) CPH and (e) FCH. Green markers denote stereo-camera measurements while red markers denote rangefinder measurements. The actual heights are constant and represented by the linear line in the graphs. We observe that height estimates from the stereo-camera method runs fairly close to the actual height. In contrast, there is more variability in height estimates of the rangefinder method from the actual height. The mean errors between the stereo-camera method and actual data are smaller than the errors between the rangefinder method and actual data i.e. 9.57cm and 26.76cm (CPH), 2.14cm and

26.11cm (FCH), 2.2cm and 9.47cm (GP1), 3.73cm and 17.89cm (GP2), 7.13cm and 7.37cm (GP3).

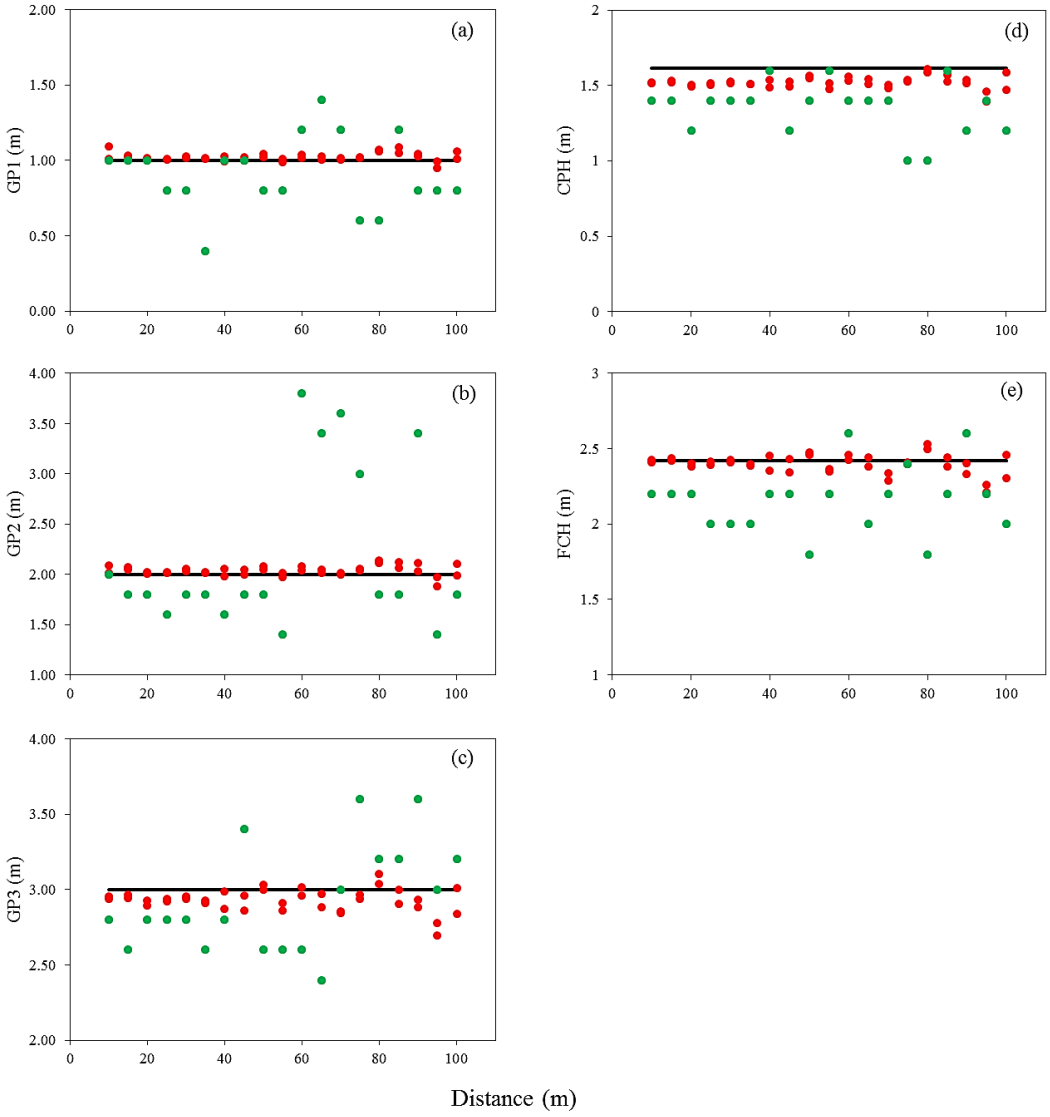

Figure 4.2.7: Comparison of estimated object height against actual height over a range of distance. Stereo-camera and rangefinder results are represented by red and green markers respectively.

Although rangefinders are easy to use and can measure both height and depth, there is inherently some error in their measurements. There are a number of factors introducing error including:

- Quality of the rangefinder.
- Target distance.
- Target characteristics.
- Pointing stability.

- Poor weather.
- Magnetic interference.

We observed the attributing factors of measurement error: target distance and pointing stability, frequently during the experimental study. ESRI (2016) gave an example that a compass degree error of 1° for a bearing measurement resulted in a horizontal error of 0.5m at a distance of 30m and 2.6m error at a distance of 150m. They also state that the difficulty in targeting small objects over large distances increases when the rangefinder is held in the operator's hand without any stabilizing support. Although the camera tripod was used as a stabilizer, measurement error still occurred. We present the distance measurements depth, d_1 and d_2 (see Figure 4.2.3) in Table 4.2.2. Given that most of the height measurements are quite small (less than 3m), d_1 and d_2 values should be approximately close to the measured depth. However, it is observed that there are many instances where d_1 and d_2 was under or overestimated, especially for GP1, GP2 and GP3 measurements (presented by the highlighted cells).

Table 4.2.2: d_1 and d_2 measurements from the rangefinder compared against depth when recording object height.

Depth	CPH		FCH		GP1		GP2		GP3	
	d_1	d_2	d_1	d_2	d_1	d_2	d_1	d_2	d_1	d_2
9.8	10	10	10	10	10	10.5	10.5	10.5	10	10
14.8	15	15	15	15	15	15	15.5	15.5	15	15
19.8	20	20	20	19	20	20.5	20.5	20	20	20
24.8	25	25	25	24.5	26	25	25	26	25	25
29.8	30.5	30.5	30	29	30	30	30.5	31.5	30	29.5
34.8	35	35.5	35	33	144.5	34	35.5	35	35.5	34
40.4	40.5	40.5	40	38	41	41	40	40	40.5	38.5
44.4	44.5	44.5	44.5	42.5	47	44.5	45	43.5	63.5	42.5
49.4	50	49.5	49	46.5	129.5	46	54.5	50	50	46.5
54.4	54.5	54	54.5	53.5	134.5	52	55.5	55.5	55.5	52
59.4	59.5	59.5	59.5	59.5	140	71	170.5	70	59.5	53.5
65	64	65	64.5	63	145	76.5	176.5	63	65	61
69.4	69.5	69.5	69.5	69.5	178.5	71	182	83	94.5	87.5
74.4	74.5	74.5	74.5	88	184	88	188	70.5	99.5	88
79.4	79.5	80	79.5	80	80.5	76.5	187.5	62	104	92.5
84.4	84.5	84.5	84.5	85.5	86.5	98.5	191.5	98	104.5	85.5
89.4	89.5	89.5	89.5	89.5	122.5	75	197	108.5	114.5	84.5
95	95	95	74.5	94.5	95.5	78	95	78	119.5	109
99.4	99.5	99.5	99.5	100.5	100.5	113	99.5	84.5	124	82

As seen from Figure 4.2.2, the measurement surface area for GP1, GP2 and GP3 is very small as compared to the measurement surface area for CPH and FCH. As such, when there is a slight instability in using the rangefinder, the projected laser

would have missed its mark and record a different point. In most cases, the measured point had a greater depth as compared to the true depth of the target (negative y-axis).

4.2.3 Discussion

Our results show that the stereo-camera method works quite well in estimating object size to acceptable accuracy within a limited measuring distance. There is an inclination for distance and some object dimensions to be underestimated as the principal distance between the camera and the target increases. Correcting stereo-images captured at different principal distance with a single set of calibration parameters is cause for the underestimation and overestimation error. It would not be feasible to calibrate the camera for all principal distances and apply specific image correction parameters to their corresponding images as we wish to maintain a level of flexibility in the methodology. However, the possibility of correcting for estimation bias from relating mensuration error to principal distance from initial calibrated camera parameters remains to be explored.

While the rangefinder works well in determining depth, it lacks mensuration flexibility. Stem diameters and canopy widths are essential factors in forestry applications. The inability to measure widths with the rangefinder increases the need for other mensuration equipment and time spent in field. Moreover, the degree of mensuration error is affected by the mensuration distance, pointing stability and size of the target object as discussed in Section 4.2.2. The stereo-camera method is cost and time efficient given that a majority of data extraction is carried out in the lab. Equipment requirements are also kept to a minimum and object size measures processed from the stereo-images are reasonably accurate. Therefore, we can consider the use of the consumer-grade stereo-camera as an alternative method in obtaining forestry data. We will address the performance of the stereo-camera against traditional dendrometry methods in Chapter 5. Dendrometric measurements such as tree height, stem diameter and crown diameter as well as aboveground biomass of the tree will be studied.

Chapter 5

Application in Complex Environments

This chapter examines 3 case studies where the methodology described in Chapters 3 and 4 is applied in more complex and uncontrolled environments. In Section 5.1, dendrometric measurements obtained from the photogrammetric method are compared against traditional dendrometry methods. This study was conducted in Kojonup, located south-east of Perth, WA. Tree height, canopy and stem diameter are measured using a hypsometer and diameter tape. These factors are essential in forest inventories and monitoring the ecosystem for sustainability and management planning. The results are presented in Section 5.1.2.

In Section 5.2, we apply the photogrammetric approach to determine metric information from shrubs and multi-stemmed trees in a case study conducted in Geraldton, located north of Perth. The dendrometric information obtained from the traditional method and the photogrammetric method is used to estimate the biomass from allometric models. This case study includes the harvest dataset from which allometric model parameters can be determined. The results are presented in Section 5.2.3.

In Section 5.3, the third case study was conducted in Williamsdale, Australian Capital Territory. Photogrammetric and harvest dataset were obtained. We estimated the aboveground biomass of the sampled trees using dendrometrics from the stereo-camera and traditional dendrometry methods. The actual measurements and biomass

is verified through destructive sampling. In contrast with the second case study, large matured paddock trees were studied in the case study rather than young trees and shrubs (< 15 years). The estimated dendrometric and biomass results are presented in Section 5.3.2.

5.1 Case Study: Kojonup

Historically, tree heights are measured as a means to quantify and monitor forest inventories (Avery and Burkhard (2011), Chave et al (2005) as well as characterizing the growth and movement of individual tree species and populations (Banin et al (2012), King and Clark (2011), and Larjavaara and Muller-Landau (2013)). It is more recently that these dendrometric measurements and indirectly, tree volumes, are used to determine carbon stocks via allometric relations between the trunk diameter, height and volume. However, traditional methods of obtaining these measurements are costly, laborious and not necessarily accurate to meet the requirements of today.

Accuracy of the data is a trade-off for the effort and complexity involved in obtaining the data. The most accurate way to measure a tree more than 10m high involves climbing to the top of the tree and doing a direct tape drop with a weight attached to the end. In most cases, the climber is unable to reach the top of the tree and require an extensible telescopic metric pole to calculate the remaining portion. This method requires experienced tree climbers with the relevant training and professional equipment in addition to being potentially dangerous and time intensive. Other methods of dendrometric measurements have been reviewed in Chapter 2. These include the trigonometric method through the use of a hypsometer, the geometric method, handheld calipers and diameter tape.

The following case study measures tree height, stem diameter at breast height (1.3m) and canopy diameter using three methods; traditional dendrometry using a diameter tape and hypsometer, terrestrial close-range photogrammetry using a consumer-grade digital stereo-camera, and aerial photogrammetry using digital surface models (DSM) generated from aerial stereo-images. The results obtained from each method are analysed and compared in Section 5.1.2.

5.1.1 Materials and Methods

5.1.1.1 Sites

The study was conducted in the agricultural area near the town of Kojonup, which is located 256km south-east of Perth, Western Australia. The study area covered 10 paddock fields located within 4 farms. Multispectral digital ortho-rectified models (DOM) and digital surface models (DSM) images covering each of the 4 farms were collected prior to the study in order to identify the samples to be surveyed. The altitude of the area ranges from 263m to 385m. The main tree species are Wandoo (*Eucalyptus wandoo*), York Gum (*Eucalyptus loxopleba*), Marri (*Corymbia calophylla*) and the South American peppercorn tree (*Schinus molle*).

5.1.1.2 Field Data

The field data was collected in fulfilment of 4 specifications:

(i) Each sample can be identified from the aerial imagery.

(ii) The sample must be distinct from the environment such that the canopies from two neightbouring trees must not intersect.

(iii) The sample must have a healthy canopy biomass.

(iv) The samples chosen must display a large variation in height.

In total, 47 trees were sampled. The image of each tree and its sample identification is presented in Appendix A. The trunk circumference is measured at an approximate height of 1.3m from the ground by a steel tape with a millimeter graduation. The diameter is calculated from the circumference by assuming that the cross-section of the trunk is circular and called diameter at breast height (DBH). DBH is one of the main attributes for forestry monitoring and allometric calculations. Spatial coordinates (longitude and latitude) were recorded with a GPS receiver in a phone through a geotagged image.

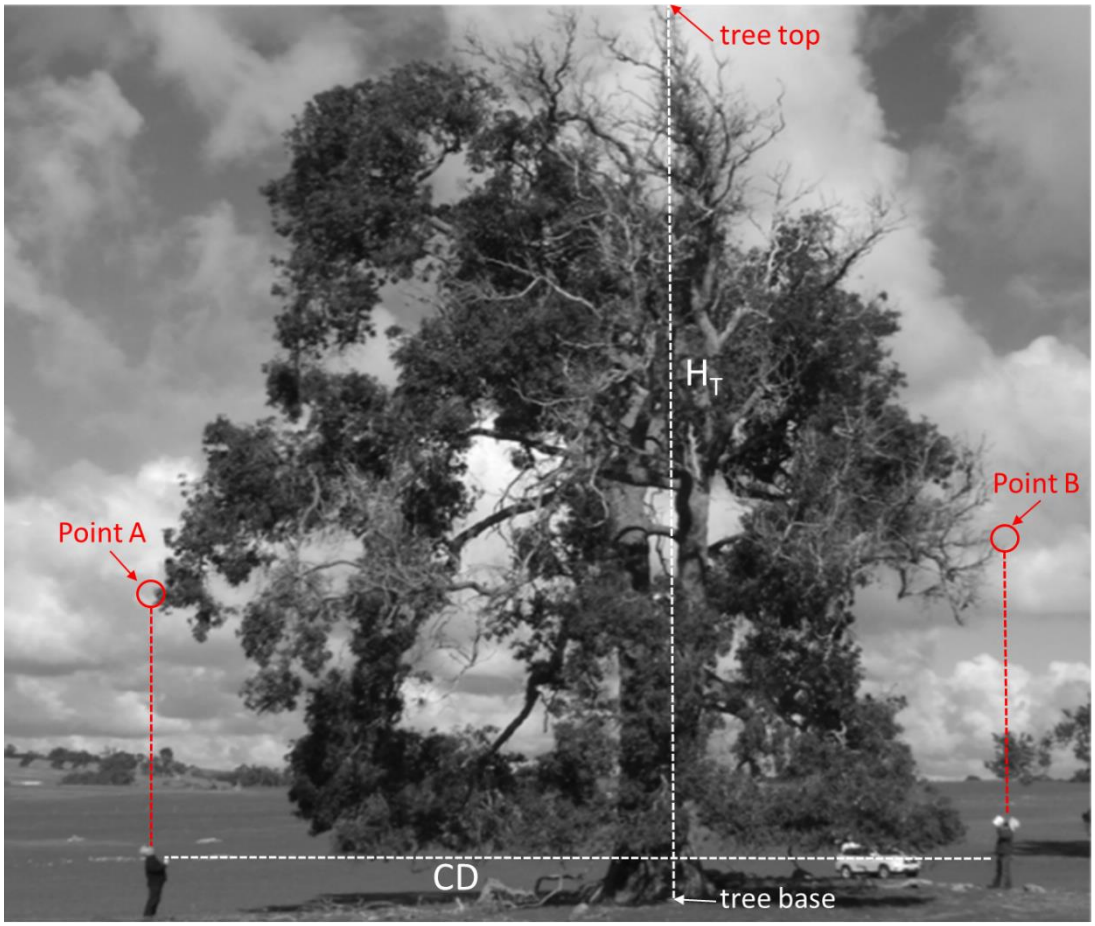

Figure 5.1.3: The estimation of canopy diameter (CD) from a rangefinder. Two operators position themselves under the endpoints of the canopy; points A and B. One operator uses the rangefinder to measure the distance between himself and the other person.

The sample is first inspected to identify the position where the canopy diameter (CD) is maximum. Once the maximum CD has been identified, two operators would position themselves directly under the endpoints A and B of the CD as seen in Figure 5.1.3. The operator at A points the rangefinder at the other operator at B and reads the distance from the rangefinder as the CD. The minimum CD is measured with the same approach only that both operators are positioned 90° clockwise or anticlockwise from their initial position. The measurement of the tree height is determined by capturing a point at the tree base (see Figure 5.1.3) and another point at the tree top with the rangefinder which then calculates the vertical height based on the linear distance and projection angle.

5.1.1.3 Photogrammetric Data

High resolution digital aerial images of the study area were captured by Landgate using a Leica ADS80 digital large format aerial camera 5300m above the ground outside Greater Perth region, Australia, in January 2010. The image data includes three-view panchromatic data for 3D surface reconstruction, and multispectral data (red, green, blue (RGB) and near infrared (NIR) bands) for ortho-rectification. Both panchromatic and multispectral data are at 50cm ground sampling distance (GSD). Figure 5.1.4 illustrates the digital aerial images for four farms: Murray, Plowman, Webb and Wilson.

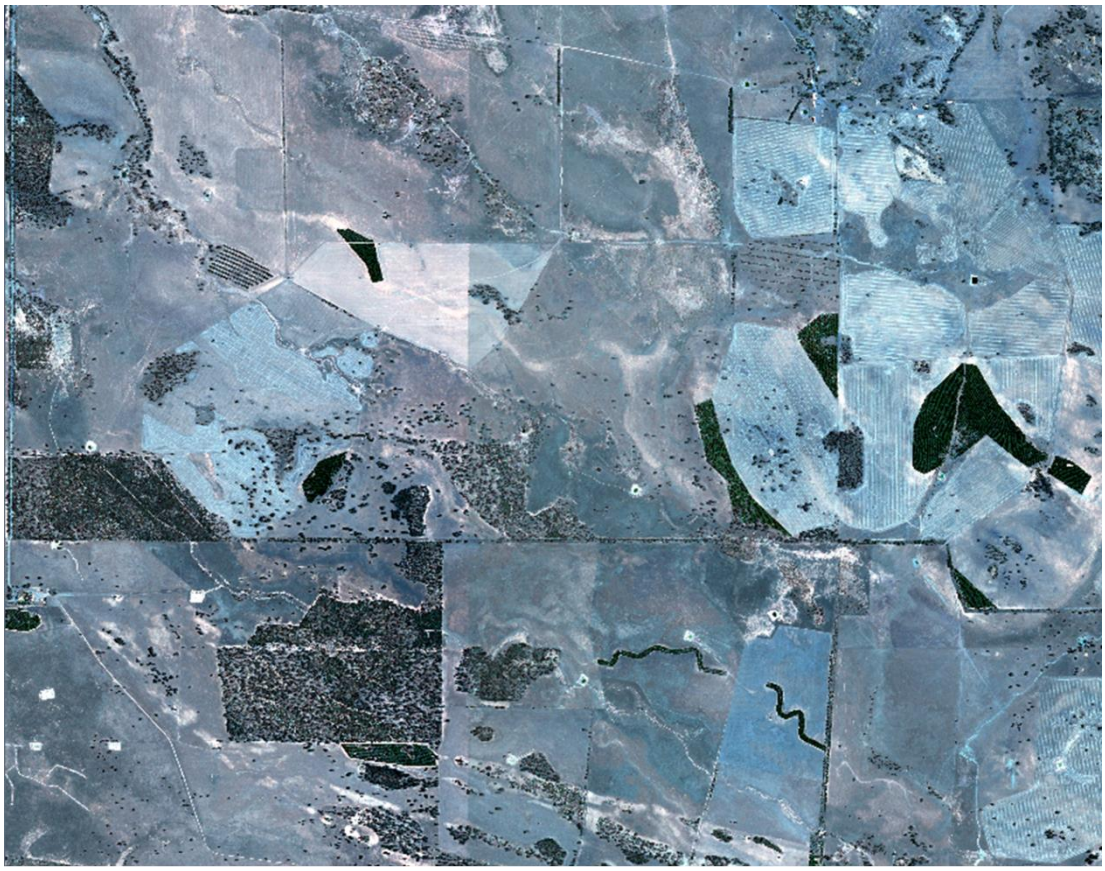

(a) Murray Paddock

(b) Plowman

(c) Webb

(d) Wilson

Figure 5.1.4: Digital ortho-image model of the four farms – (a) Murray, (b) Plowman, (c) Webb and (d) Wilson.

Terrestrial photogrammetric data was collected using a FujiFilm FinePix REAL 3D W3 consumer grade stereo-camera calibrated at 5m. Operational parameters were set to automatic mode with the largest frame size <16:9>. The frame size 3648×2736 pixels gives approximately 10 million image points. We maintain a fixed focal length for all images by not using any of the zoom functions in the camera. This makes it easier to model the associative distortions.

Not every tree has a single trunk stem at breast height (1.3m) and some will have trunks that diverge from the main trunk below 1.3m. When objects overlap one another under the optical rules of a linear perspective, more than one set of stereo-images is required to offset the lack of details due to occlusion. Therefore, the terrestrial photogrammetric data for each sample is collected in a series of stereo-image pairs depicting different perspectives of the target object. Figure 5.1.5 illustrates the photogrammetric network used when obtaining the photogrammetric data, whereas Figure 5.1.6 represents one such example of the multi-perspective data for the sample i.e. Sample T05.

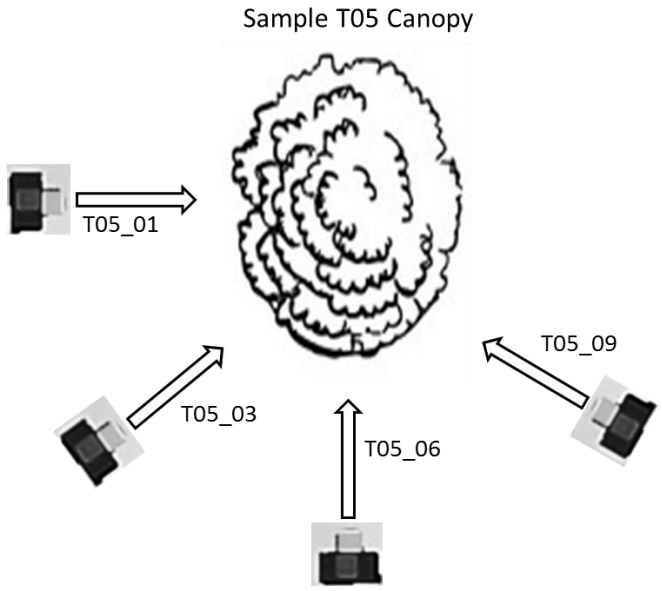

Figure 5.1.5: An example of the photogrammetric network for taking stereo-images of each sample. The stereo-images are labelled accordingly to the tree sample T05 i.e. T05_01, T05_03, T05_06 and T05_09.

(a) T05_01

(b) T05_03

(c) T05_06

(d) T05_09

Figure 5.1.6: A representation of the multi-perspective images captured from sample T05 from differing viewing angles as illustrated by the photogrammetric network in Figure 5.1.5. Starting at initial position (a), we move approximately 45° anti-clockwise to (b) and capture the image T05_03, then move another 45° and 90° anti-clockwise to capture the images T05_06 and T05_09 at (c) and (d) respectively.

Control points (CP) provide object space points in the image for which their relative location is known. This is a fundamental step to convert coordinates in the 2D image space into object coordinates in 3D object space. CP markers were employed in the form of a 0.55×0.55m square quadrat with the target points located at each end- and mid-point of the quadrat edges. With more than one known height and width measurement, the measurement error can be reduced according to Hengl and Križan (1997) and real-time scale against image data can be established.

5.1.1.4 Dendrometric measurements

Dendrometric measurements from the rangefinder and tape measure were recorded on site during the field survey. Image data from the stereo-camera, DSM and DOM had to be processed and analysed in the lab, before any dendrometric measurements can be extracted.

5.1.1.4.1 Terrestrial Photogrammetric Data from Stereo-camera

The left and right images from the stereo-camera FujiFilm FinePix REAL 3D W3 are extracted from the MPO file in JPEG format using third party software and converted to TIFF format. The TIFF images were calibrated and rectified for all intrinsic distortion with the calibration parameters in Table 5.1.1.

Table 5.1.1: Calibration parameters for FujiFilm FinePix REAL 3D W3.

Left Camera		Right Camera	
c	7.28666	c	7.27896
x_0	-0.31691	x_0	-0.11697
y_0	-0.12643	y_0	-0.07415
k_1	2.289E-03	k_1	2.039E-03
k_2	-6.458E-05	k_2	-2.834E-05
k_3	1.081E-06	k_3	1.360E-07
p_1	9.290E-04	p_1	1.312E-03
p_2	1.934E-04	p_2	-8.095E-05
b_1	1.163E-02	b_1	1.165E-02
b_2	-9.469E-04	b_2	-1.719E-04

This process eliminates any radial lens distortion and minimizes the errors that may arise during the measurement. The rectified images are then viewed in ERDAS ER Mapper, a powerful remote sensing software that allows users to visualise, enhance and combine images for easy and efficient data interpretation. Image segmentation is applied when the target object and its boundaries cannot be located from its environment. For example, we set some threshold boundaries for the RGB bandwidths to improve the contrast of the object against some environmental background such as grass and the sky.

The scale factor is calculated from the control frame with known dimensions (see Section 5.1.1.3) and using CP markers located in each image. H, CD and DBH are then estimated by converting image object dimensions (in pixels) to true measurements from the rectified images.

5.1.1.4.2 Dendrometric measurements from 2010 DSM and DOM

Digital aerial photographs of Greater Metropolitan Perth from 2010 have been processed photogrammetrically that included aerial triangulation by Landgate, DSM generation using CSIRO proprietary software and ortho-rectification from the derived DSM (Caccetta et al (2011)). The DSM and DOM raster vectors were viewed in ERDAS ER Mapper. The raster vectors contains ground distance information in its cell values and multispectral information RGB and NIR which have been assigned the corresponding bandwidths B1, B2, B3 and B4. Each sample

is located on the DSM and DOM from the GPS coordinates that were recorded in an EXIF image file captured during the field survey.

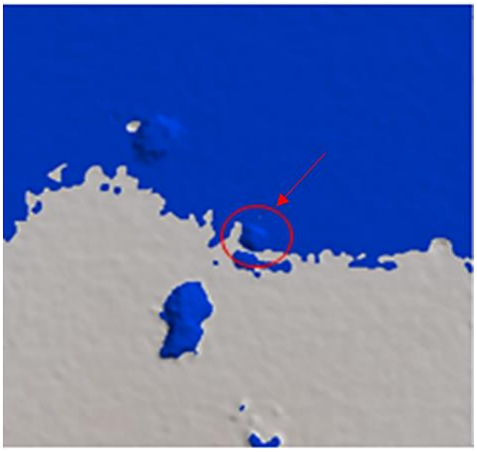

(a) DSM

(b) True colour DOM

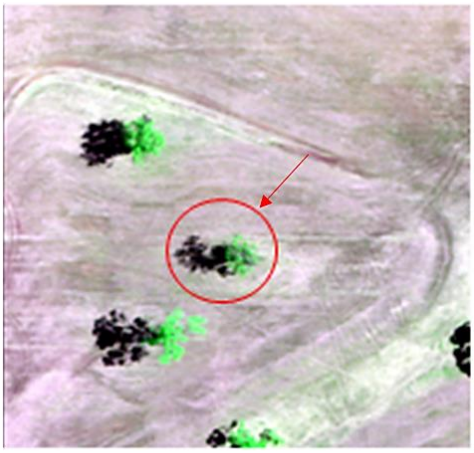

(c) DOM with adjusted bandwidths

Figure 5.1.7: The tree sample is located and marked on the DSM and DOM using GPS coordinates recorded during the field survey. Height is approximated from the DSM in (a). (b) is an example of the DOM in true colour where identifying tree canopy from its shadow is difficult. Reassigning bandwidth values to RGB results in (c) where the canopy is coloured in bright green, the shadow in black and the ground a pale red.

Maximum and minimum CD is measured from the DOM. In true colour (Figure 5.1.7(a)), it is hard to separate the canopy from underlying shadows by visual inspection. In order to improve the contrast between the tree canopy, shadow and ground, we reassigned the bandwidths of RGB to Red (B1), near Infrared (B4) and Green (B2). The resulting DOM in Figure 5.1.7(b) shows a clear separation between

the tree canopy and its shadow, making the process of measuring canopy diameter much simpler. The canopy is fitted into an ellipsoid where the maximum and minimum CD is measured as the major and minor lengths of the ellipsoid.

The DSM (Figure 5.1.7(c)) contains elevation values of the Earth's surface in the raster vector cell values. Tree height (H) is approximated by taking the difference of the highest cell value within the elevated contour of the tree (tree top) and outside the borders of the contour (tree base).

5.1.2 Results

We present the results for the dendrometric measurements (H, CD and DBH) made by the stereo-camera, rangefinder, tape measure, DSM and DOM. We also make a comparison on the performance and accuracy of these methods of measurement for field surveys.

5.1.2.1 Tree height

Individual tree heights for 47 samples measured in the field and lab from the stereo-camera (FujiFilm FinePix REAL 3D W3), rangefinder and DSM from 2010 are compared statistically against each other (see Table 5.1.2). The height of the tree is defined by Schreuder et al (1993) as the vertical distance from ground level to its uppermost point. In the case of leaning trees, measuring the length of the tree axis from ground level to its tip is a more appropriate choice given that an underestimation of standing volume will occur otherwise.

Mean height from the stereo-camera is 16.99m, comparative to the mean heights of 14.75m from the rangefinder and 10.88m from the DSM. It is predicted that the mean H for the stereo-camera could be higher with the inclusion of height values for T02, T03, T07 and T16. Standard deviation is approximately 4.5m, with higher results from the stereo-camera and DSM approach, indicating that there is a good variation of H in the sample. This satisfies one of the initial sampling requisites stated in Section 5.1.1.2.

Table 5.1.2: Tree heights (m) for 47 samples measured through the use of a stereo-camera (FujiFilm FinePix REAL 3D W3), a rangefinder and through the DSM raster vector.

TREE HEIGHT (m)						
Sample #	Mensuration Equipment Used			Difference between		
	Camera	Rangefinder	DSM (2010)	Camera & Rangefinder	Camera & DSM	Rangefinder & DSM
T01	17.311	14.5	12.315	2.811	4.996	2.185
T02	NA	11	4.933	NA	NA	6.067
T03	NA	14.8	4.338	NA	NA	10.462
T04	15.282	13.4	7.63	1.882	7.652	5.77
T05	13.307	10.2	5.738	3.107	7.569	4.462
T06	18.684	16.4	14.179	2.284	4.505	2.221
T07	NA	15.4	6.992	NA	NA	8.408
T08	20.310	17.4	11.842	2.910	8.468	5.558
T09	16.136	16.4	14.309	-0.264	1.827	2.091
T10	17.412	14	10.409	3.412	7.003	3.591
T11	13.715	10.2	11.961	3.515	1.754	-1.761
T12	12.779	12.6	15.368	0.179	-2.589	-2.768
T13	17.224	18	15.453	-0.776	1.771	2.547
T14	16.746	16.2	14.401	0.546	2.345	1.799
T15	12.974	9.4	16.208	3.574	-3.234	-6.808
T16	NA	5.8	NA	NA	NA	NA
T17	18.488	12.6	14.448	5.888	4.040	-1.848
T18	24.415	23	5.177	1.415	19.238	17.823
T19	20.325	17.6	7.796	2.725	12.529	9.804
T20	22.937	21.4	15.775	1.537	7.162	5.625
T21	19.264	17.2	7.353	2.064	11.911	9.847
T22	13.409	11.2	6.16	2.209	7.249	5.04
T23	22.141	20.6	15.344	1.541	6.797	5.256
T24	19.900	17.2	16.19	2.700	3.710	1.01
T25	20.054	17.6	17.873	2.454	2.181	-0.273
T26	18.597	17.4	11.022	1.197	7.575	6.378
T27	14.540	12.6	7.963	1.940	6.577	4.637
T28	17.861	18.6	15.982	-0.739	1.879	2.618
T29	14.068	14.6	8.004	-0.532	6.064	6.596
T30	16.411	13.8	12.178	2.611	4.233	1.622
T31	8.470	7.2	5.057	1.270	3.413	2.143
T32	18.430	16.8	8.714	1.630	9.716	8.086
T33	10.909	10.2	7.334	0.709	3.575	2.866
T34	9.334	9.2	4.718	0.134	4.616	4.482
T35	17.681	16.5	16.496	1.181	1.185	0.004
T36	35.338	26.6	24.902	8.738	10.436	1.698
T37	17.376	13.6	15.838	3.776	1.538	-2.238
T38	22.626	15.8	8.338	6.826	14.288	7.462
T39	21.193	18	18.055	3.193	3.138	-0.055
T40	13.586	10.4	5.527	3.186	8.059	4.873
T41	23.820	26	10.314	-2.180	13.506	15.686
T42	15.308	15.8	13.019	-0.492	2.289	2.781
T43	12.894	10.8	8.479	2.094	4.415	2.321
T44	12.266	11.4	9.399	0.866	2.867	2.001
T45	11.207	9.2	5.672	2.007	5.535	3.528
T46	14.144	13	7.737	1.144	6.407	5.263
T47	11.833	11.8	3.65	0.033	8.183	8.15
Mean Height	16.993	14.753	10.882	1.961	5.730	4.065
Standard Dev.	4.845	4.427	4.772	2.015	4.367	4.485

The absence of some H measurements from the stereo-camera is mainly attributed to the inability to place the control frame in the image in addition to the occlusion of image points from the image. Some of the reasons are as follow:

(i) The sample T16 in Figure 5.1.8 has a full foliage that grew out close to the base of the tree. The control frame was not placed in the image because the foliage would have obscured most parts of the frame from any viewing angle. In addition, the foliage occluded the tree base and stem diameter at breast height from sight and prevented the reading of the target's image points. Without the scale factor or target image points, tree height cannot be calculated.

(ii) Occlusion of image points occur predominantly from large pieces of dead wood or debris around the base of the tree. Since tree base coordinates cannot be accurately measured, tree height is therefore not calculated.

(iii) Because the control frame was not designed to stand independently, uneven terrain made it difficult to put the control frame in a secure position and had to be excluded from the image.

Figure 5.1.8: An example of T16 where height is not measured. The control frame was not placed in the image as the foliage grew too close to the ground and would obscure the frame, preventing the reading of the CP markers.

From the DSM, H could not be read for T16 as seen in Table 5.1.2. It is likely that this sample fall within the omission error stated by Hingee (2013) when he generated ground elevation models (GEM) from the same DSM dataset. The omission error can stem from the DSM generation processes such as stereo-matching issues in or near trees, smoothed object edges or errors from moving vehicles. Because CD of the same sample can be measured from the DOM as shown in Table 5.1.3, this proves that the tree was not omitted from the DSM due to unaccounted tree growth within the time difference in terrestrial and aerial photogrammetric data i.e. the tree was a sapling or too small to be detected when aerial photogrammetric data was captured in 2010.

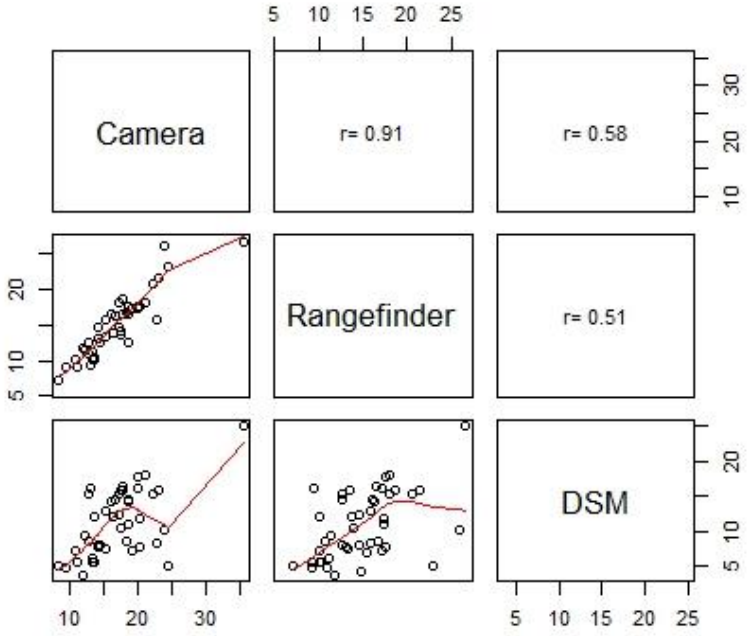

Figure 5.1.9: A 3×3 plot matrix with the lower triangle as pairwise plots for H_T values between methods and the correlation between methods in the upper triangle.

We plot the H values of each method in a 3×3 scatterplot matrix to determine if there is a linear correlation between methods (see Figure 5.1.9). The methods (stereo-camera, rangefinder and DSM) are written in the diagonal from top left to bottom right, corresponding to the $(i,j)^{th}$ entry. The lower triangle of the plot matrix contains individual scatterplots of H values for the following pairs while the upper triangle is the corresponding correlation value between methods:

(i) Stereo-camera and rangefinder.

(ii) Stereo-camera and DSM.

(iii) Rangefinder and DSM.

There is a strong correlation (r = 0.91) between the results from the stereo-camera and the rangefinder and moderately strong between the pairs stereo-camera and DSM (r = 0.58), and rangefinder and DSM (r = 0.51). This can be seen by the non-linear fitted regression line of the plots in the 3rd row of Figure 5.1.9.

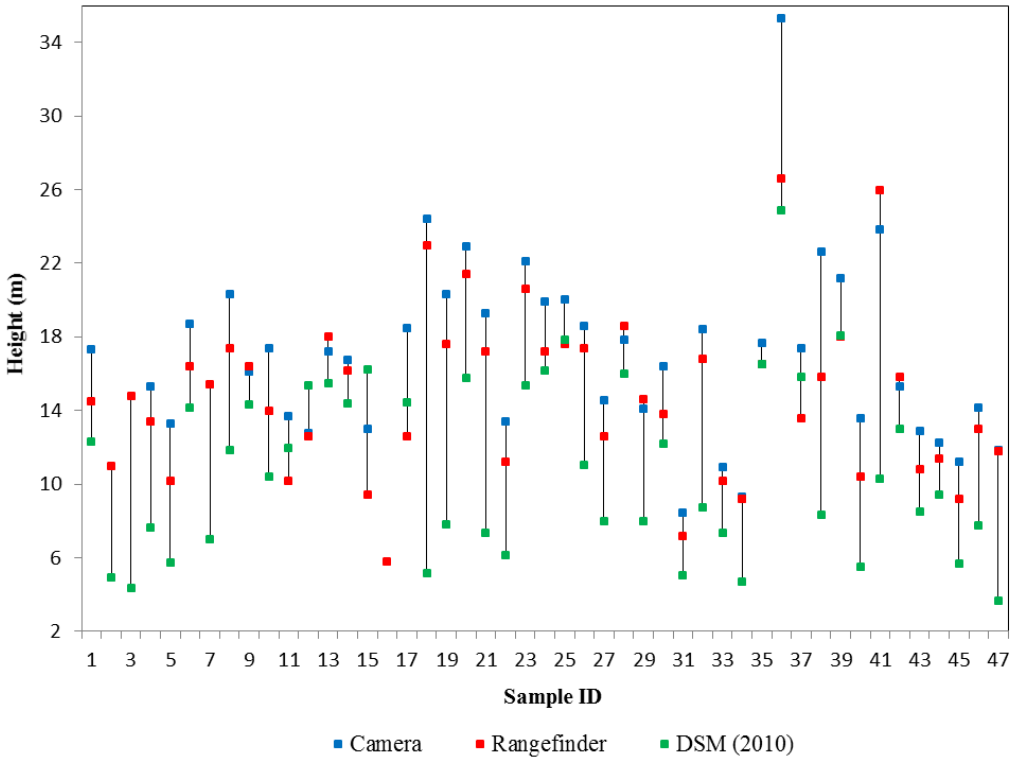

Figure 5.1.10: An illustrative comparison of H values between the stereo-camera, rangefinder and DSM (2010).

One shortcoming of using the rangefinder is that the height is measured from shooting straight up from the base. When dealing with trees that lean, there is a chance that the highest point recorded for height determination is not the highest point of the tree. Leaning trees is a source for errors in height estimation when using a rangefinder (sine or tangent method). Forestry inventories perceive true tree height to be the length of the tree axis from its base to its tip (Bragg (2007), and Schreuder et al (1993)) for trees that lean. As with any measurement, operator error is a common occurrence. This is especially so in the case of mistaken identity where the highest point of one tree is perceived as another. Figure 5.1.11 presents some examples of underestimating H when the point identified as the highest point

(illustrated by the circle) is not actually the highest point (identified by the arrow) of the tree. The figure also presents the samples (T10, T36, T38 and T40) where some of the largest differences in H were observed between the stereo-camera and rangefinder from Figure 5.1.10.

(a) T10 (b) T36

(c) T38 (d) T40

Figure 5.1.11: Examples of how the rangefinder can record a tree top point that is not the real highest point of the tree.

It should be pointed out that the rangefinder not only produces two major sources of errors: offset between measured distance and crown-top position and tree-top occlusion, it can also underestimate the distance between the observer and the tree of interest in the presence of dense understory vegetation or intervening obstacles (Hunter et al (2013)) i.e. leaves, branches or dead wood debris.

5.1.2.2 Canopy diameter

Individual canopy diameters (CD) for 47 samples measured in the field and lab from the rangefinder and DOM from 2010 are compared statistically against each other

(see Table 5.1.2). CD measurements consist of the maximum CD (representing maximum foliage spread) and the diameter perpendicular to the longest CD (minimum CD). Crown area can be calculated from these two measurements (Hulet et al (2014)). Figure 5.1.12 and 5.1.13 represent the maximum and minimum CD measures from the rangefinder (red marker) and DOM (green marker) and their differences.

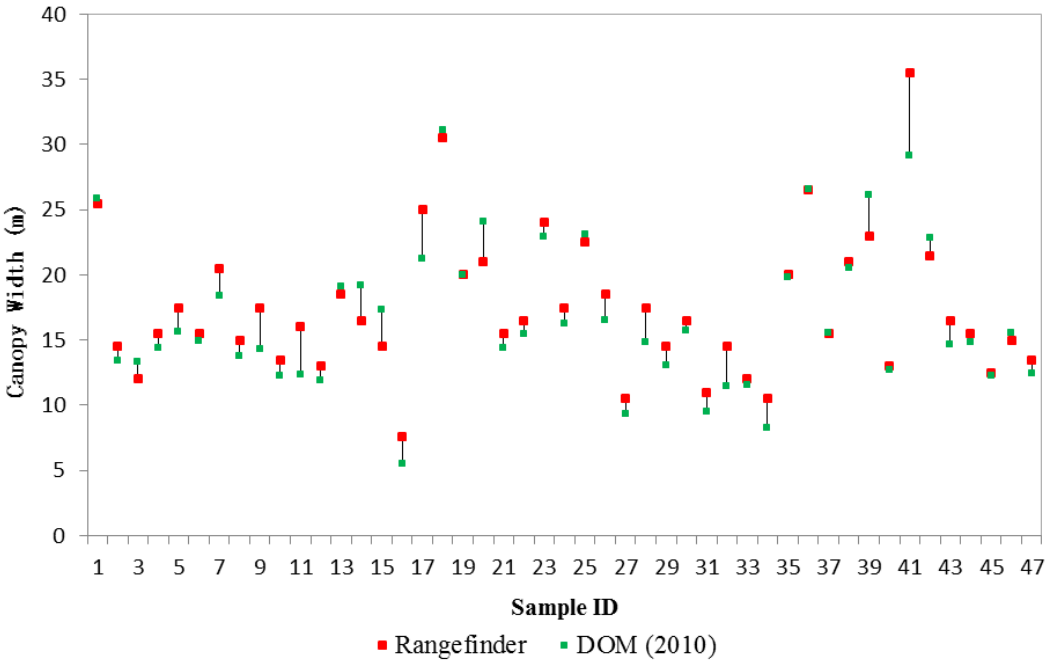

Figure 5.1.12: Comparison of maximum CD between rangefinder and adjusted DOM.

Maximum CD estimates obtained from the adjusted DOM generally fall below estimates from the rangefinder. The largest differences in maximum CD range between 3 – 6m (see Figure 5.1.12). We expect the DOM measurements to be underestimated given that CD measurements were estimated from 2010 data. However, there were some outliers in samples T14, T15, T20, T39 and T42 where estimates from the DOM is at least 1m greater than rangefinder estimates. We hypothesize that the error came from misidentifying the locations at which crown diameter is maximum, resulting in an underestimation of CD from the rangefinder. It is likely that most, if not all, CD measurements from the rangefinder will lie above DOM estimates when the maximum crown width has been correctly identified in the field survey.

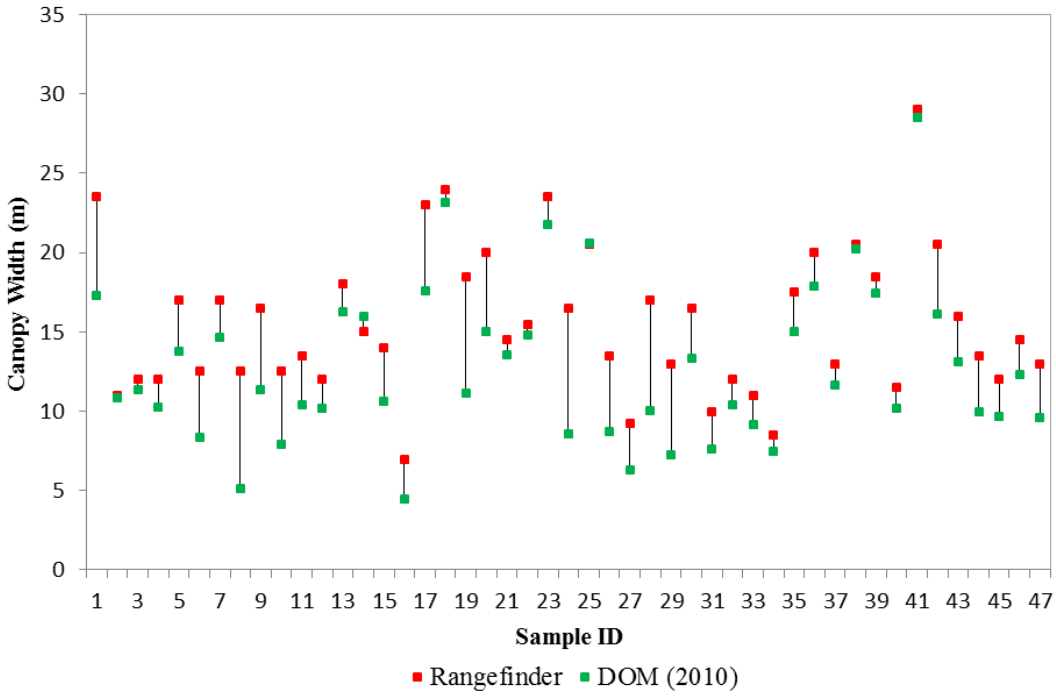

Figure 5.1.13: Comparison of minimum CD between rangefinder and DSM.

On the other hand, minimum CD estimates from the adjusted DOM is consistently below rangefinder measures with the largest differences between 4 – 7.4m (see Figure 5.1.13). This is within the expectation that there was some crown growth from 2010 to 2013. We observe that large differences between minimum CD measurements from the rangefinder and DOM appear more frequently as opposed to maximum CD values. This is further proven in Table 5.1.3 when comparing the count rate of diameter differences more than 15%. Such instances for maximum CD appeared 10 times as opposed to 27 times for minimum CD.

Table 5.1.3: Canopy diameter (m) for 47 samples measured through the use of a rangefinder and from the DOM raster vector.

CANOPY (m)						
Sample #	Maximum			Minimum		
	Rangefinder	DSM	Error (%)	Rangefinder	DSM	Error (%)
T01	25.5	25.87	1.45%	23.5	17.3	-26.38%
T02	14.5	13.46	-7.17%	11	10.87	-1.18%
T03	12	13.32	11.00%	12	11.38	-5.17%
T04	15.5	14.4	-7.10%	12	10.26	-14.50%
T05	17.5	15.66	-10.51%	17	13.78	-18.94%
T06	15.5	14.89	-3.94%	12.5	8.37	-33.04%
T07	20.5	18.42	-10.15%	17	14.63	-13.94%
T08	15	13.8	-8.00%	12.5	5.13	-58.96%
T09	17.5	14.34	-18.06%	16.5	11.33	-31.33%
T10	13.5	12.26	-9.19%	12.5	7.95	-36.40%
T11	16	12.31	-23.06%	13.5	10.39	-23.04%
T12	13	11.9	-8.46%	12	10.16	-15.33%
T13	18.5	19.09	3.19%	18	16.31	-9.39%
T14	16.5	19.23	16.55%	15	15.98	6.53%
T15	14.5	17.34	19.59%	14	10.65	-23.93%
T16	7.6	5.53	-27.24%	6.95	4.44	-36.12%
T17	25	21.24	-15.04%	23	17.62	-23.39%
T18	30.5	31.1	1.97%	24	23.14	-3.58%
T19	20	19.97	-0.15%	18.5	11.11	-39.95%
T20	21	24.07	14.62%	20	15	-25.00%
T21	15.5	14.4	-7.10%	14.5	13.55	-6.55%
T22	16.5	15.47	-6.24%	15.5	14.82	-4.39%
T23	24	22.9	-4.58%	23.5	21.79	-7.28%
T24	17.5	16.22	-7.31%	16.5	8.59	-47.94%
T25	22.5	23.1	2.67%	20.5	20.6	0.49%
T26	18.5	16.54	-10.59%	13.5	8.76	-35.11%
T27	10.5	9.29	-11.52%	9.2	6.34	-31.09%
T28	17.5	14.82	-15.31%	17	10.02	-41.06%
T29	14.5	13.1	-9.66%	13	7.27	-44.08%
T30	16.5	15.77	-4.42%	16.5	13.34	-19.15%
T31	11	9.51	-13.55%	10	7.63	-23.70%
T32	14.5	11.44	-21.10%	12	10.38	-13.50%
T33	12	11.52	-4.00%	11	9.19	-16.45%
T34	10.5	8.3	-20.95%	8.5	7.51	-11.65%
T35	20	19.82	-0.90%	17.5	15.03	-14.11%
T36	26.5	26.53	0.11%	20	17.9	-10.50%
T37	15.5	15.54	0.26%	13	11.66	-10.31%
T38	21	20.56	-2.10%	20.5	20.22	-1.37%
T39	23	26.12	13.57%	18.5	17.42	-5.84%
T40	13	12.7	-2.31%	11.5	10.16	-11.65%
T41	35.5	29.12	-17.97%	29	28.51	-1.69%
T42	21.5	22.81	6.09%	20.5	16.13	-21.32%
T43	16.5	14.64	-11.27%	16	13.14	-17.88%
T44	15.5	14.82	-4.39%	13.5	9.96	-26.22%
T45	12.5	12.29	-1.68%	12	9.69	-19.25%
T46	15	15.52	3.47%	14.5	12.32	-15.03%
T47	13.5	12.42	-8.00%	13	9.58	-26.31%

5.1.2.3 Stem diameters at breast height

Stem diameters measured at breast height have been separated into two sets of results; one examines the accuracy of measurements from trees with a single trunk at 1.3m (single stem trees) while the other looks at trees with more than one trunk at 1.3m (multi-stem trees). We apply the analysis to the results from the stereo-camera and tape measure given that DBH cannot be inferred from aerial photogrammetric data.

Of the 47 samples, 39 are single stem trees. From Figure 5.1.14, the majority of DBH measurements from both stereo-camera and tape measure are comparatively close.

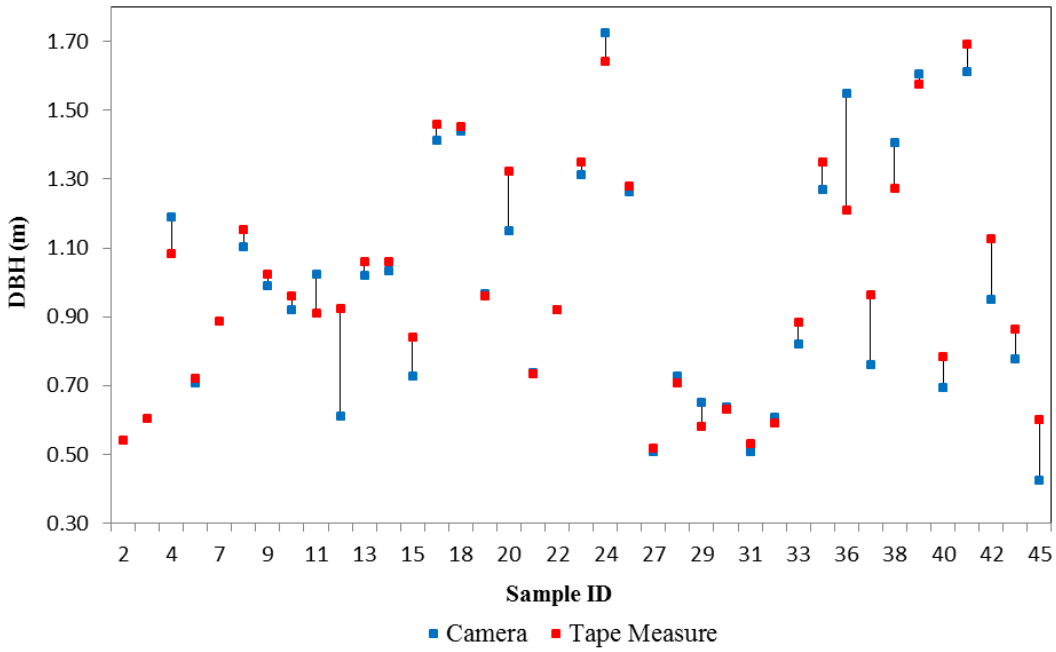

Figure 5.1.14: A comparison of DBH for single stem trunk at 1.3m between the stereo-camera and tape measure.

Amongst the samples with large differences in DBH (highlighted in Table 5.1.4), samples T12 and T36 have an error of approximately 30cm (28 – 33%) from Table 5.3. According to Chave et al (2004), a tree of diameter 30cm has a typical error of 0.27cm (95% confidence). Since our minimum DBH from the study is at least 50cm, the DBH errors between the stereo-camera and tape measure measurements are considered within the acceptable range. It should also be pointed out that DBH from tape measures is calculated by dividing the trunk circumference by π, by assuming

that the cross-section of the trunk is circular. This measurement is an error in the case where the cross-section of the trunk is not circular. We can also attribute the difference in measurements between the two methods to the viewing angle of the captured image for a non-circular trunk if measurement is made at the widest or narrowest section of the trunk. Weaver et al (2015) found significant differences in diameters measured using a diameter tape and calipers. It is commonly accepted that diameter tape measurements will more likely lead to different results than caliper or sector-fork measurements, due to variations in tree bole and bark shape (Weaver et al (2015), McArdle (1928)).

Table 5.1.4: DBH (m) for trees with a single trunk at 1.3m measured with a tape measure and from a stereo-camera (FujiFilm FinePix REAL 3D W3).

Single Stem DBH (m)			
Sample #	Camera	Tape Measure	Error (%)
T02	NA	0.543	-
T03	NA	0.606	-
T04	1.19	1.085	9.68%
T06	0.708	0.721	-1.80%
T07	NA	0.887	-
T08	1.104	1.154	-4.33%
T09	0.990	1.024	-3.37%
T10	0.920	0.961	-4.25%
T11	1.022	0.912	12.08%
T12	0.611	0.924	-33.91%
T13	1.019	1.059	-3.81%
T14	1.034	1.061	-2.54%
T15	0.728	0.839	-13.25%
T17	1.411	1.459	-3.29%
T18	1.439	1.453	-0.99%
T19	0.966	0.962	0.43%
T20	1.150	1.323	-13.09%
T21	0.739	0.733	0.82%
T22	0.920	0.922	-0.19%
T23	1.314	1.348	-2.55%
T24	1.726	1.641	5.18%
T25	1.262	1.281	-1.47%
T27	0.508	0.517	-1.69%
T28	0.728	0.706	3.11%
T29	0.650	0.58	12.08%
T30	0.639	0.632	1.10%
T31	0.507	0.53	-4.43%
T32	0.608	0.591	2.95%
T33	0.820	0.885	-7.40%
T35	1.270	1.351	-5.98%
T36	1.550	1.211	28.01%
T37	0.761	0.964	-21.03%
T38	1.405	1.273	10.35%
T39	1.606	1.575	1.99%
T40	0.695	0.785	-11.45%
T41	1.613	1.692	-4.66%
T42	0.952	1.126	-15.48%
T43	0.778	0.863	-9.84%
T45	0.424	0.6	-29.33%

There are 8 cases of multi-stemmed trees in the Kojonup study. There is increased complexity in measuring DBH for multi-stemmed trees due to occlusion occurrences

as mentioned in Section 5.1.1.3. This necessitates capturing multiple images of the tree sample from different viewing angles in order to identify all trunks at breast height from the base of the trunk. Multi-stem DBH measurements are presented in Table 5.1.5 and Figure 5.1.15.

DBH was not measured for sample T16 due to occlusion as seen in Figure 5.1.8. Difficulties were faced in identifying and measuring the trunks for T46 and T47. Overcast skies during time of data collection created low light levels and resulted in image underexposure for samples T37 – T47 i.e. darker images.

Table 5.1.5: DBH (m) for multi-stemmed trees at 1.3m measured with a tape measure and from a stereo-camera (FujiFilm FinePix REAL 3D W3).

Multi-stem DBH (m)			
Sample #	Branch #	Camera	Tape Measure
T01	1	0.552	0.524
	2	0.448	0.477
	3	0.447	0.454
	4	0.439	0.443
	5	0.373	0.369
T05	1	0.491	0.735
	2	0.475	0.643
	3	0.291	0.384
T16	1	NA	0.344
	2	NA	0.143
	3	NA	0.088
T26	1	0.548	0.544
	2	0.441	0.46
	3	0.439	0.335
T34	1	0.337	0.365
	2	0.319	0.346
	3	0.254	0.265
T44	1	0.761	0.713
	2	0.526	0.531
T46	1	NA	0.732
	2	NA	0.61
	3	NA	0.504
T47	1	NA	0.606
	2	NA	0.427
	3	NA	0.232

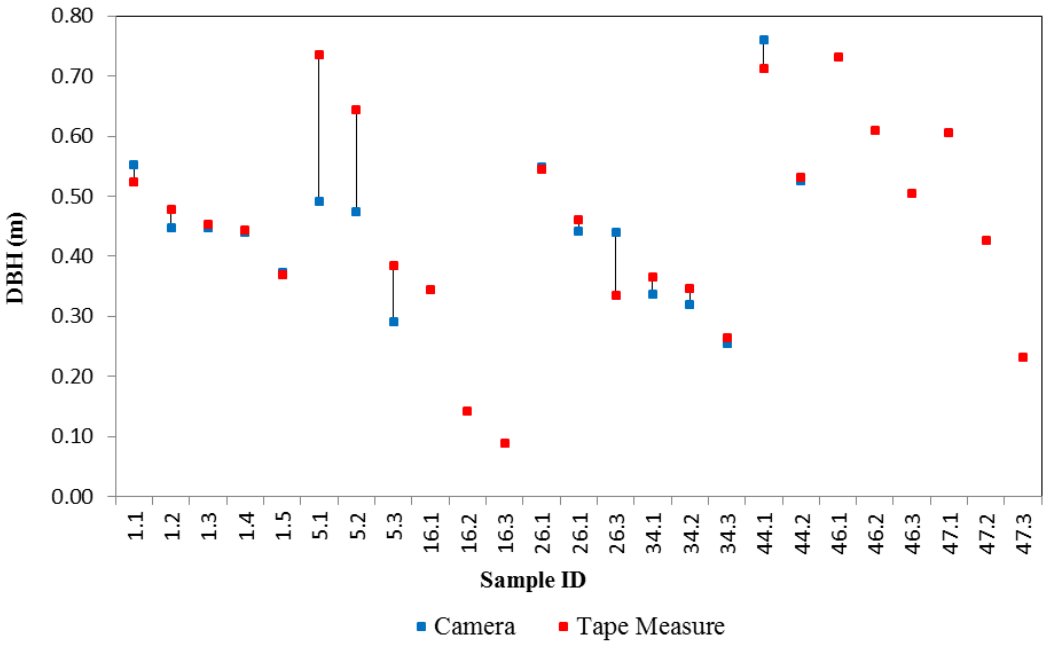

Figure 5.1.15: DBH for multi-stem trunks at 1.3m.

Sample ID in Figure 5.1.15 is read in the form “tree ID” and “trunk number corresponding to tree ID” separated by a decimal. Maximum error from T05 registers as 24cm and 16cm respectively. Since the average trunk diameter is 45cm, this error falls within the acceptable range. DBH measurements from the stereo-camera, excepting cases where DBH cannot be obtained, is comparable to the measurements calculated from the tape measure.

5.1.3 Discussion

The results show that the methodology used in this research can be effectively used to estimate H, DBH and CD to satisfactory accuracy. The method works well in measuring DBH from single stem trees at breast height from a single image. Multiple images captured at different positions are required when taking stereo-images for a multi-stem trunk. This is to account for any part that will be obscured from one perspective. The lower figures of tree height and canopy width obtained from aerial images is explained by the tree growth within the time difference between the DSM scans and actual data collection for the stereo-camera and rangefinder. DBH of a tree cannot be measured from aerial photography but can be measured through terrestrial based photogrammetry using stereo-cameras. Results from the stereo-camera are

comparative to using a rangefinder or DSMs generated from aerial photographs, and can be considered as a cost and time effective alternative in obtaining data for forestry applications.

Weather conditions were observed to have a large effect on the quality of the image and the ability to distinguish tree characteristics. Overcast skies results in underexposed images (more shadows and darker images) that affects the identification of tree characteristics through loss of shadow detail i.e. foliage from stem, stem from stem, foliage from background and stem from background. Wet weather can cause water droplets on the camera lenses during image acquisition and affect the overall quality of the image.

However, in order to make a meaningful comparison between the accuracy of dendrometric measurements between a rangefinder and a stereo-camera, it is necessary that true tree height can be accurately measured. This is difficult with larger trees unless intensive forestry surveys are undertaken.

With relative accurate measures of tree height and DBH, tree biomass can be estimated from allometric equations. The next case study in Section 5.2 includes destructive sampling to obtain harvest dataset. We apply the photogrammetric approach to measure tree height and DBH against more hands-on methods and compare both results.

5.2 Case Study: Geraldton

In this section, we will examine the accuracy of dendrometric measurements for small–medium trees (less than 10m) from a consumer-grade stereo-camera and a pair of DSLR cameras against traditional methods using a height stick and calliper. The dendrometrics obtained from each method is used to predict AGB which is subsequently assessed with the actual biomass of the sample harvested in the field. The results in Section 5.2.3 indicate that the photogrammetric method works well in predicting tree height but has limitations in identifying stems and measuring their diameter from trees/shrubs with a high density of basal stems at breast height. This affects the effectiveness of the allometric model in predicting AGB. The conclusions drawn from the biomass estimated by each method disagree in the allometric model which performs better in estimating AGB.

5.2.1 Materials and Methods

5.2.1.1 Sites

The study was conducted in a restoration plantation managed by the Auscarbon Group in 2013. The plantation, Tomora is located near Geraldton, a coastal city in the mid-west region of Western Australia, 424km north of Perth. It is a part of Auscarbon's "Environmental Plantings" project with over 40 specimens of trees and shrubs planted in variable mixtures using 2 ways: direct seeding where seed form a range of species is tilled into the ground and hand planting where a smaller range of species was manually planted as small seedlings. The main species in the plantation are York Gum (*Eucalyptus loxophleba*), Mallee (*Eucalyptus horistes*), Jam (*Acacia acuminata*), Tan Wattle (*Acacia hemiteles*), Salt Bush (*Atriplex*), Poverty Bush (*Eremophila*) and a few others. However, the harvest dataset in this study only comprises of 4 tree species. They are

- Mallee *(Eucalyptus horistes).*
- York Gum *(Eucalyptus loxophleba).*
- Tan Wattle *(Acacia hemiteles).*
- Native Poplar *(Codonocarpus continifolius).*

The trees and shrubs were replanted in a configuration as seen in Figure 5.2.1. A random selection of tree seedlings and shrubs represented by a circle marked S are planted 2.5m apart from one another in a single row. Two rows separated by a 4m gap is grouped into a pair of rows of which they are separated by another pair of rows by a 10m gap.

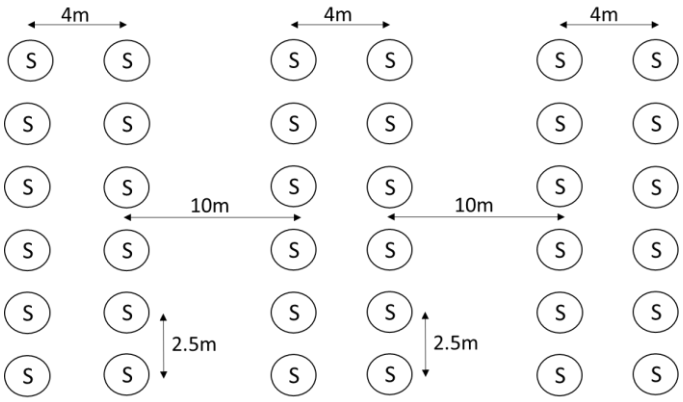

Figure 5.2.1: An illustration of the plantation configuration by Auscarbon in Tomora.

Figure 5.2.2: An example of the plantation configuration provided by Geoff McArthur (Auscarbon).

5.2.1.1.1 Fallow Paddock, Tomora

The species Mallee is located at Fallow Paddock (28˚52.158S and 115˚58.811E) in Tomora. The topographic position is low, with a flat terrain made up of sandy clay loams. Seedlings were planted in 1995 and the samples were 18 years old when felled. The sample consists of 4 Mallee trees and have been given the identities EH01, EH02, EH03 and EH04 respectively. They are a medium-sized multi-stemmed tree with a potential growth height of 8m.

5.2.1.1.2 Ram Paddock, Tomora

The species sampled in Ram Paddock is the Native Poplar (28˚52.158S and 115˚58.811E), Tan Wattle (28˚52.158S and 115˚58.811E) and York Gum (28˚52.158S and 115˚58.811E). The topographic position where four 5 year old Native Poplar trees – ID NP01, NP02, NP03 and NP04, is relatively high with gravelly loam soil. This pyramidal shrub or tree has a potential growth up to 10m. Of the Tan Wattle and York Gum, one biomass sample is obtained from each species, with the sample ID as TW01 and EL01 respectively. Both species are 5 years old. The Tan Wattle is a medium-sized shrub growing up to 4m and the York Gum a mid-sized tree that can grow up to 10m.

5.2.1.2 Field Biomass Measurement

A plot size 20×20m square (Coomes et al (2002), and Hall et al (2001)) is measured out and allocated a plot number. Trees are marked out and numbered while the tree species, tree age and site information are recorded.

Image acquisition is first carried out before manual field measurements began. Standing tree height was first measured. The sampled trees or shrubs are either small or medium-sized, therefore a 3m solid height stick marked to 0.1m accuracy with extensions up to 6m was used to estimate tree height. Stem diameter that are greater than 1cm was measured with a diameter tape, up to 1mm accuracy, at breast height. Any stem diameters that are less than 1cm was counted and recorded accordingly. It is later assumed that the stems (<1cm) are 0.6cm in diameter on average. The sample is then felled for aboveground biomass estimation. AGB was determined by the sum of two components:

- Small branches and foliage (crown).
- Larger woody branches and stem (stemwood).

The fresh weight of each individual tree and its components was obtained in situ from an electronic weighing scale with 300kg capacity and precision of 50g. Belowground biomass (BGB) was not taken into account in this case study as we are more concerned with estimating AGB using aboveground dendrometric measurements from the stereo-camera.

5.2.1.3 Photogrammetric Data

Once the selected trees for felling has been marked out, a pair of Canon 5D Mark II digital cameras were mounted 0.5m apart on a horizontal bar attached to a tripod and positioned horizontally from the tree or shrub in a stereo-camera configuration. The distance between the camera and the target tree is not measured. A control frame of known dimension is position 0.5m from the tree to provide a scale factor in the subsequent computational analysis. The shortest focal length (maximum wide angle) was used in imaging the entire tree. A synchronizer device connected to both cameras enabled the image acquisition for both cameras to be taken at the same instance, thus negating any matching error that can occur from minute changes in the position of tree features. Images of a close-up view of stem distribution at breast height was also captured. The Canon 5D Mark IIs were calibrated at 5m and operational parameters were set to image ratio <3:2> with resolution 5616×3744 pixels giving approximately 21.1 million image points.

Image acquisition from the FujiFilm FinePix REAL 3D W3 is obtained after the Canon 5D Mark IIs from the same locations. The FujiFilm FinePix REAL 3D W3 had also been calibrated at 5m while its operational parameters were set to automatic mode with frame size <16:9> and resolution 3648×2736 pixels. Image data for the FujiFilm FinePix REAL 3D W3 and Canon 5D Mark II is illustrated in Appendices B.1 and B.2.

5.2.1.4 Extracting Tree Metric Information from FujiFilm FinePix REAL 3D W3 and Canon 5D Mark II

Image extraction for the FujiFilm FinePix REAL 3D W3 follows the process described in Section 3.4.2.1. From the Canon pseudo stereo-cameras, JPEG left and right images were obtained separately from each camera differentiated by their serial numbers 495 (left camera representative) and 153 (right camera representative). The images are then converted to TIFF format. All TIFF images from the FujiFilm and Canon cameras were calibrated and rectified for all intrinsic distortion using the calibration parameters in Tables 5.1.1 and 5.2.1.

Table 5.2.1: Left and Right camera calibration parameters for Canon 5D Mark II.

Left Camera		Right Camera	
c	24.50310	c	24.44050
x_0	-0.35440	x_0	-0.42700
y_0	-0.11380	y_0	0.03290
k_1	1.450E-05	k_1	1.602E-05
k_2	1.980E-08	k_2	2.670E-08
k_3	-5.965E-11	k_3	-9.187E-11
p_1	4.935E-05	p_1	5.156E-05
p_2	1.172E-05	p_2	7.689E-06
b_1	9.225E-07	b_1	-5.930E-07
b_2	4.218E-05	b_2	-6.127E-05

As explained in Chapter 3, this process removes any lens distortion that can affect measurement later. The rectified images are then viewed in ERDAS ER Mapper. Image segmentation is applied when the target object and its boundaries cannot be located from its environment. We set some threshold boundaries for the RGB bandwidths to improve the contrast of the object against some environmental background such as grass and the sky.

The scale factor is determined from the control frame (a cross shaped construct made from two PVC pipes of lengths 2000mm and 1000mm and outside diameter 33mm). H, CD and DBH are estimated by converting image object dimensions (in pixels) to true measurements from the rectified images. DBH and H measured from the stereo-images will be used in the estimation of AGB using allometric equations.

5.2.2 Estimating Aboveground Biomass (AGB) using Allometric Models

AGB allometric models have commonly been formulated using the natural logarithm (ln) of either one variable alone or in combination involving first and second-order polynomials of these variables (Nogueira et al (2014), and Williams et al (2005)). These predictor variables include stem diameter, wood density, tree height and canopy diameter. Although logarithmically-transformed equations that use stem diameter and specific wood density as predictor variables show good accuracy in estimating AGB (Nogueira et al (2014)), our dataset contained the two basic measures of H and DBH which limits our selection of allometric models for this study.

5.2.2.1 Model Formulation and Selection

Out of many studies in estimating AGB from allometric relationships, temperate forests (Husch et al (1982), and Ter-Mikaelian and Korzukhin (1997), Muukkonen (2007)) and regions in the humid tropics (Brown et al (1989 and 1995), Chave et al (2005), Hunter et al (2013), Mate et al (2014), and Nogueira et al (2014)) are most commonly published.

Allometric relationship is affected from the variation in tree species in their canopy architecture and wood density (Chave et al (2005)). In order to obtain more accurate volume and biomass estimates of a particular tree or forest types, species specific equations are preferred. However, owing to species and locality limitations in current published studies in biomass estimations, generalised biomass estimation equations are a viable alternative where their precision may be acceptable for regional-scale applications and forest types and locations in which they were developed (Paul et al (2013)). Thus, we examined allometric studies in Australia for regional estimates of AGB. This includes studies by O'Grady et al (2000), Werner and Murphy (2001), Brack and Richards (2002), Suganuma et al (2006), Williams et al (2005), Montagu et al (2005), and Specht and West (2003).

Eight candidate models deemed as the more commonly used formulations for estimating AGB were taken from Williams et al (2005) and Montagu et al (2005). The models are log-log models relating AGB to some predictor variables. These variables were chosen to range from D or H alone, to different combinations of both variables. H is used to examine the practicality of incorporating height in the relationship to improve the accuracy of AGB estimation. In later context, we refer to D as the equivalent DBH for single and multi-stem trees and DBH as any stem diameter measured at breast height. The models are listed in Table 5.2.2 below:

Table 5.2.2: 8 general allometric models (Williams et al (2005) and Montagu et al (2005)).

Model ID	Model Description
1	$\ln(AGB) = \beta_0 + \beta_1 \ln(H)$
2	$\ln(AGB) = \beta_0 + \beta_1 \ln(DH^2)$
3	$\ln(AGB) = \beta_0 + \beta_1 \ln(DH)$
4	$\ln(AGB) = \beta_0 + \beta_1 (\ln(D))^2 + \beta_2 \ln(H)$
5	$\ln(AGB) = \beta_0 + \beta_1 \ln(D)$
6	$\ln(AGB) = \beta_0 + \beta_1 \ln(D^2H)$
7	$\ln(AGB) = \beta_0 + \beta_1 \ln(D) + \beta_2 \ln(H)$
8	$\ln(AGB) = \beta_0 + \beta_1 \ln(D) + \beta_2 (\ln(H))2$

In the above table, AGB is the aboveground biomass (kg tree^{-1}), H is tree height (m), D is equivalent stem diameter at breast height (cm) and β_0, β_1 and β_2 are parameter estimates. Given that variance increased with tree size, a common method when developing volume equation involves transforming the data and applying linear regression.

5.2.2.2 Equivalent stem diameter at breast height (D)

Trees have either single or multiple stems at breast height. Given that allometric models use a single DBH measurement to estimate AGB, adjustments have to be made in consideration of multiple DBH measurements from multi-stemmed trees

(Mate et al (2014), Nogueira et al (2014), and Poultouchidou et al (2013)). In which case, an equivalent DBH (D) is calculated from the diameter of all *n* number of stems at breast height with Equation (5.2.1).

$$\boldsymbol{D} = \sqrt{\sum_{\boldsymbol{i=1}}^{\boldsymbol{n}} \boldsymbol{dbh_i}^{\boldsymbol{2}}} \tag{5.2.1}$$

where dbh_i is the diameter of the i^{th} stem at breast height.

Among the stem diameters measured at breast height, stems with diameter <1cm (small stems) were not measured in field and a stem count was undertaken instead. An email (G. McArthur 2016, personal communication, 28 April) states that the diameter for small stems is assumed to be 0.6cm based on a predictive average. This average is later used in the equivalent DBH calculations.

5.2.3 Results

We present the results of dendrometric measurements obtained from analysing stereo-images captured by a pair of Canon 5D Mark II cameras and a handheld FujiFilm FinePix REAL 3D W3 camera and compare it with field measurements using a height stick, diameter tape and an electronic weighing scale. The comparison results are presented in four parts:

(i) Tree height.
(ii) Canopy width.
(iii) DBH count and measurement.
(iv) AGB estimation using generalised allometric models.

5.2.3.1 Tree height

We obtained the tree height of 10 samples from the rectified images taken with the pseudo stereo-camera Canon 5D Mark IIs and stereo-camera FujiFilm FinePix REAL 3D W3 and compare the results against height measurements recorded from a 3m height stick in situ. The results are presented in Table 5.2.3, including an estimated height based on a pole-to-tree height ratio, the means and standard

deviations of the corresponding results and the difference between the methods and ratio approximation.

Table 5.2.3: Tree/shrub heights (m) for 10 samples recorded from a height stick in field, processed digital images from the Canon 5D Mark II and FujiFilm FinePix REAL 3D W3 and an estimated height based on pole-to-tree/shrub ratio.

TREE HEIGHT (m)							
Sample #	Mensuration Equipment Used			Pole-Tree Ratio Height Estimation	Difference between		
	Height stick	Canon	FujiFilm		Stick & Ratio	Canon & Ratio	FujiFilm & Ratio
EH01	2.75	2.668	2.552	2.749	0.00	0.08	0.20
EH02	2.70	3.801	4.038	4.085	1.38	0.28	0.05
EH03	3.40	3.704	4.294	4.305	0.90	0.60	0.01
EH04	4.10	4.516	3.592	3.642	0.46	0.87	0.05
NP01	4.55	3.639	3.826	3.929	0.62	0.29	0.10
NP02	5.00	4.607	4.979	4.693	0.31	0.09	0.29
NP03	4.30	3.618	3.641	3.578	0.72	0.04	0.06
NP04	5.20	5.388	5.102	5.200	0.00	0.19	0.10
TW01	2.70	2.382	2.279	2.309	0.39	0.07	0.03
EL01	3.50	3.074	3.131	3.229	0.27	0.15	0.10
Mean	3.820	3.740	3.743	3.772	0.506	0.267	0.098
Standard Dev	0.947	0.915	0.928	0.871	0.423	0.270	0.084

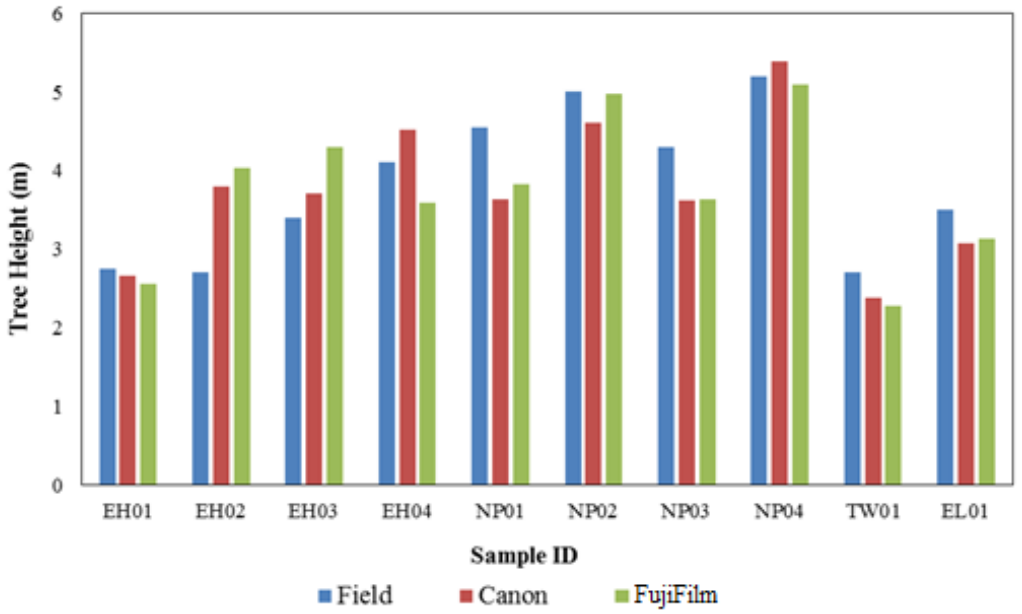

Figure 5.2.3: An illustrative comparison of tree height between field measurements, Canon 5D Mark II and FujiFilm FinePix REAL 3D W3.

Samples EH02 and EH03 display a large difference in the height stick and stereo-camera methods in Figure 5.2.3. According to a tree-pole ratio calculated in Table 5.2.2, the heights determined from the stereo-camera is actually closer to the true height as opposed to the measurement recorded from the height stick. We attribute this error as a human error in reading the tree height off the height stick. It is expected for the same error to occur when measuring taller trees (>4m) with the height stick due to the limitation on its length.

The height stick had a length of 3m. To increase this length for measuring taller trees, we had extended the length by bracing the height stick on another 1m long PVC pole or having a field operator lift up the pole to the highest possible height. This action resulted in a tendency for the height stick to lean near the tree top which would have affected the reading of tree height off the pole. Contrary to our expectations, the height stick was fairly accurate in estimating tree heights that were greater than 4m.

Out of all the results, the FujiFilm cameras appears to perform best given that the height difference between the FujiFilm FinePix REAL 3D W3 and the ratio approximation is the least (see Table 5.2.2) at an absolute maximum difference of 0.3m as opposed to the absolute maximum difference of 0.87m and 1.38m between the stick-to-ratio approximation and Canon-to-ratio approximation. This observation is further corroborated by the mean of these differences with the FujiFilm-to-ratio mean difference at a minimum of 0.098m. The mean difference between the stick-to-ratio approximation and Canon-to-ratio approximation is 5 and 2.5 times greater than the FujiFilm-to-ratio approximation. Given that the largest sample stands at 5m, an error of 0.5m causes at least a 10% inaccuracy error.

5.2.3.2 Canopy width

Although field measurements for canopy width was not undertaken, we still compare canopy width measurements obtained from both cameras to verify that the results from the FujiFilm FinePix REAL 3D W3 camera is comparable to the Canon 5D Mark II. One factor affecting the accuracy in photogrammetry is the degree of resolution. The higher the resolution of the images, the chances of achieving high accuracy increases because objects in the image can be more precisely located. According the camera specifications stated in Table 3.4.1, the highest resolution of

the Canon 5D Mark II provides more than twice the effective pixels (potential matching points) than the FujiFilm FinePix REAL 3D W3 which implies an increase chance of accuracy in measuring objects.

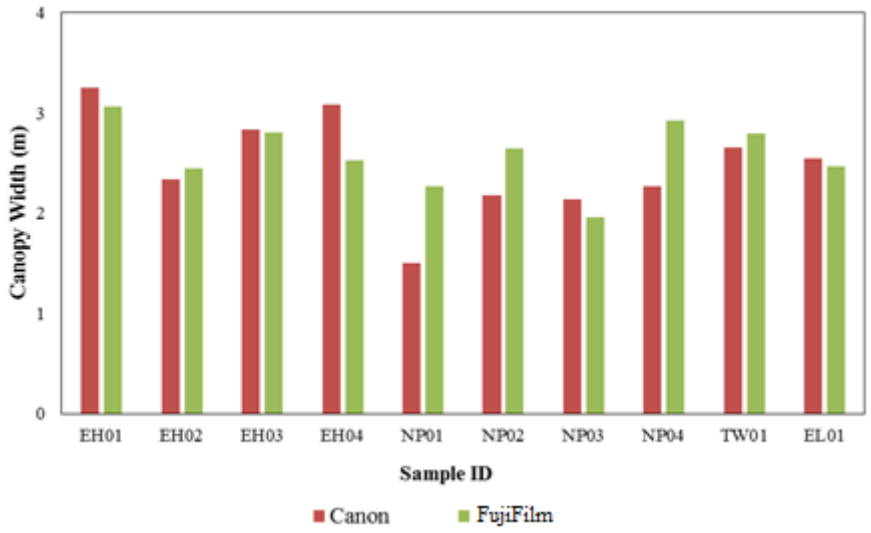

Figure 5.2.4: Comparison of canopy width between the Canon 5D Mark II and FujiFilm FinePix REAL 3D W3.

Canopy widths measured from the FujiFilm stereo-images appear to be comparable to the Canon 5D Mark II measurements as seen in Figure 5.2.4 with a few exceptions. The canopy widths for samples EH04, NP01, NP02 and NP04 are not as close as other samples i.e. EH01, with the largest difference observed from NP01 is approximately 0.7m. There is however some uncertainty in the measurement of canopy width from the Native Poplar trees (sample IDs NP01 – NP04) due to its shape. It tends to be canonical in outline with sub-branches extending almost horizontally from the main trunk. As the canopy foliage tend to grow close to the ground, it is uncertain if there is a minimum height from which the canopy width is to be measured. With the exception of the Native Poplar samples, the FujiFilm FinePix REAL 3D W3 appears to perform well against the Canon 5D Mark II with comparable results and can be considered a viable option for photogrammetric applications.

5.2.3.3 Stem count and DBH estimation

All samples in the Geraldton case study are multi-stem trees or shrubs (see Appendix B). Field measurements taken by traditional means, as represented by the blue markers, were used as a reference to compare DBH measurements from both sets of cameras. Tree or shrub diameter was measured for all branches at breast height (1.3m) in centimetres. Branches that have diameters less than 1cm were counted and assumed to be 0.6cm in diameter. The equivalent DBH (D) is calculated from Equation (5.2.1). We take the sum of squares of all diameters from branches with diameters greater than 1cm and add that amount to the product of the stem count (for <1cm diameter stems) with the square of the averaged diameter (0.6cm). D is the square root of the total sum of the diameters measured or assumed.

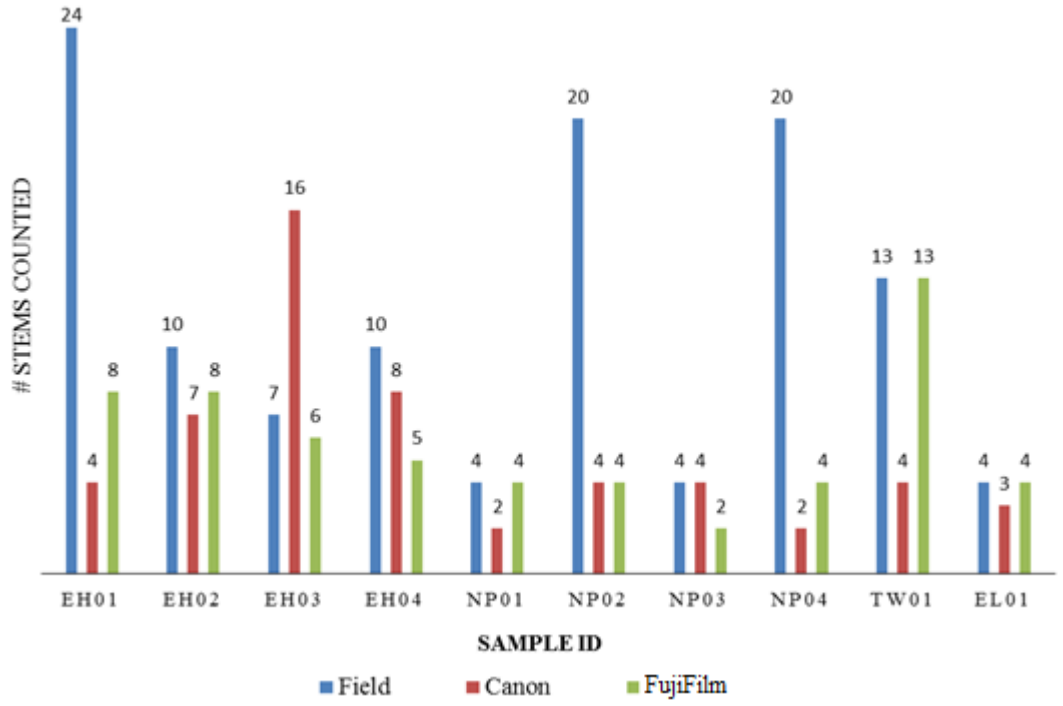

Figure 5.2.5: Stem count for stems >1cm from field measurements and through stereo-images obtained by the Canon 5D Mark II and FujiFilm FinePix REAL 3D W3.

A stem count for stems with diameters >1cm is illustrated in Figure 5.2.5 from traditional field measurements in situ and identified from the cameras' stereo-images after image processing. Stem identification is a difficult process with shrubby plants and woody trees that have high density of basal stems at breast height in computer

vision. Although multiple images from viewing angles is necessary in the identification of stems from occlusion, it is still a complex problem to identify each branch separately and measure them when the density of basal stems is extremely high and have been occluded from leaf foliage and other branches. An example can be seen from a magnified image of branch and foliage spread at breast height for samples NP and TW01 in Figure 5.2.6(a) and 5.2.6(b).

(a) Close-up view of sample NP02 at 1.3m (dotted line)

(b) Close-up view of sample TW01 at 1.3m (dotted line)

Figure 5.2.6: A close-up view of samples (a) NP02 and (b) TW01 illustrating the difficulty of identifying stems and measuring the DBH due to high frequency of occlusion at 1.3m depicted by the dotted line.

As such, the number of stems with diameters >1cm counted from the stereo-images are generally less than the actual stem count made from field measurements. Additionally, the calculation for D from stereo-camera measured DBH excluded stems that are <1cm, resulting in a lower estimate for D for some samples from the Canon 5D Mark II and FujiFilm FinePix REAL 3D W3 cameras (see Table 5.2.4 and Figure 5.2.7).

Table 5.2.4: Equivalent DBH of a multi-stem tree/shrub calculated from Equation (5.2.1).

Equivalent DBH for Multi-stem trees/shrubs (cm)						
Sample #	Mensuration Equipment Used			Abs. Difference between		
	Tape Measure	Canon	FujiFilm	Tape & Canon	Tape & FujiFilm	Canon & FujiFilm
EH01	11.507	8.262	2.440	3.244	9.066	5.822
EH02	9.940	11.198	12.902	1.258	2.962	1.704
EH03	7.435	7.639	9.648	0.204	2.212	2.009
EH04	10.617	8.985	10.322	1.632	0.296	1.337
NP01	9.699	6.922	10.303	2.777	0.604	3.380
NP02	11.111	14.847	9.813	3.737	1.298	5.035
NP03	9.189	7.018	7.204	2.171	1.985	0.186
NP04	10.793	8.551	10.567	2.242	0.226	2.016
TW01	7.873	2.115	4.106	5.758	3.767	1.991
EL01	5.856	4.780	7.785	1.076	1.929	3.005
Mean	9.402	8.032	8.509	2.410	2.435	2.648
Standard Dev	1.825	3.427	3.188	1.580	2.596	1.711

For the Canon 5D Mark IIs, sample EH02 and NP02 are two conflicting cases where the calculated D is larger than the tape measure estimation in spite of having a lower stem count. In EH02 (see Appendix B), the tree is observed to be shedding its bark in long strips on multiple height levels of the tree as typical of a Eucalypt. In the process of measuring DBH from EH02 stems, bulk weight from loose hanging bark could have been measured as part of the diameter. The errors from overestimating

individual DBH would have propagated to D since it is calculated from the square root of the sum of squares of all individual DBH measures. For NP02 (see Appendix B), it is more likely a case of operator error where two or more overlapping branches at breast height could have been misinterpreted as a single branch as thus overestimated. Again, this would have resulted in an overestimated D. Overestimations of D from the FujiFilm FinePix REAL 3D W3 can also be attributed to operator error in misinterpreting and identifying stems for DBH measurements.

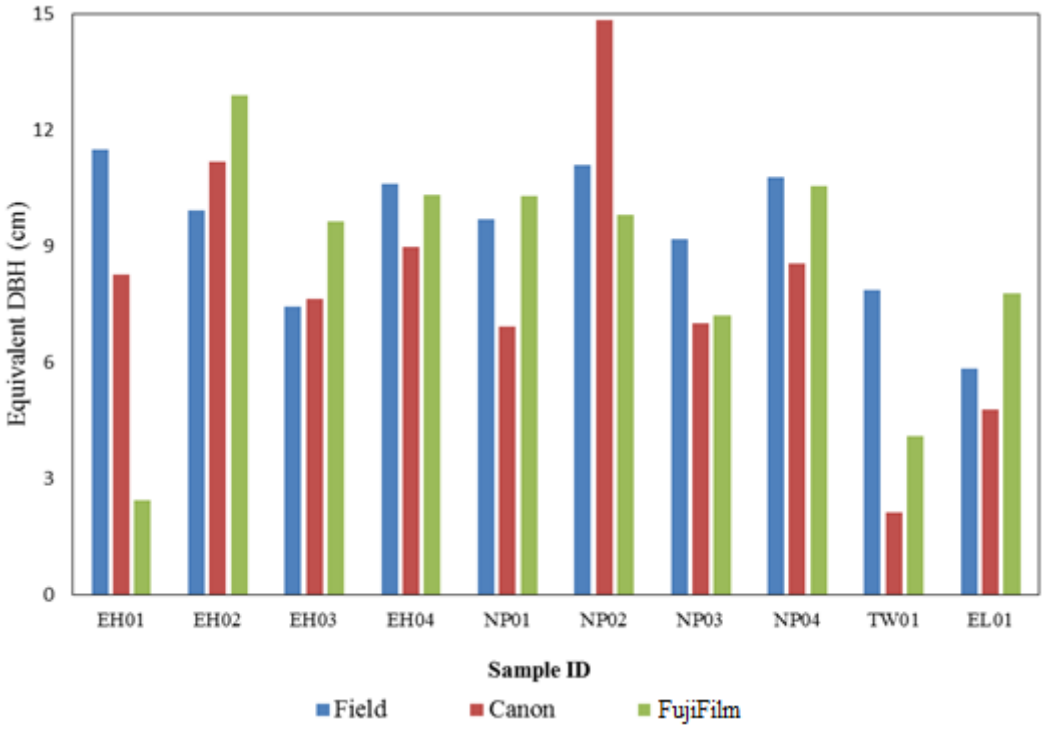

Figure 5.2.7: Illustrative comparison of D calculated from Equation (5.2.1) of field measurements and Canon 5D Mark II and FujiFilm FinePix REAL 3D W3 images.

5.2.3.4 AGB estimation from generalised allometric models

Linear and multiple regression parameters were derived from fitting field measured AGB weights, height measurements and D in the generalised allometric models proposed by William et al (2005) and mentioned in Section 5.2.2.1. The eight models that related ln(AGB) to predictor variables ln(D), ln(H) and linear and or quadratic combinations of the two variables are presented in Table 5.2.5 below.

Table 5.2.5: Selected allometric models with single and multivariable regression parameters and fit statistics.

Model	Inputs	β_0	Parameters β_1 and β_2							RMSE	Adj. R^2
			ln(D) (cm)	$(\ln(D))^2$ (cm^2)	ln(H) (m)	$(\ln(H))^2$ (m^2)	ln(DH) (m^2)	$\ln(D^2H)$ (m^3)	$\ln(DH^2)$ (m^3)		
1	ln(H)	3.0737			0.3345					0.3802	-0.077
2	$\ln(DH^2)$	1.8382							0.3456	0.3344	0.167
3	ln(DH)	0.8939					0.7411			0.2852	0.394
4	$(\ln(D))^2 + \ln(H)$	1.5104		0.4304	-0.1066					0.1322	0.851
5	ln(D)	-0.4942	1.8035							0.1278	0.878
6	$\ln(D^2H)$	0.0286						0.6054		0.2211	0.636
7	ln(D) + ln(H)	-0.4351	1.8380		-0.1034					0.1256	0.866
8	$\ln(D) + (\ln(H))^2$	-0.5139	1.8507			-0.0479				0.1246	0.868

Of these models, Model 1 that uses height as a single predictor variable gave the poorest fit as indicated by the root mean square error (RMSE) with a highest value of 0.3802. Model 5 that uses D as the only predictor is superior to Model 1 with a relative low RMSE value of 0.1278. However, Models 7 and 8 with RMSE values of 0.1256 and 0.1246 have shown that they are better when the predictor ln(D) is involved with some combination of ln(H). Models 4, 5, 7 and 8 also show that there is a good fit of the data (adjusted R^2 values are >0.85), indicating that more than 85% of the variation in ln(AGB) can be explained by ln(D) and/or some linear and quadratic combination of ln(D) and ln(H).

Figure 5.2.8 illustrates comparative plots of predicted AGB against observed data (on a log-log scale) for all eight models. The plots are consistent with the RMSE results observed in Table 5.2.5. The scatterplot for Model 1 illustrates a relatively horizontal trend in the data points from which we infer that there is poor correspondence between the fitted values of AGB and the original observed values of AGB for the samples in the harvest dataset. Adjusted R^2 increases with decreasing values of RMSE (see Table 5.2.5) and the best model is based on Model 8 which includes both ln(D) and $(\ln(H))^2$.

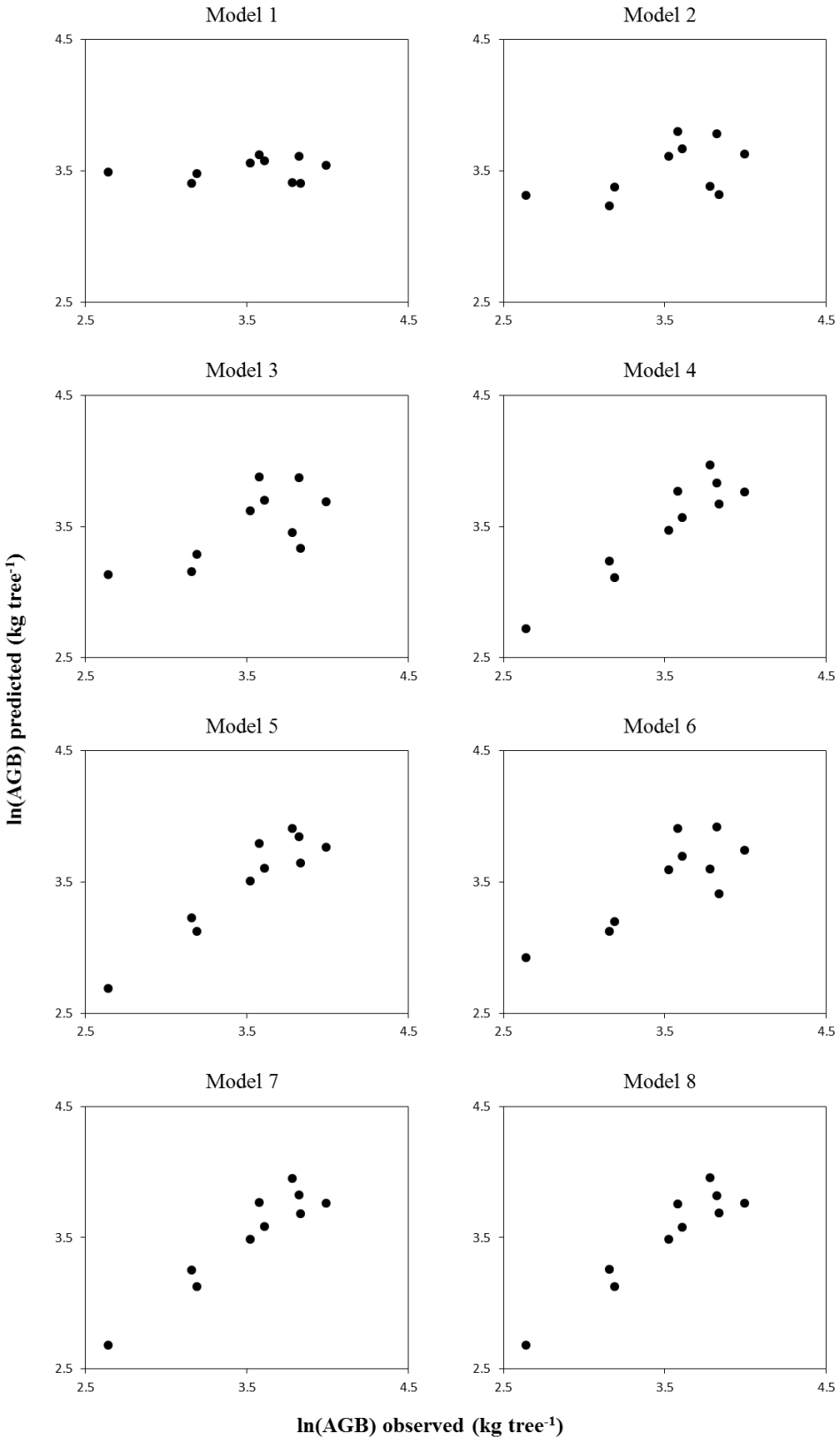

Figure 5.2.8: Plots comparing predicted ln(AGB) against observed ln(AGB) for the eight models.

Table 5.2.6(a): Table of observed and predicted values of ln (AGB) calculated from regression parameters in Table 5.2.5, height and DBH_e values in Tables 5.2.3 and 5.2.4 using allometric models 1 – 4 and the corresponding RMSE.

Sample #	Observed ln(AGB) (kg tree^{-1})	Predicted ln(AGB) (kg tree^{-1})											
		Model 1			Model 2			Model 3			Model 4		
		Field	Canon	FujiFilm	Field	Canon	FujiFilm	Field	Canon	FujiFilm	Field	Canon	FujiFilm
EH01	3.782	3.412	3.402	3.387	3.382	3.246	2.794	3.454	3.186	2.249	3.971	3.327	1.759
EH02	3.834	3.406	3.520	3.541	3.318	3.596	3.687	3.332	3.674	3.824	3.674	3.832	4.117
EH03	3.190	3.483	3.512	3.561	3.377	3.446	3.629	3.288	3.371	3.654	3.112	3.107	3.495
EH04	3.992	3.546	3.578	3.501	3.630	3.639	3.529	3.690	3.638	3.571	3.762	3.343	3.681
NP01	3.610	3.581	3.506	3.523	3.670	3.400	3.571	3.701	3.285	3.617	3.570	2.943	3.660
NP02	3.823	3.612	3.585	3.611	3.783	3.826	3.737	3.871	4.025	3.776	3.834	4.394	3.480
NP03	3.522	3.562	3.504	3.506	3.613	3.400	3.414	3.619	3.291	3.315	3.472	2.968	3.011
NP04	3.578	3.625	3.637	3.619	3.800	3.744	3.779	3.879	3.733	3.849	3.770	3.190	3.620
TW01	3.155	3.406	3.364	3.349	3.238	2.697	2.896	3.159	2.092	2.551	3.237	1.672	2.297
EL01	2.639	3.493	3.449	3.455	3.315	3.155	3.336	3.132	2.886	3.261	2.721	2.429	3.184
RMSE		0.380	0.359	0.371	0.334	0.331	0.449	0.285	0.442	0.601	0.132	0.641	0.760

Table 5.2.6(b): Table of observed and predicted values of ln (AGB) calculated from regression parameters in Table 5.2.5, height and DBH_e values in Tables 5.2.3 and 5.2.4 using allometric models 5 – 8 and the corresponding RMSE.

Sample #	Observed ln(AGB) (kg tree^{-1})	Predicted ln(AGB) (kg tree^{-1})											
		Model 5			Model 6			Model 7			Model 8		
		Field	Canon	FujiFilm	Field	Canon	FujiFilm	Field	Canon	FujiFilm	Field	Canon	FujiFilm
EH01	3.782	3.912	3.314	1.115	3.599	3.179	1.676	3.950	3.345	1.108	3.958	3.348	1.095
EH02	3.834	3.648	3.863	4.118	3.410	3.762	3.970	3.683	3.867	4.121	3.689	3.872	4.126
EH03	3.190	3.124	3.173	3.594	3.198	3.283	3.655	3.126	3.167	3.580	3.127	3.167	3.579
EH04	3.992	3.767	3.466	3.716	3.743	3.599	3.629	3.761	3.444	3.723	3.763	3.441	3.728
NP01	3.610	3.603	2.995	3.712	3.697	3.153	3.665	3.584	2.987	3.713	3.581	2.987	3.716
NP02	3.823	3.849	4.371	3.624	3.918	4.220	3.765	3.824	4.365	3.596	3.818	4.367	3.589
NP03	3.522	3.506	3.020	3.067	3.597	3.166	3.202	3.491	3.013	3.061	3.489	3.013	3.061
NP04	3.578	3.796	3.376	3.758	3.907	3.647	3.870	3.767	3.335	3.730	3.759	3.322	3.722
TW01	3.155	3.227	0.857	2.053	3.128	1.461	2.237	3.255	0.852	2.076	3.258	0.837	2.068
EL01	2.639	2.693	2.327	3.207	2.927	2.603	3.204	2.684	2.324	3.219	2.682	2.321	3.222
RMSE		0.128	0.827	0.962	0.221	0.624	0.785	0.126	0.830	0.962	0.125	0.835	0.967

To test the viability of using dendrometric measurements from stereo-cameras in estimating AGB, we used the following:

- Generalised allometric models (Table 5.2.2).
- Regression parameters derived from fitting field measured AGB weight, H and D (Table 5.2.5).
- Tree or shrub height measurements from the Canon 5D Mark II and FujiFilm FinePix REAL 3D W3 (Table 5.2.3).
- D estimations from the Canon 5D Mark II and FujiFilm FinePix REAL 3D W3 (Table 5.2.4).

It is observed that the predicted AGB from both Canon 5D Mark II's and FujiFilm FinePix REAL 3D W3's H and D measurements contradicted the predicted results from field measurements. Based on our previous analysis of predicted AGB from field measurements, Model 1 (ln(H)) gave the poorest fit (high RMSE 0.3802) whereas Models 5 (ln(D)), 7 (ln(D) + ln(H)) and 8 (ln(D) + $(\ln(H))^2$) performed best with more than 85% good fit of data and low RMSE values of 0.1278, 0.1256 and 0.1246 respectively. However, based on the RMSE values in Tables 5.2.6(a) and 5.2.6(b), Model 1 (H as the only predictor variable) gave a better fit to the data with RMSE values of 0.359 (Canon) and 0.371 (FujiFilm). Poorer fit of the data was observed in Models 5, 7 and 8 where RMSE values are at (0.827, 0.962), (0.830, 0.962) and (0.835, 0.967) respectively. The agreement between the predicted and observed logarithmically transformed AGB values is very poor when D was used as a predictor variable. The results suggest that the model estimating AGB using H as the only predictor is the best model when we input dendrometric measurements from the stereo-cameras, whereas models with D as a predictor variable would not perform as accurately.

We believe that the poor fit of data observed in models that use D as a predictor variable (in linear or quadratic combinations) is a result from the D errors as discussed in Section 5.2.3.3. Since the regression parameters were derived from field measurements as reference, any underestimation or overestimation in D calculated from the stereo-cameras would have greatly affected the fit of the data and predicted AGB. We also believe that Model 1 appears to be the best model because our height estimates from the stereo-cameras were more accurate than field measurements when compared against the estimates using the tree-pole ratio.

Table 5.2.7(a): Table of observed and predicted values of AGB back transformed from ln (AGB) of Models 1 – 4 in Table 5.2.6(a).

Sample #	Observed AGB (kg tree^{-1})	Predicted AGB (kg tree^{-1})											
		Model 1			Model 2			Model 3			Model 4		
		Field	Canon	FujiFilm	Field	Canon	FujiFilm	Field	Canon	FujiFilm	Field	Canon	FujiFilm
EH01	43.900	30.328	30.023	29.580	29.415	25.692	16.346	31.629	24.197	9.482	53.034	27.852	5.809
EH02	46.250	30.143	33.795	34.486	27.612	36.443	39.906	27.994	39.398	45.766	39.423	46.151	61.405
EH03	24.300	32.559	33.504	35.203	29.290	31.367	37.659	26.780	29.111	38.617	22.469	22.351	32.960
EH04	54.150	34.663	35.801	33.163	37.704	38.046	34.076	40.063	38.027	35.570	43.037	28.297	39.689
NP01	36.950	35.892	33.308	33.869	39.270	29.951	35.569	40.471	26.711	37.218	35.534	18.981	38.851
NP02	45.750	37.042	36.042	36.990	43.931	45.891	41.963	47.999	56.004	43.642	46.255	80.962	32.466
NP03	33.850	35.220	33.244	33.313	37.068	29.975	30.376	37.288	26.872	27.523	32.207	19.455	20.300
NP04	35.800	37.531	37.980	37.294	44.687	42.258	43.785	48.364	41.785	46.947	43.389	24.294	37.325
TW01	23.450	30.143	28.907	28.481	25.475	14.836	18.095	23.553	8.105	12.823	25.458	5.321	9.942
EL01	14.000	32.876	31.481	31.673	27.516	23.453	28.109	22.924	17.914	26.065	15.199	11.349	24.145

Table 5.2.7(b): Table of observed and predicted values of AGB back transformed from ln (AGB) of Models 5 – 8 in Table 5.2.6(b).

Sample #	Observed AGB (kg tree-1)	Predicted AGB (kg tree^{-1})											
		Model 5			Model 6			Model 7			Model 8		
		Field	Canon	FujiFilm	Field	Canon	FujiFilm	Field	Canon	FujiFilm	Field	Canon	FujiFilm
EH01	43.900	49.981	27.504	3.049	36.552	24.034	5.344	51.951	28.352	3.028	52.366	28.451	2.990
EH02	46.250	38.385	47.590	61.442	30.278	43.022	52.977	39.773	47.793	61.620	40.010	48.018	61.919
EH03	24.300	22.738	23.875	36.373	24.494	26.656	38.673	22.776	23.726	35.886	22.813	23.736	35.854
EH04	54.150	43.233	31.993	41.085	42.231	36.580	37.671	43.000	31.324	41.386	43.081	31.207	41.589
NP01	36.950	36.724	19.987	40.948	40.312	23.408	39.047	36.022	19.831	40.977	35.911	19.822	41.120
NP02	45.750	46.924	79.152	37.505	50.314	68.018	43.179	45.794	78.685	36.461	45.533	78.827	36.204
NP03	33.850	33.316	20.491	21.482	36.491	23.720	24.575	32.810	20.354	21.343	32.758	20.350	21.344
NP04	35.800	44.531	29.262	42.862	49.744	38.341	47.933	43.240	28.083	41.670	42.889	27.718	41.363
TW01	23.450	25.212	2.356	7.794	22.834	4.311	9.370	25.915	2.345	7.972	25.992	2.308	7.908
EL01	14.000	14.781	10.249	24.704	18.669	13.498	24.635	14.641	10.217	24.997	14.614	10.185	25.073

From back transformed AGB estimations using field dendrometric measurements, we observe systematic overestimation biases ranging from 4.8% - 38.95% in sample NP04 and 4.38% - 134.8% for EL01 across all models. Samples EH02 and EH04 on the other hand is systematically underestimated with biases ranging from -40.30% to -13.49% and -36.0% to -20.16%. Overall, the mean bias of all eight models overestimates AGB in comparison with field measurements. The models with the lowest mean estimation bias and smallest range of bias are found to be Models 4 $((\ln(D))^2 + \ln(H))$, 5 $(\ln(D))$, 7 $(\ln(D) + \ln(H))$ and 8 $(\ln(D) + (\ln(H))^2)$.

The comparison of predicted results with observed values, following back transformation in Tables 5.2.7(a) and 5.2.7(b) indicated that the Canon 5D Mark II performed slightly better than the FujiFilm; differences in predicted and observed are not as large. However, mean biases for the FujiFilm all eight models is smaller (between -9.0% to 7.1%) than the Canon 5D Mark II (between -23.5% to 6.7%). From the mean bias, AGB is generally underestimated using predictor values from the Canon 5D Mark II and FujiFilm FinePix REAL 3D W3, with only Model 1 holding a mean bias of 6.7% (Canon) and 7.1% (FujiFilm).

5.2.4 Discussion

In this study, stereo-cameras were tested against traditional methods in a plantation with small to medium sized trees and shrubs. The accuracy of height, canopy width and diameter measurements were examined. Tree heights obtained from stereo-cameras Canon 5D Mark II and FujiFilm FinePix REAL 3D W3 are more accurate than the traditional method of measurement from a height stick when comparing against height estimates based on tree-pole ratios. The measurements of canopy width between the Canon 5D Mark II and FujiFilm FinePix REAL 3D W3 is comparable with little difference in predicted values. Both stereo-cameras however performed quite poorly in measuring DBH from woody stems and shrubs with large numbers of basal stems at breast height. The high density of basal stems causes increased occlusion and mistaken identification when measured in the viewing software ERDAS ER Mapper, thereby affecting DBH measurement. Visualization from multiple viewing angles does not alleviate the problem and can even cause

double counting in stem diameter measurement unless branches have been individually marked for recognition purposes.

We also considered the viability of estimating AGB using H and D measurements from the stereo-cameras. Linear and multiple regression parameters were derived from fitting field measured AGB weights, H and D in the generalised allometric models proposed by William et al (2005). The best models in predicting AGB were achieved by D and/or some linear and quadratic combination of D and H.

The resulting AGB estimations from stereo-camera D and H measurements contradict the results obtained from field measurements. The RMSE values implied that using height as the only predictor variable (Model 1) is the best model for AGB estimation. Since height estimations from the stereo-cameras are shown to be quite accurate against the true height (Table 5.2.3), we attribute a large proportion of the associative error from the allometric models in estimating AGB to the equivalent DBH estimates obtained from stereo-camera measurements. The error is especially pronounced in allometric Model 5 which uses D as the only predictor variable.

The data used in this study had a small sample size; 10 samples of 4 different species. With such a small sample, the parameter estimates can be quite sensitive to each data point due to the inherent instability in the parameter and regression variance estimates. Increasing the sample size would produce stable parameter and regression variance estimates (Williams et al (2005)), resulting in a better AGB estimation using the allometric models. Total uncertainty at the single tree level of the biomass estimation process consists of tree variables measurement uncertainty and uncertainty from the use of allometric models to predict biomass of a new individual (Chave et al (2004), Zianis (2008)).

Based on previous results in Section 5.1, it is possible that the estimation of AGB will perform better with more mature trees that have distinct basal trunks at breast height considering that the DBH measurements from the stereo-camera is acceptably accurate against tape measurements (Tables 5.1.4 and 5.1.5). Further studies and more samples are required to validate the use of stereo-camera dendrometric measurements to approximate AGB from allometric equations and displace traditional methods in field surveys.

5.3 Case Study: Williamsdale

In this section, we will examine the accuracy of dendrometric measurements for matured paddock trees from a consumer-grade stereo-camera against field measurements obtained from harvested trees. Standing tree height was measured with a hypsometer and estimated from stereo-images. A measuring tape was used to measure the length of the tree after it was felled. Stem diameter was measured with a diameter tape and estimated from the stereo-images at 3 points: 10cm from ground, 50cm from ground and at breast height. The dendrometrics obtained from the photogrammetric method was used to predict AGB which is subsequently assessed with the actual biomass of the sample harvested in the field.

The results in Section 5.3.2 indicate that the photogrammetric method performs quite well in estimating tree height, stem diameter and AGB. There is an inclination for tree height to be underestimated, with a mean error of approximately 7%. Stem diameter for both the photogrammetric and tape measure method are comparable at breast height. Errors between stem diameter estimates at 10cm and 50cm from the ground are much larger. This can be attributed to the non-circular cross-section of the trunk at those heights. The biomass estimated by the photogrammetric method agree more with the harvest dataset whereas the biomass predicted from field measured dendrometrics fall short of the actual weight.

5.3.1 Materials and Methods

5.3.1.1 Study Site

The site formed part of a CSIRO environmental planting study being conducted by a team of technicians and contractors from CSIRO in Williamsdale, Australian Capital Territory. Physical measurements were made by this team and provided for purposes of comparison with the photogrammetric approach, which were jointly collected by the thesis author. The survey site is predominantly metasedimentary soils on flat moderate slopes. The tree species measured and harvested are Yellow Box (*Eucalyptus melliodora*), Red Gum (*Eucalyptus blakleyi*), Candlebark Gum (*Eucalyptus rubida*), Apple Box (*Eucalyptus bridgesiana*) and Scribbly Gum, (*Eucalyptus racemosa*).

5.3.1.2 Biomass estimation

Aboveground and belowground tree biomass was estimated through direct harvest by a team of field technicians. A total of 20 samples were collected spanning the tree species mentioned in Section 5.3.1.1. Before harvest sampling, a measuring tape was used to determine basal stem diameter (10cm). Diameters at 30cm and 50cm and breast height (1.3m, DBH), tree length was measured after the tree is felled.

Trees were felled and the fresh mass of the following component parts were measured in the field:

(i) Live crown (all foliage and twigs).

(ii) Tree bole and remaining branches.

Sub-samples of each biomass component were taken to determine the dry-mass correction factor after fresh-mass measurement. Approximately three replicate subsamples (disks from trunks and large branches, and small branches and foliage) were sampled for moisture content. The subsamples were subsequently weighed and oven-dried at 70° to a constant mass in the laboratory. On a tree-by-tree basis, moisture contents were calculated for each component and used to calculate the dry weight (Paul et al (2008, 2013)). The CSIRO team's procedure to determine stem wood density using the water displacement method is as follows: a number of wedges are removed from individual trees depending on disc size. These subsamples, including remaining disc material were dried at 70° to a constant mass. Stem density (ρ) is calculated as the dry weight of wood divided by its volume (Paul et al (2008, 2013)).

5.3.1.3 Photogrammetric and rangefinder data

Photogrammetric data was acquired using a FujiFilm FinePix REAL 3D W3 consumer grade stereo-camera, concurrent with distance and tree heights measures from a Nikon Forestry 550 rangefinder. The camera's operational parameters were set to automatic mode with the largest frame size <16:9>, with a frame size of 3648×2736 pixels to generate approximately 10 million image points. The focal length is fixed without any use of the zoom functions.

A series of stereo-images were captured for 19 samples (see Appendix C) based on the photogrammetric network stated in Section 5.1.1.3. At the time of image acquisition, GPS coordinates (longitude and latitude) were recorded in a geotagged image. In addition, tree height and horizontal distance were recorded from the range-finder at each stereo-image capture point.

5.3.1.4 Image Processing and retrieving tree metric information

The stereo-images were processed as described in Section 3.4.2.3 and corrected for all intrinsic distortion using calibration parameters in Table 5.1.1 and executable programs developed by CSIRO. This process is a fundamental step in eliminating any radial lens distortion and minimizes potential errors in object measurement. ERDAS ER Mapper is used to view and enhance the images for object measurement. Image segmentation is applied when the target object and its boundaries cannot be easily distinguished from its environment; we set some threshold boundaries for the RGB bandwidths to improve the contrast of the object against some environmental background such as grass and the sky.

The reference framework is a square panel of 55.5cm with CP markers centered at each midpoint and endpoint along all the edge lengths. We determine the scale factor from the reference frame (see Section 5.1.1.3) and estimate H, and DBH from image coordinates.

5.3.2 Results

We present the results of dendrometric measurements obtained from analysing stereo-images captured by a handheld FujiFilm FinePix REAL 3D W3 camera and compare it with field measurements corresponding to 14 samples out of the 20 that are harvested. Some samples from the harvest data have been excluded from the comparison for the following reasons:

- The harvesting process had begun before the photogrammetric data collection started.

- The field technicians harvesting the samples did not have sufficient time to harvest all the samples captured in the stereo-images.

The comparison results are presented in three parts:

(i) Tree height.

(ii) Stem diameters.

(iii) AGB estimation using generalised allometric models.

5.3.2.1 Tree height

Repeated measurements are necessary for obtaining statistical stability and assessing accuracy and precision (Bruce (1975)). In this study, we recorded several measurements of tree height and horizontal distance for each individual sample from the Nikon Forestry 550 hypsometer/rangefinder based on the process explained in Section 5.3.1.3. Multiple measurements of tree height from 19 samples have also been carried out using the rectified images of the stereo-camera. The height for each individual tree is then presented as the average of all height measurements for that particular sample. This enables us to reduce any bias from over or underestimation as mentioned in previous chapters. The results are presented in Table 5.3.1, including the means, standard error of the means and the absolute difference between the methods. It can be seen that from the 25 samples, the results of 14 sampled trees are compared between the harvesting, rangefinder and stereo-camera method.

Table 5.3.1: Tree height (m) of 25 samples recorded through harvesting or from a rangefinder and processing stereo-images from the FujiFilm FinePix REAL 3D W3 camera.

Tree Height (m)						
Sample #	Mensuration Equipment			Absolute Difference between		
	Camera	Rangefinder	Field	Camera & Rangefinder	Camera & Field	Rangefinder & Field
S1	-	-	14.7	NA	NA	NA
S2	-	-	19.4	NA	NA	NA
S3	16.15	16.60	17.6	0.45	1.45	1.00
S4	11.90	12.67	13	0.78	1.10	0.33
S5	14.90	14.58	16	0.33	1.10	1.42
S6	16.93	16.66	17.5	0.27	0.57	0.84
S7	13.00	13.68	-	0.67	NA	NA
S8	11.39	12.13	12	0.73	0.61	0.12
S9	24.44	26.64	28	2.21	3.56	1.36
S10	-	-	20	NA	NA	NA
S11	-	-	16	NA	NA	NA
S12	17.83	17.05	18	0.78	0.17	0.95
H1	15.42	14.71	16	0.71	0.58	1.29
H2	15.54	15.80	16	0.26	0.46	0.20
H3	21.99	23.68	-	1.69	NA	NA
H4	15.24	14.13	16	1.11	0.76	1.87
H5	19.74	21.14	21	1.40	1.26	0.14
H6	17.72	19.73	21	2.01	3.28	1.27
H7	13.98	14.84	15	0.86	1.02	0.16
H8	20.79	20.75	-	0.04	NA	NA
H9	20.56	21.40	-	0.84	NA	NA
H10	13.97	14.83	-	0.86	NA	NA
H11	17.02	19.06	19.5	2.04	2.48	0.44
H12	-	-	19.5	NA	NA	NA
H13	-	-	13	NA	NA	NA
Mean	16.76	17.37	17.46	0.950	1.314	0.813
Standard Dev.	3.492	3.952	3.620	0.639	1.053	0.580

Mean height is 16.76m, 17.37m and 17.46m for the stereo-camera, rangefinder and harvest method respectively. Of the 3 methods, the absolute error between the rangefinder and field measured height is the smallest with a mean difference of 0.813m and lowest value of uncertainty. In comparison, the results from the stereo-camera exhibit a tendency to underestimate tree height. We assumed that the height from the felled trees is the most accurate measure. Brown (1971) states that for cameras calibrated for a particular finite distance, targets at different distances will display slightly different quantities of radial distortion. This implies that the stereo-images we have rectified from previous camera calibration parameters (see Section 4.2) cannot correct all distortion parameters arising from the variability of distance in

image capture in the field and is cause for the discrepancy of tree height measurement from the stereo-camera. A simple analysis on the tree height to horizontal distance ratio from our rangefinder recordings shows the ratio to be at least 1:2 for the target to fit within the image field of view. This indicates that the error source in taller trees can subsequently be attributed to the increased uncorrected radial distortion from the increasing difference between fieldwork target distance and the initial camera calibration distance. One example would be samples S8 and S9 of heights 12m and 28m respectively (from field measure). The absolute difference in height between the stereo-camera and field measure is calculated at 0.61m and 3.56m and can be seen by the large disparity in Figure 5.3.1 below.

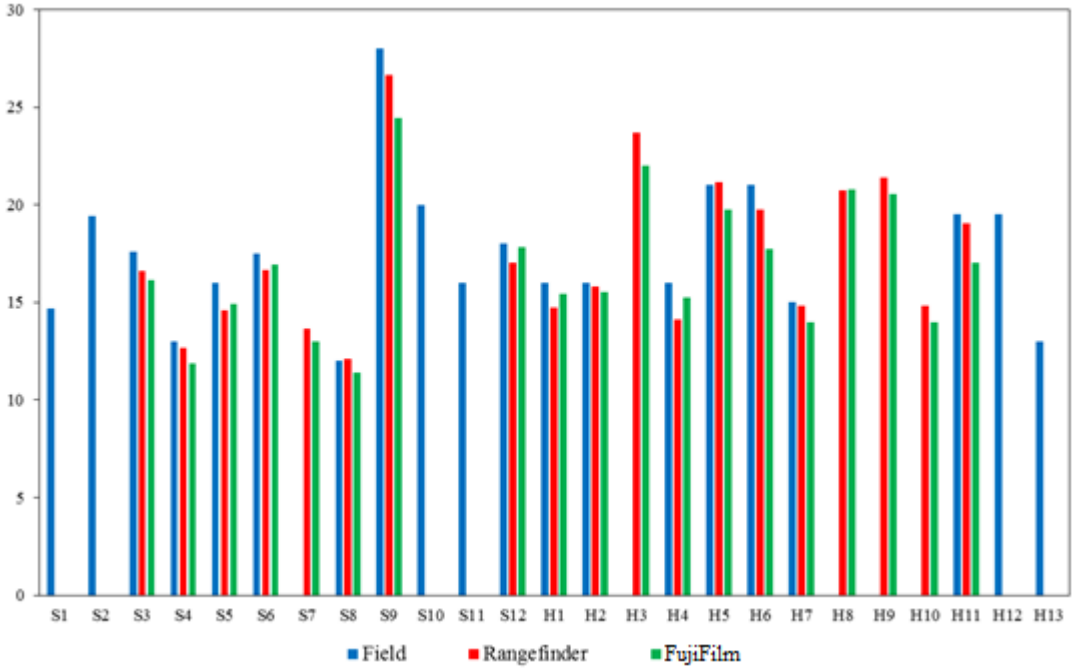

Figure 5.3.1: An illustrative comparison of tree height between field measurements, a rangefinder and the FujiFilm FinePix REAL 3D W3 camera.

5.3.2.2 Stem diameters

Field measurements taken by traditional means, as represented by the blue columns in Figure 5.3.1, were used as a reference to compare DBH measurements from both sets of cameras. Trunk diameters are measured at 3 heights for comparison: 10cm from ground, 50cm from ground and breast height at 1.3m. The notations for each measurements is D10, D50 and DBH respectively. The equivalent DBH and D50 is

calculated in the case of multi-stemmed trunks and is represented by the notation D and D50e respectively.

Table 5.3.2: Equivalent DBH of single or multi-trunk trees calculated from Equation (5.2.1).

Equivalent DBH (D) for trees (cm)			
Sample #	Mensuration Equipment		Absolute Difference
	Camera	Field	
S1	-	88.60	NA
S2	-	111.10	NA
S3	92.69	85.30	7.39
S4	116.23	135.46	19.24
S5	99.53	106.50	6.97
S6	76.23	81.00	4.77
S7	80.26	-	NA
S8	64.26	69.94	5.67
S9	123.15	132.00	8.85
S10	-	94.80	NA
S11	-	91.00	NA
S12	100.65	102.00	1.35
H1	119.80	91.40	28.40
H2	114.37	103.10	11.27
H3	104.69	-	NA
H4	110.44	102.50	7.94
H5	80.38	82.00	1.62
H6	123.51	138.80	15.29
H7	81.90	81.00	0.90
H8	90.14	-	NA
H9	60.77	-	NA
H10	77.15	-	NA
H11	96.92	97.55	0.63
H12	-	106.30	NA
H13	-	67.22	NA
Mean	95.42	98.38	8.591
Standard Dev.	19.508	19.892	7.889
Standard Error			2.958

A paired t-test was used to test for any statistical difference in the stem diameters measured by the different methods. It revealed that differences in measurements between the field and stereo-camera method were not significant (t = -0.1911). Mean D for the stereo-camera method and field method is 95.42cm and 98.38cm, where the mean absolute difference is 8.591cm. We see from Table 5.3.2 and Figure 5.3.2 that a majority of D is underestimated by the stereo-camera method. Figure 5.3.2 is an

illustrative comparison of D measurements between the stereo-camera and field method, and represented by the green and blue bar graphs.

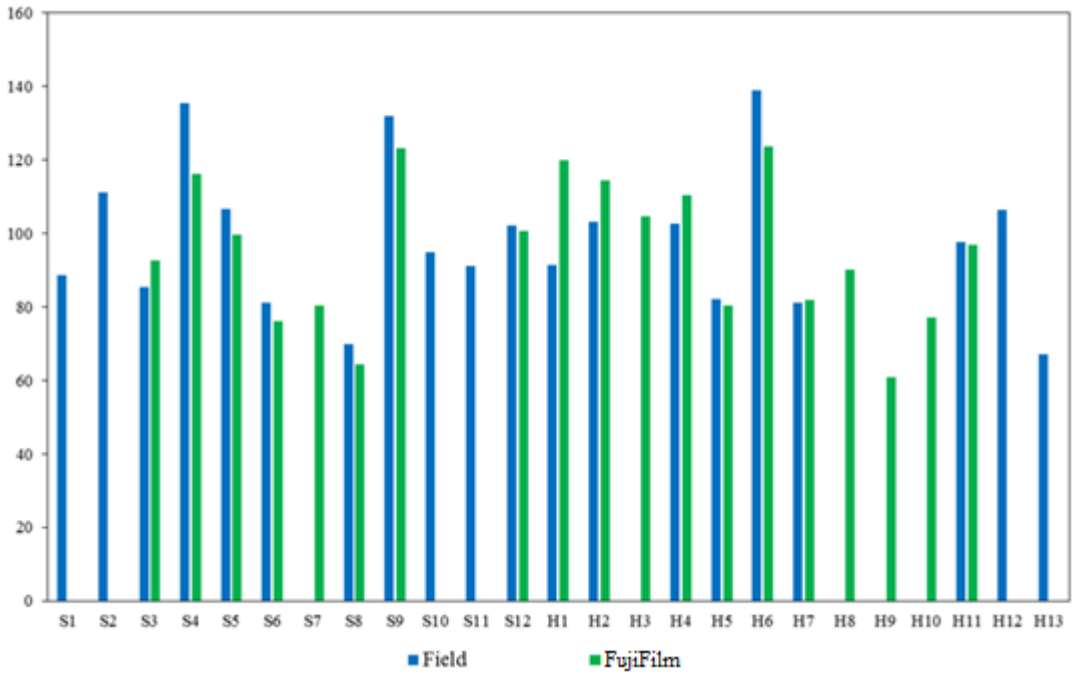

Figure 5.3.2: An illustrative comparison of the equivalent DBH (cm) from field measurements and FujiFilm FinePix REAL 3D W3 stereo-images.

There is a significant difference in diameter measurements between the field and stereo-camera method for sample S4, H1, H2 and H6 with the absolute difference ranging from 11.27 – 28.40cm. With the exception of H1, the samples S4, H2 and H6 are multi-stemmed trees at breast height. According to Paul et al (2014), there is a greater measurement error for diameters of multi-stemmed trees. Measurement error also occurs for trunks that have a non-circular cross-section, in which calliper instruments give a better estimate of sectional area than from the girth measure (Husch et al (2003)).

For samples H6 and S4, D is underestimated by the stereo-camera method. From Figure 5.3.3, breast height is marked on the image by a red line. We see that in the case of H6, recent growth from the main trunk has resulted in multiple branches at breast height. As mentioned in Section 5.2.3.3, a large cluster of stems in stereo-images often results in occlusion and difficulty in identifying all stems for measurements. As such, the number of stem diameters measured for H6 would be less than the actual number of stems at breast height and is cause for the

underestimation bias in D. Although the trunks are distinguishable for S4, we are unable to fully explain the significant difference in D measurement. It can only be presumed that the breast height was interpreted differently between the 2 methods which can cause such a large disagreement in D.

Figure 5.3.3: A close-range image of the trunk for samples H6, S4 and H1.

In considering sample H1, DBH was measured at the height denoted by the solid white line from the rectified image. The position of breast height was found by back transforming 1.3m (breast height) into pixels and determined from the tree base. This breast height is represented by the solid white line in Figure 5.3.3. We observe that there is a canker or protrusion occurring on the right end of the trunk at the camera measured breast height. The forestry approach to measure DBH in such cases is to measure either as close as possible above the canker and account for taper or take an average of the diameters above and below the canker (Husch et al (2003)). We therefore hypothesis that the DBH for sample H1 measured in field is recorded at a level above the protrusion, represented by the dotted line. This would then explain the overestimation error for H1 in Table 5.3.2 between the field and stereo-camera method.

Table 5.3.3 summarises stem diameter measurements recorded 10cm from the ground from both the stereo-camera and tape measure method. A paired t-test was used to test whether the diameters measured by the different methods were statistically different from one another. It revealed that differences in measurements between the field and stereo-camera method were significant (t = 3.638).

Table 5.3.3: Comparison of D10 (cm) between field and stereo-camera measurement.

Diameter at 10cm (D10) for trees (cm)			
Sample #	Mensuration Equipment		Absolute Difference
	Camera	Field	
S1	-	111.40	NA
S2	-	145.00	NA
S3	171.93	128.00	43.93
S4	192.43	193.40	0.97
S5	156.40	137.00	19.40
S6	105.51	117.20	11.69
S7	214.96	-	NA
S8	113.62	95.00	18.62
S9	189.89	182.90	6.99
S10	-	146.40	NA
S11	-	110.00	NA
S12	170.77	148.00	22.77
H1	154.40	145.00	9.40
H2	140.24	122.10	18.14
H3	162.04	-	NA
H4	129.88	114.50	15.38
H5	112.75	101.00	11.75
H6	172.99	171.50	1.49
H7	97.84	89.50	8.34
H8	138.98	-	NA
H9	106.63	-	NA
H10	90.98	-	NA
H11	122.11	110.00	12.11
H12	-	146.50	NA
H13	-	91.50	NA
Mean	144.44	130.30	14.357
Standard Dev.	35.624	29.654	10.681
Standard Error			3.449

Paul et al (2014) states that measurement error in stem diameters increases with lower levels of the tree, where their errors for DBH were in agreement with those noted by Gregoire et al (1989). It is also noted that multi-stemmed trees are a source of greater measurement error for diameters compared to single-stemmed trees. We see from Table 5.3.3 that the error between stereo-camera and field measured D10 tend to be large; mean error is 14.38cm and the standard error is 3.45cm. We believe that error source from both field and stereo-camera measured D10 can be attributed to the following reasons:

- The presence of exposed roots at 10cm from the ground results in a larger diameter measurement due to the roots being detected as the trunk when the actual bole is smaller.
- Diameter measurements from rectified images is dependent on the image perspective. Errors are more liable to occur in trunks with an elliptical bole. In field measurements, a typical stem diameter is approximated from the trunk circumference under the assumption that trunk bole is circular. Suppose that an elliptical bole has maximum and minimum length of 10cm and 6cm. The circumference is then approximated as 51.05cm. If stem diameter is calculated from the abovementioned assumption, then the diameter should be 16.25cm. However, stem diameter for non-circular boles is calculated as the average between the maximum and minimum length of the bole, which turns out to be 8cm. If we calculate the diameter from a photogrammetric point of view, the stem diameter can range between 6 – 10cm due to the image perspective.

Diameters retrieved from the stereo-images display a strong tendency to overestimate stem diameters at 10cm height. It is possible that by taking the average value of multiple D10 measurements from different viewing angles, we can reduce estimation error.

Table 5.3.4 summarises stem diameter measurements recorded 50cm from the ground from both the stereo-camera and tape measure method. Due to the presence of multiple stems at 50cm for a few samples, the equivalent diameters (D50e) is retrieved from the stereo-images and represented in the table below. A paired t-test was used to test whether the diameters measured by the different methods were statistically different from one another. It revealed that differences in measurements between the field and stereo-camera method were not statistically significant ($t = -1.153$), indicating that measurement error decreases at higher levels of measuring height (Paul et al (2014), Gregoire et al (1989)).

Table 5.3.4: Comparison of D50 and D50e (cm) between field and stereo-camera measurement.

Diameter at 50cm (D50) for trees (cm)			
Sample #	Mensuration Equipment		Absolute Difference
	Camera	Field	
S1	-	96.00	NA
S2	-	125.00	NA
S3	118.58	115.50	3.08
S4	168.50	169.50	1.00
S5	117.75	119.70	1.95
S6	84.17	91.80	7.63
S7	108.66	-	NA
S8	37.60	73.50	35.90
S9	157.82	156.10	1.72
S10	-	117.40	NA
S11	-	100.50	NA
S12	139.06	120.00	19.06
H1	117.59	117.00	0.59
H2	110.73	109.40	1.33
H3	130.23	-	NA
H4	104.89	100.50	4.39
H5	94.44	94.00	0.44
H6	126.63	181.00	54.37
H7	80.17	87.50	7.33
H8	102.13	-	NA
H9	74.00	-	NA
H10	91.44	-	NA
H11	102.38	103.40	1.02
H12	-	119.00	NA
H13	-	85.00	NA
Mean	108.78	114.09	9.986
Standard Dev.	30.030	27.604	16.085
Standard Error			4.550

We see from Table 5.3.4 that there is a significant difference in diameter measurements between the field and stereo-camera method for sample S8, S12 and H6 with errors ranging from 19.06 – 54.37cm. It is observed that with the exception of S12, both S8 and H6 are multi-stemmed trees at the 50cm height level. As mentioned before, multi-stemmed trees are a source of greater measurement error for diameters compared to single-stemmed trees and can explain the large measurement error for these samples. In S12, there is some indication of root spread at the 50cm

height level which would have inflated the girth measurement and explained the large difference between the field and stereo-camera method.

5.3.2.3 AGB estimation

Linear and multiple regression parameters were derived from fitting field measured AGB weights, H and D of 20 samples in the generalised allometric models from Section 5.2.2.1. The eight models that relate ln(AGB) to predictor variables ln(D), ln(H) and linear and or quadratic combinations of the two variables are presented in Table 5.3.5 below. Initially, we fit the data from the 14 samples mentioned in Sections 5.3.2.1 and 5.3.2.2 since a comparative analysis can be conducted from those samples between methods. The resulting linear and multiple regressions parameters and adjusted R^2 is presented in Table 5.3.5. However, increasing the sample size would produce stable parameter and regression variance estimates and provide a better AGB estimation according to Williams et al (2005).

Table 5.3.5: Fitted regression parameters derived from 14 samples.

Model	Inputs	β_0	Parameters β_1 and β_2							RMSE	Adj. R^2
			ln(D) (cm)	$(\ln(D))^2$ (cm^2)	ln(H) (m)	$(\ln(H))^2$ (m^2)	ln(DH) (m^2)	$\ln(D^2H)$ (m^3)	$\ln(DH^2)$ (m^3)		
1	ln(H)	4.262			1.580					0.3541	0.4204
2	$\ln(DH^2)$	4.650							0.724	0.2928	0.6039
3	ln(DH)	5.528					1.141			0.2807	0.6365
4	$(\ln(D))^2$ + ln(H)	2.918		0.120	1.160					0.2846	0.5944
5	ln(D)	1.490	1.584							0.3594	0.4108
6	$\ln(D^2H)$	6.714						0.727		0.2945	0.6016
7	ln(D) + ln(H)	0.282	1.136		1.147					0.2812	0.6035
8	ln(D) + $(\ln(H))^2$	1.960	1.146			0.189				0.2895	0.5807

We then fit the data from all 20 harvest samples into the allometric models and retrieve the regression parameters, adjusted R^2 and p-values on the regression coefficients as given in Tables 5.3.6 and 5.3.7.

Table 5.3.6: Regression parameters derived from 20 field measured samples.

Model	Inputs	β_0	Parameters β_1 and β_2							RMSE	Adj. R^2
			ln(D) (cm)	$(\ln(D))^2$ (cm^2)	ln(H) (m)	$(\ln(H))^2$ (m^2)	ln(DH) (m^2)	$\ln(D^2H)$ (m^3)	$\ln(DH^2)$ (m^3)		
1	ln(H)	3.220			1.940					0.3596	0.4934
2	$\ln(DH^2)$	3.968							0.844	0.2905	0.6695
3	ln(DH)	5.028					1.321			0.2742	0.7055
4	$(\ln(D))^2$ + ln(H)	2.014		0.148	1.277					0.2777	0.6802
5	ln(D)	-0.435	2.006							0.3453	0.5331
6	$\ln(D^2H)$	6.370						0.853		0.2830	0.6864
7	ln(D) + ln(H)	-1.169	1.388		1.253					0.2739	0.6889
8	ln(D) + $(\ln(H))^2$	0.593	1.413			0.208				0.2814	0.6715

Table 5.3.7: P-values for regression parameters derived from 14 and 20 field measured samples.

Model	Regression parameters p-values					
	14 samples			20 samples		
	β_0	β_1	β_2	β_0	β_1	β_2
1	0.0101	0.0072		0.0191	0.0003	
2	0.0002	0.0007		0.0001	0.0000	
3	0.0000	0.0004		0.0000	0.0000	
4	0.0446	0.0306	0.0239	0.0734*	0.0035	0.0053
5	0.5283*	0.0080		0.8239*	0.0002	
6	0.0000	0.0007		0.0000	0.0000	
7	0.8870*	0.0266	0.0241	0.4722*	0.0027	0.0057
8	0.3353*	0.0295	0.0339	0.7243*	0.0029	0.0094

According to Tables 5.3.6 and 5.3.7, we observe a general increase in the coefficients of the predictor variables whereas the constant coefficient is reduced from the increase in sample size. The adjusted R^2 has increased for all models when 20 samples were fitted to the allometric model, indicating that the addition of more data has improved the model fit. The constant coefficients for Models 5, 7, and 8 derived from the 14 sample size is not meaningful given that $p > 0.05$. (*) marks the p-values where the corresponding regression coefficient is not significant. When the data set increases, the constant coefficient becomes increasingly insignificant whereas p-values for the predictor variables coefficients have decreased, thereby increasing the significance of those coefficients in representing the change in AGB.

In order to verify the normality and collinearity of linear and multiple regression models, we examine the residual statistics of the regression model using the probability plot (Q-Q plot) from the standardized residuals. From Figure 5.3.4, the residuals for all models appear normal and closely follow a linear trend.

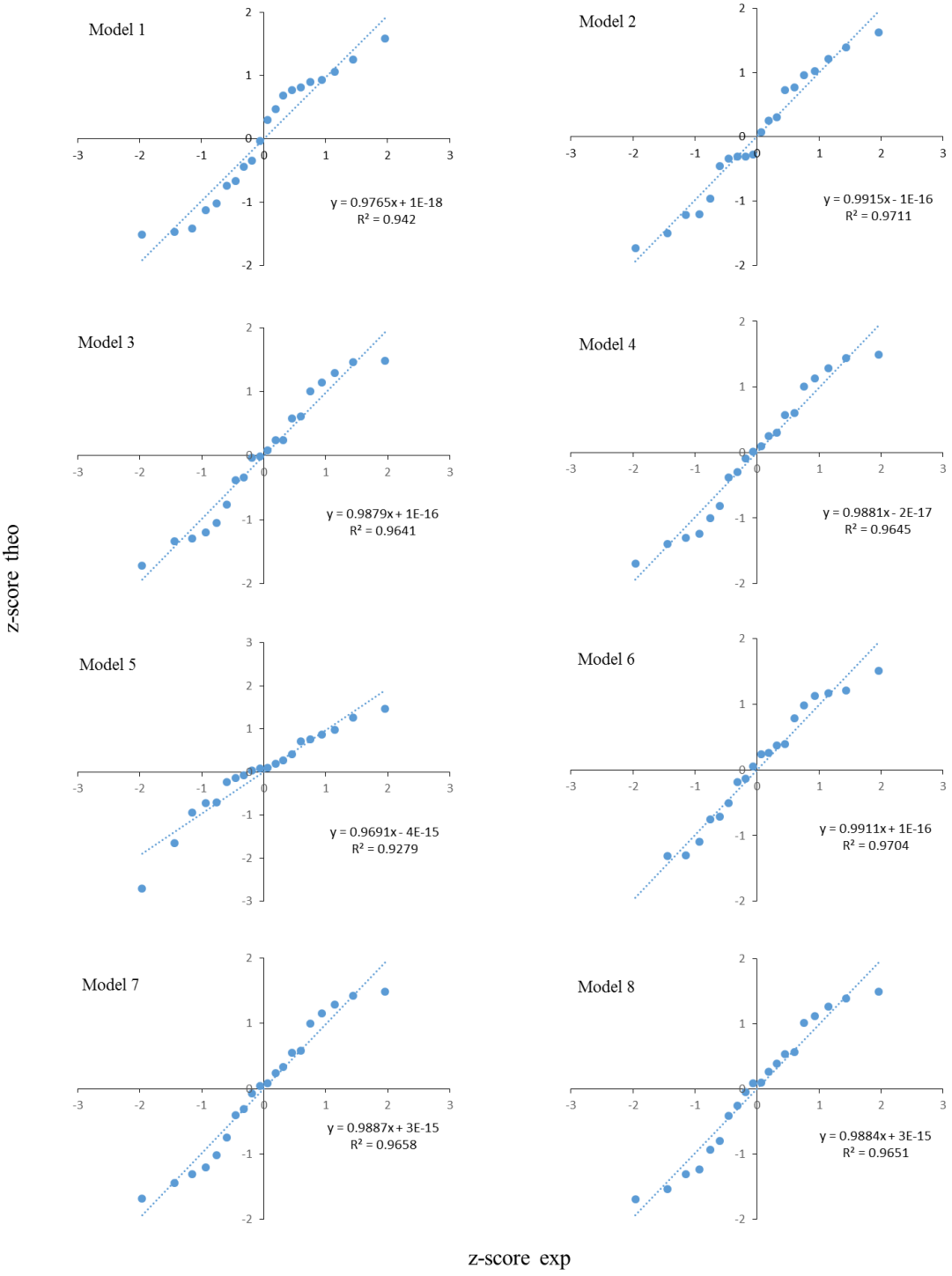

Figure 5.3.4: Q-Q plots of observed and theoretical quantiles of the standardized residuals for the allometric models.

Out of the 8 models, Model 1 and 5 that uses height or the equivalent diameter at breast height as a single predictor variable performs the worst in estimating AGB as indicated by the root mean square error (RMSE) with the highest value of 0.3596 and 0.3453. The models that use a combination of D and H as predictor variables appear to perform better than the models with a single predictor variable given their RMSE value of less than 0.3. Models 3, 4, 6 and 7 imply that the data better fits allometric models that uses H in the first degree with some linear or quadratic combination of D, while the models 2 and 8 that involves H in the second degree results in a slightly larger bias in AGB estimation. Despite this, the adjusted R^2 and RMSE values for these 6 models exhibit a small difference in predicting AGB where the mean difference is approximately 0.01 and thereby not very significant.

Figure 5.3.5 illustrates comparative plots of predicted AGB against observed data (logarithmically transformed) for all eight models. As mentioned previously, the closeness of RMSE and adjusted R^2 values between the models with more than one predictor variable is cause for an insignificant difference between the models. From observing Figure 5.3.5, there appears to be no differences in predicting AGB from any of the 6 models. We then back-transform AGB from ln(AGB) and plot the predicted AGB against the harvest weight presented in Figure 5.3.6. Between models 3 and 4, and 7 and 8, there is a negligible change in AGB estimates. The difference in predicted AGB compared to the harvested weight ranges from 0.006% – 4.929% (models 3 and 4), and 0.001% – 5.686% (models 7 and 8). These 4 models appear to perform best, out of which models 3 and 7 that used D and H in the first degree as predictor variables have the lowest RMSE and highest adjusted R^2 values.

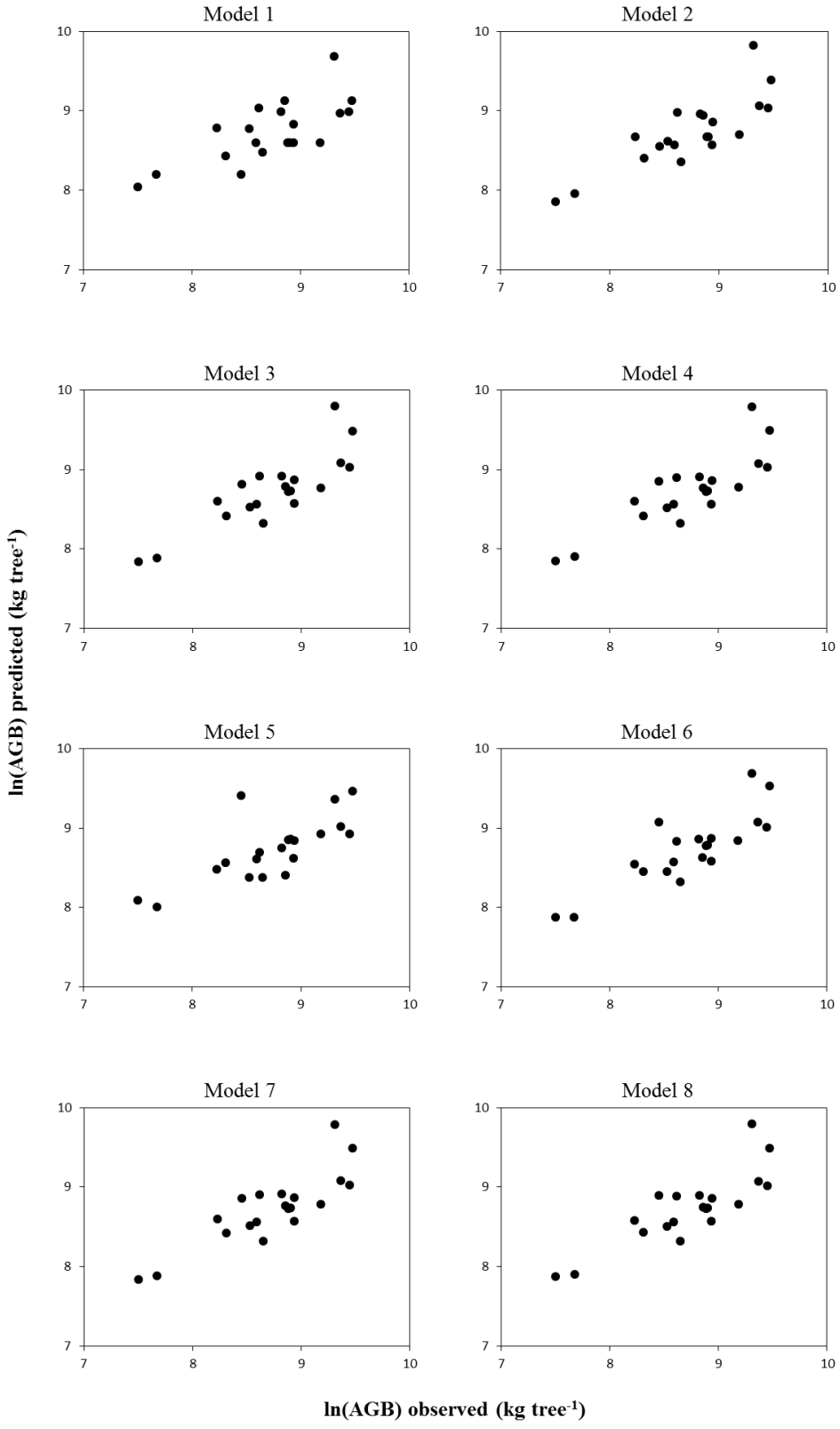

Figure 5.3.5: Plots comparing predicted ln(AGB) against observed ln(AGB) for the eight models.

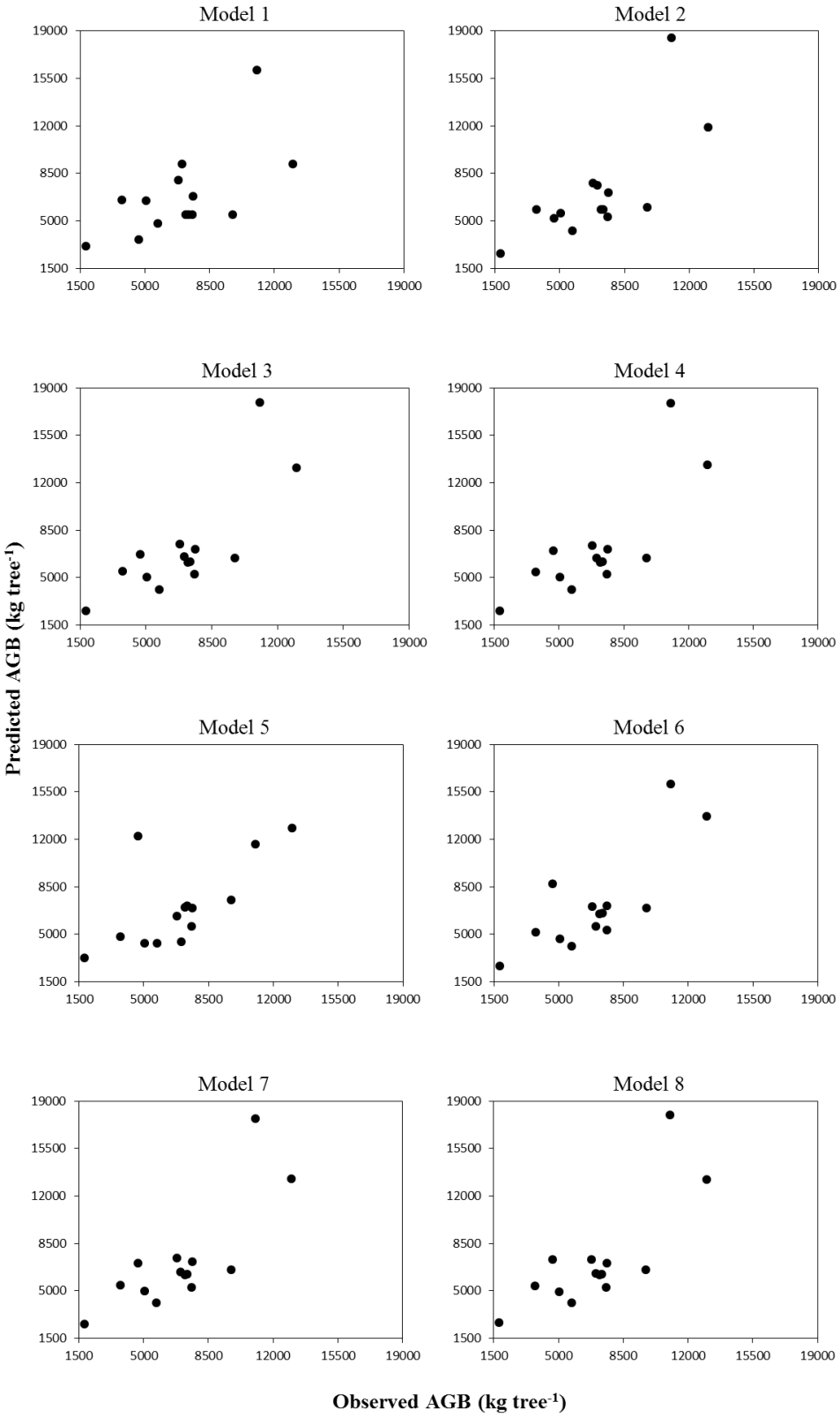

Figure 5.3.6: Plots comparing predicted AGB against observed AGB for the eight models back-transformed from ln(AGB) from field measurements.

Table 5.3.8(a): Table of observed and predicted values of ln (AGB) calculated from regression parameters in Table 5.3.6, height and D values in Tables 5.3.1 and 5.3.2 using allometric models 1 – 4 and the corresponding RMSE.

Sample #	Observed ln(AGB) (kg tree^{-1})	Predicted ln(AGB) (kg tree^{-1})							
		Model 1		Model 2		Model 3		Model 4	
		Field	FujiFilm	Field	FujiFilm	Field	FujiFilm	Field	FujiFilm
S3	8.228	8.786	8.618	8.674	8.599	8.605	8.601	8.597	8.597
S4	8.452	8.198	8.025	8.553	8.274	8.816	8.497	8.850	8.518
S5	9.184	8.601	8.463	8.701	8.524	8.773	8.589	8.774	8.591
S6	8.527	8.775	8.710	8.621	8.514	8.529	8.405	8.522	8.402
S8	7.500	8.042	7.941	7.860	7.701	7.837	7.657	7.853	7.681
S9	9.310	9.687	9.422	9.826	9.538	9.795	9.524	9.792	9.519
S12	8.938	8.829	8.811	8.863	8.836	8.871	8.841	8.866	8.835
H1	8.933	8.601	8.530	8.572	8.738	8.571	8.880	8.567	8.892
H2	8.902	8.601	8.544	8.673	8.712	8.730	8.828	8.730	8.836
H4	8.885	8.601	8.507	8.668	8.650	8.722	8.757	8.722	8.763
H5	8.856	9.128	9.008	8.939	8.818	8.786	8.679	8.771	8.666
H6	9.473	9.128	8.799	9.383	8.998	9.481	9.103	9.497	9.112
H7	8.648	8.475	8.339	8.361	8.252	8.326	8.248	8.325	8.250
H11	8.823	8.985	8.720	8.960	8.725	8.918	8.730	8.907	8.725
RMSE		0.354	0.390	0.293	0.297	0.281	0.261	0.285	0.260

Table 5.3.8(b): Table of observed and predicted values of ln (AGB) calculated from regression parameters in Table 5.3.6, height and D values in Tables 5.3.1 and 5.3.2 using allometric models 5 – 8 and the corresponding RMSE.

Sample #	Observed ln(AGB) (kg tree^{-1})	Predicted ln(AGB) (kg tree^{-1})							
		Model 5		Model 6		Model 7		Model 8	
		Field	FujiFilm	Field	FujiFilm	Field	FujiFilm	Field	FujiFilm
S3	8.228	8.485	8.651	8.545	8.613	8.595	8.602	8.582	8.599
S4	8.452	9.413	9.105	9.076	8.739	8.857	8.533	8.895	8.585
S5	9.184	8.930	8.794	8.842	8.666	8.784	8.601	8.785	8.608
S6	8.527	8.381	8.259	8.452	8.320	8.516	8.390	8.503	8.378
S8	7.500	8.086	7.917	7.879	7.691	7.840	7.657	7.876	7.704
S9	9.310	9.361	9.221	9.686	9.451	9.783	9.516	9.797	9.514
S12	8.938	8.843	8.817	8.869	8.838	8.871	8.841	8.862	8.832
H1	8.933	8.623	9.166	8.581	9.012	8.572	8.901	8.569	8.909
H2	8.902	8.865	9.073	8.787	8.939	8.739	8.846	8.739	8.852
H4	8.885	8.853	9.003	8.777	8.863	8.731	8.773	8.730	8.781
H5	8.856	8.406	8.365	8.628	8.542	8.762	8.657	8.743	8.638
H6	9.473	9.461	9.227	9.526	9.182	9.492	9.117	9.487	9.114
H7	8.648	8.381	8.403	8.320	8.279	8.323	8.250	8.324	8.262
H11	8.823	8.754	8.741	8.861	8.734	8.910	8.730	8.896	8.723
RMSE		0.359	0.326	0.295	0.260	0.281	0.258	0.289	0.261

Table 5.3.9(a): Table of observed and predicted values of AGB back transformed from ln (AGB) of Models 1 – 4 in Table 5.3.8(a).

Sample #	Observed AGB (kg tree^{-1})	Predicted AGB (kg tree^{-1})							
		Model 1		Model 2		Model 3		Model 4	
		Field	FujiFilm	Field	FujiFilm	Field	FujiFilm	Field	FujiFilm
S3	3744.07	6539.22	5531.50	5850.38	5425.04	5460.64	5437.61	5416.28	5416.36
S4	4683.43	3632.61	3057.47	5183.74	3921.07	6741.65	4897.68	6972.50	5001.98
S5	9736.95	5435.06	4734.91	6007.22	5032.25	6454.80	5373.88	6466.68	5382.57
S6	5051.53	6467.31	6062.32	5546.90	4981.93	5061.87	4471.15	5025.68	4453.94
S8	1807.62	3110.02	2810.96	2592.20	2210.46	2533.37	2115.03	2573.41	2167.54
S9	11043.32	16099.58	12362.95	18515.51	13878.21	17944.32	13679.11	17888.91	13611.59
S12	7618.80	6830.69	6704.62	7066.19	6874.63	7123.15	6910.36	7083.53	6870.73
H1	7581.42	5435.06	5062.24	5280.04	6236.81	5274.67	7184.13	5254.97	7274.04
H2	7345.70	5435.06	5136.15	5844.98	6073.38	6184.09	6824.08	6184.56	6879.40
H4	7221.32	5435.06	4948.17	5816.26	5708.53	6136.61	6352.72	6135.33	6392.80
H5	7017.01	9212.41	8171.97	7624.07	6754.51	6544.99	5875.29	6445.11	5803.69
H6	13003.31	9212.41	6625.16	11887.16	8086.99	13114.45	8982.61	13325.84	9067.35
H7	5697.33	4795.29	4184.87	4276.22	3834.12	4129.58	3819.29	4127.73	3828.44
H11	6790.42	7978.47	6127.04	7789.13	6157.36	7463.90	6183.59	7383.38	6152.05

Table 5.3.9(b): Table of observed and predicted values of AGB back transformed from ln (AGB) of Models 5 – 8 in Table 5.3.8 (b).

Sample #	Observed AGB (kg tree^{-1})	Predicted AGB (kg tree^{-1})							
		Model 5		Model 6		Model 7		Model 8	
		Field	FujiFilm	Field	FujiFilm	Field	FujiFilm	Field	FujiFilm
S3	3744.07	4840.30	5717.76	5140.74	5503.07	5405.68	5444.38	5337.26	5424.60
S4	4683.43	12242.29	9003.76	8739.75	6239.01	7025.49	5082.00	7291.78	5351.65
S5	9736.95	7555.56	6595.75	6921.18	5803.31	6527.28	5435.50	6532.62	5476.03
S6	5051.53	4363.21	3863.39	4683.71	4104.98	4995.50	4404.47	4927.57	4348.33
S8	1807.62	3249.64	2742.53	2642.35	2187.89	2539.21	2115.31	2634.33	2216.54
S9	11043.32	11622.21	10111.03	16089.45	12725.63	17729.57	13576.20	17977.25	13553.10
S12	7618.80	6928.71	6745.37	7109.30	6892.34	7125.72	6911.11	7058.42	6847.17
H1	7581.42	5559.69	9567.58	5332.03	8199.93	5279.51	7340.37	5263.26	7398.25
H2	7345.70	7079.42	8717.07	6548.47	7624.20	6239.94	6947.35	6239.87	6987.78
H4	7221.32	6997.01	8126.22	6483.59	7065.67	6189.61	6460.66	6188.62	6507.28
H5	7017.01	4471.94	4296.19	5587.59	5123.15	6385.79	5748.50	6269.35	5641.69
H6	13003.31	12854.47	10171.84	13714.63	9722.92	13254.90	9111.49	13189.10	9077.76
H7	5697.33	4363.21	4460.71	4106.60	3941.40	4117.86	3829.27	4123.30	3874.34
H11	6790.42	6334.96	6253.70	7053.29	6211.78	7404.35	6187.91	7304.35	6143.94

We next tested how the dendrometric measurements from the stereo-camera perform in estimating AGB. The inputs are:

- Generalised allometric models (Table 5.2.2).
- Regression parameters derived from fitting 20 samples of field measured AGB weight, H and D (Table 5.3.6).
- Tree height measurements retrieved from rectified stereo-images (Table 5.3.1).
- D measurements retrieved from rectified stereo-images (Table 5.3.2).

From Tables 5.3.8(a), 5.3.8(b), 5.3.9(a) and 5.3.9(b), we observed that the predicted AGB from the stereo-camera's H and D measurements agrees with the predicted results from field measurements. Based on our previous analysis of predicted AGB from field measurements, Models 1 (ln(H)) and 5 (ln(D)) gave the poorest fit (high RMSE 0.354 and 0.359) whereas Models 3 (ln(DH)) and 7 (ln(D) + ln(H)) performed best with more than 68% good fit of data and low RMSE values at 0.281 and 0.281 respectively. The following is true when we apply image measured D and H into the models. Models 1 and 5 remain the poorest model in predicting AGB whereas models 3, 7, and 8 performed well.

When using the models to estimate AGB, the results obtained from the photogrammetric method are better than the ones obtained from the field measured data. It is observed that RMSE values for most models using the stereo-camera method is lower than their counterparts from the field method e.g. Model 7's RMSE value is 0.281 for the field method and 0.258 for the stereo-camera method. Similar to the field method, there appears to be no difference in predicting AGB from the model pairs (3, 4) and (7, 8). We then back-transform AGB from ln(AGB) and plot the predicted AGB against the harvest weight presented in Figure 5.3.7. Between the model pairs (3, 4) and (7, 8), there is a negligible change in AGB estimates. The difference in predicted AGB compared to the harvested weight ranges from 0.089% – 2.905% (models 3 and 4), and 0.209% – 5.758% (models 7 and 8). These 4 models appear to perform best, out of which models 4 and 7 that uses and H in the first degree as a predictor variable have the lowest values.

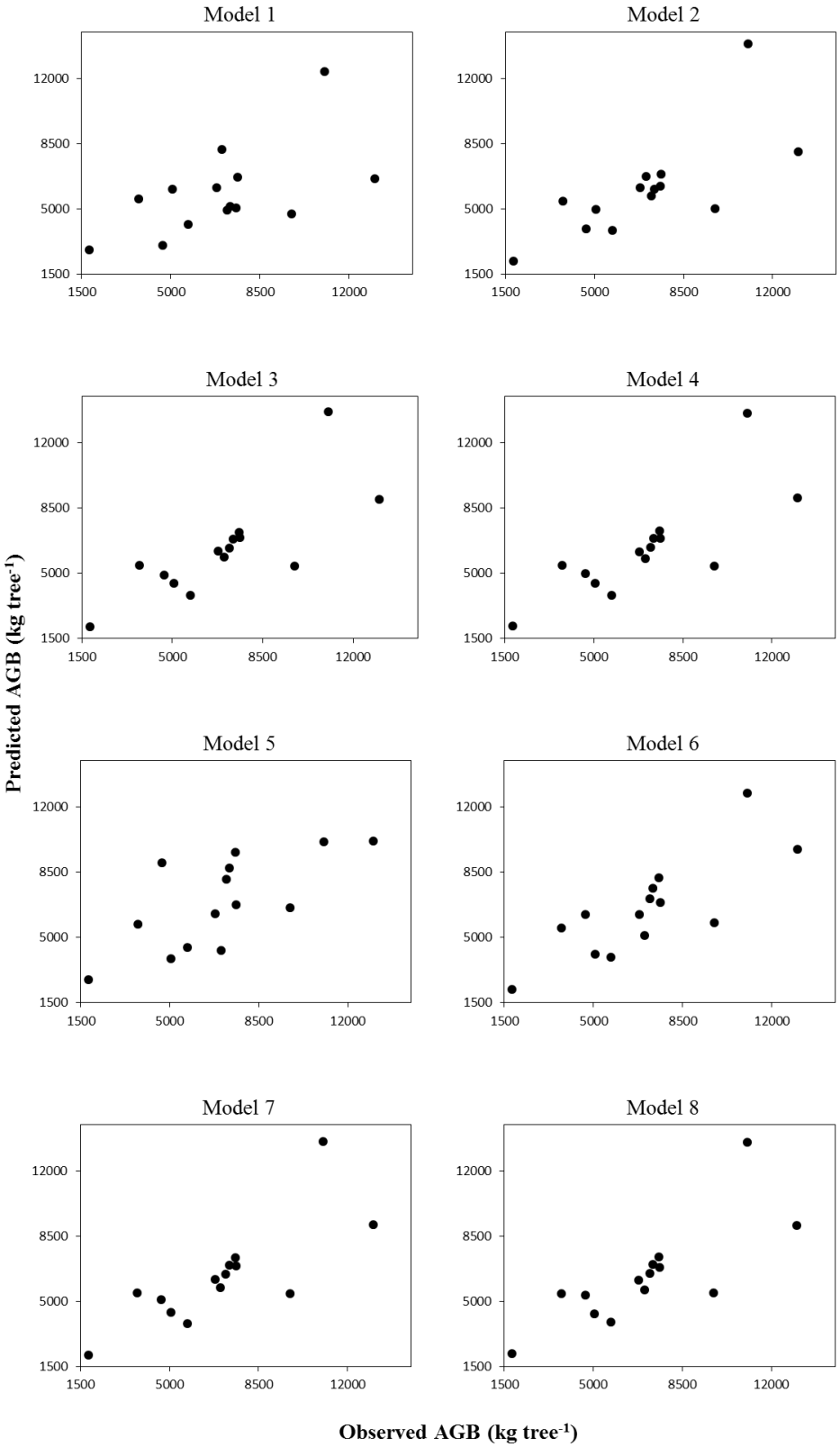

Figure 5.3.7: Plots comparing predicted AGB against observed AGB for the eight models back-transformed from ln(AGB) from stereo-camera measurements.

5.3.3 Discussion

In this study, a stereo-camera was tested against traditional forestry measurement methods in several paddocks for mature paddock trees. The accuracy of height, and diameter measurements were examined. Tree heights retrieved from the stereo-camera is comparable to field measures, with an inclination to underestimate true height. The underestimation is attributed to lens distortion which had not been fully corrected for due to differences in the principal distances between camera calibration and actual fieldwork. The bias is larger for taller trees but not as significant in smaller trees; height difference between methods is approximately 1.5m. For stem diameter measurement, there is a greater propensity for measurement errors to occur at lower levels of the tree trunk. Stem diameter results have shown that while there is no significant difference in both methods of measuring D and D50e, there is a significant difference between the methods in measuring D10 which concurs with the observations made by Paul et al (2014) and Gregoire et al (1989). The stereo-camera has the advantage in that we can take multiple measurements of D and H from the rectified images and calculated the average stem diameter and height. This allows us to reduce potential bias in the measurement in addition to countering the diameter measurement errors from the circular cross-sectional trunk assumption in traditional methods.

We also consider the viability of estimating AGB using H and D measurements from the stereo-camera. Linear and multiple regression parameters were derived from fitting field measured AGB weights, H and D in the generalised allometric models stated in Section 5.2.2.1. The number of samples in this study was of decent size (25 samples). However, only 14 samples could be used in the comparison analysis due to dissimilarity in the dataset between the harvest data and photogrammetric data. In spite of the reduced sample size, the regression parameter estimates were not as sensitive to the data points as seen in Section 5.2.

The best models in predicting AGB were explained by a linear and/or quadratic combination of D and H, with H in the first degree as the predictor variable. The resulting AGB estimations from stereo-camera D and H measurements are in agreement with the results obtained from field measurements and appears to perform better in predicting AGB. The RMSE values agree that models 3, 4 and 7 are the best models for AGB estimation. Although there are some cases where there is relatively

large bias in stereo-camera measurement diameters and heights, the overall AGB prediction does not seem to be severely affected. The potential sources of errors identified in the previous sections can be rectified by ensuring that we have the appropriate camera calibration parameters for a certain principal distance or relating distance to distortion errors to correct for under or overestimation bias in object measurement. We can also mitigate errors in stem diameter measurements with a more rigorous photogrammetric network i.e. increasing the number of stereo-images captured from different viewing angles.

As mentioned in Section 5.2.4, we hypothesis that AGB estimation will perform better in more matured trees that have distinct basal trunks at breast height. This is in consideration that our DBH measurements from the stereo-camera is fairly accurate against tape measurements in Section 5.1's case study. From our results, we show that AGB estimation using dendrometric measures from stereo-images in generalized allometric models are in agreement with traditional methods of dendrometric measures and even appear to perform better. Height and stem diameter estimates are generally in agreement with those measured with a rangefinder or in field with a few outliers. Therefore, the use of consumer-grade digital cameras is a viable method in forestry inventories and contributing to non-destructive sampling in biomass estimation.

Chapter 6

Conclusions and Further Recommendations

In this thesis, we explored the value of a consumer-grade digital stereo-camera to conduct non-destructive dendrometric measurements for forest monitoring and biomass estimation instead of traditional methods which can be destructive and time-consuming. With the implementation of REDD, the accurate determination of the spatio-temporal variation of carbon stocks is crucial. Amongst remote sensing technologies, the photogrammetric potential of consumer-grade digital cameras has been frequently reported in the literature for forest inventory. However, a majority of the literature are based on single camera techniques and very few in stereo-camera techniques. The objective of this research is to develop and validate a photogrammetric method for dendrometric measurements as an alternative cost and time-efficient non-destructive forestry sampling method. In summary, we have addressed the following issues in this thesis:

- Developed a close-range stereo photogrammetric procedure in a proximal monitoring environment.

A step by step guidance (Section 3.4) was developed, which included 5 main procedures: calibration of the digital stereo-camera (left and right lens), establishing a photogrammetric network for comprehensive multi-view image capture, providing

control information for image scaling and restitution, object identification and spatial measurement from the corrected images using photogrammetry. By following these procedures, it is possible for non-experts to use digital stereo-cameras for dendrometric measurements in environmental monitoring.

- Optimised procedures for imaging, processing and analyzing data

In Chapter 4, we examine an object measurement procedure proposed in previous literature (Mustafah et al (2012), and Hsu and Wang (2016)). Object-to-sensor distance can be estimated from disparity values between stereo-images. Measurement of disparity from one matched feature point results in bias in the disparity value, and significantly affects distance measurement if feature points are incorrectly measured. Taking the average of every matched feature point disparity for a stereo-image pair reduces the uncertainty and computational errors. Application of spatial scale to the model is critical for ensuring distance and volume estimates are accurate. Pre-camera calibration affects the accuracy of predicting object dimensions that are measured outside of the calibration distance. The object size was found to be increasingly underestimated as the principal distance is further from the camera calibrated distance. Uncertainties in perfectly eliminating lens distortions for consumer-grade digital cameras may have influenced the accuracy in object measurement. The results suggest that radial lens distortion has not been perfectly corrected for when the principal distance is greater than the camera calibrated distance.

- Liaise with other researchers in the fields of biomass estimates, tree growth models, and monitoring landscape changes to consolidate the information together.

In Chapter 5, we present three case studies in which the performance of the stereo-camera to determine tree metrics in landscape environments was examined. The aim of the study was to test the accuracy of these dendrometric measurements and biomass estimations against other traditional methods and destructive sampling. We examined if accuracy is affected by a variety of factors. The first case study

(Section 5.1) compared the tree height, canopy diameter and stem diameters of paddock trees measured with 3 methods:

- Traditional dendrometry instruments including a laser rangefinder/hypsometer to measure tree height, canopy width and tree-to-sensor distance and a diameter tape to measure stem diameters at breast height.
- DSM and DOM generated from digital aerial images.
- Terrestrial stereo-images captured with a consumer-grade digital stereo-camera.

Tree height and canopy diameter are generally underestimated in the DSM and DOM, which can be attributed to the difference in the time frame in which the results from other methods were compared with. Tree height and stem diameter measured from terrestrial stereo-images performed quite well, and is mostly consistent with the results obtained by traditional methods.

In the second and third case studies (Sections 5.2 and 5.3), this thesis has demonstrated that dendrometric measurements from the stereoscopic method can effectively estimate AGB using existing allometric models. Metric information from multi-stemmed young shrubs and trees were measured in the second study with 3 methods:

- Traditional dendrometry instruments including a height pole to measure tree height, a calliper to measure stem diameter and a weighing scale to determine fresh aboveground tree weight.
- Stereo-images captured with a pair of non-metric digital cameras in stereoscopic configuration.
- Stereo-images captured with a consumer-grade digital stereo-camera.

The harvest dataset was used to determine allometric model parameters. The dendrometric information obtained from the above methods were used to estimate the biomass from the allometric models. The stereo-cameras performed better in estimating tree height but had limitations in identifying every stem for each tree sample due to high occlusion of stems. Field measured dendrometrics produced biomass estimates that suggest that the allometric models using stem diameter or some combination of stem diameter and height is better at predicting biomass. On the other hand, dendrometrics from the stereo-camera method suggest that the allometric

model with height as the only predictor variable is a better model in estimating biomass. The contradictory results observed indicate that the predictor variable, stem diameter, has a significant impact on the accuracy of AGB estimation.

In Section 5.3, we also estimate the aboveground biomass of the sampled trees using allometric models. The actual measurements and biomass is verified through destructive sampling. Predictive measurements were obtained from:

- Traditional dendrometry instruments including a laser rangefinder/hypsometer to measure tree height, and tree-to-sensor distance, a diameter tape to measure stem diameters at breast height, 50cm above ground and 10cm above ground, a tape measure to estimate the length of the tree, and a scale to determine aboveground biomass weight.
- Stereo-images captured with a consumer-grade digital stereo-camera.

In contrast with the second case study, large matured paddock trees were studied in the third case study rather than young trees and shrubs (< 15 years). The photogrammetric method generally underestimates tree height; however, the mean error is approximately 7%. Stem diameter measured from the stereo-images is comparable to field measured stem diameters at height levels of 50cm and 1.3m. The biomass estimates from the stereo-camera dendrometrics agree more with the harvest dataset whereas the biomass predicted from field measured dendrometrics fall short of the actual weight.

Parameters that affect the accuracy of the dendrometric measurements, and in extension, aboveground biomass include camera calibration parameters, the complexity of the background scene, complexity of the tree structure (i.e. high density of stem count at 1.3m measurement height), lighting and weather. Stand-alone individual trees have subject characteristics such as canopy foliage and stem branching that can be clearly defined against other background details and measured to great accuracy. They also provide the best opportunity to capture tree images from the full 360˚ viewing angle in order to identify tree stems that have been occluded from a single viewing angle.

The accuracy of tree metric estimates achieved by stereoscopic sensors is comparable to the traditional method for matured trees with well-defined trunks in a sparsely populated environment. The AGB estimated using the dendrometric information from this dataset is reasonably accurate with generalized allometric models. We observed that where there is high occlusion of stems and foliage, it is

difficult to correctly identify and measure stem diameter of each branch at breast height. The error in measurement subsequently translates to systematic error in AGB estimation. Although multi-view stereo-photogrammetry can address the occlusion problem, there is a risk of double-counting in stem diameter measurement. This is a challenging problem that requires future study.

In conclusion, this thesis has demonstrated the ability of stereo-photogrammetry to produce reasonably accurate dendrometric measurements for biomass estimation, as well as outlined some factors that influence the degree of accuracy in those measurements. As a remote sensing, non-contact and non-destruction technology, the stereo-camera has the semi-automation potential, low cost, low weight and time-efficient on-site prospects for forestry applications. Unlike the TLS method which requires specialized equipment and some degree of skill training, the stereo-photogrammetric method is simpler in the photography and object mensuration process to estimate tree dendrometrics. The accuracy of the tree metric estimates that stereo-photogrammetry can achieve with a hand-held consumer grade digital camera makes it an attractive consideration for dendrometric measurements on low tree density field plots when compared to traditional methods.

6.1 Further Recommendations

Studies conducted in developing generic equations for AGB biomass estimates are limited to specific regions. Additionally, in some research regarding AGB estimation through allometric models, the equations that are used have been cited from previous literature conducted in another region. It remains to be determined whether the AGB estimates obtained from the applying stereo-camera dendrometric measurements to generic allometric equations is satisfactorily accurate. Investigations into species- and location-specific allometric models can improve the quality of AGB estimates from stereo-photogrammetry dendrometric measurements. By using a suitable allometric model when predicting AGB, the uncertainties associated with the estimation can be reduced (Chave et al (2004), and Petrokofsky et al (2012)).

This thesis reported uncertainties in perfectly eliminating lens distortions for consumer-grade digital cameras through self-calibration. These uncertainties affect the accuracy achievable in predicting object dimensions that have been measured

outside of the calibrated distance. Given that the distance at which the photogrammetric data is captured varies according to the size of the target object, calibrating the camera according to each principal distance is inefficient. An additional study is needed to develop a predictive algorithm that corrects any image distortion that remains uncorrected when the threshold for the calibrating distance has been crossed. This would perhaps increase the accuracy of the predicted tree height, canopy width, stem diameter, and by extension, biomass when most of the distortion have been accounted for.

Appendix A

Kojonup image data from stereo-camera FujiFilm FinePix REAL 3D W3


T01


T02


T03


T04


T05


T06


T07


T08


T09


T10


T11


T12

Appendix A


T13


T14


T15


T16


T17


T18


T19


T20


T21


T22


T23


T24


T25


T26


T27


T28


T29


T30


T31


T32


T33


T34


T35


T36


T37


T38


T39


T40


T41


T42

T43

T44

T45

T46

T47

Appendix B

B.1 Geraldton image data from stereo-camera FujiFilm FinePix REAL 3D W3


EH01


EH02


EH03


EH04


NP01


NP02


NP03


NP04


EL01


TW01

B.2 Geraldton image data from pseudo stereo-camera Canon 5D Mark II

EH01

EH02

EH03

EH04

NP01

NP02

NP03

NP04

EL01

TW01

Appendix C

Williamsdale image data from stereo-camera FujiFilm FinePix REAL 3D W3


H01


H02


H03


H04


H05


H06


H07


H08


H09


H10


H11


S03

Appendix C

S04

S05

S06

S07

S08

S09

S12

Bibliography

K.B. Atkinson. “Close Range Photogrammetry and Machine Vision”. Whittles Publishing, UK, 1996.

Anon. *Field measurement procedures for carbon accounting.* National Carbon Accounting System Technical Report **22** (2002). Australian Greenhouse Office, Canberra.

T.E. Avery and H. Burkhard. “Forest Measurements” 5th Edition, McGraw – Hill, New York, 2011.

A. Baccini, S.J. Goetz, W.S. Walker, N.T. Laporte, M. Sun, D. Sulla-Menashe, J. Hackler, P.S.A. Beck, R. Dubayah, M.A. Friedl, S. Samanta and R.A. Houghton. *Estimated carbon dioxide emissions from tropical deforestation improved by carbon-density maps.* Nature Climate Change **2** (2012), 182 – 185.

I. Balenović, H. Marjanovi and M. Benko. *Application of aerial photographs in forest management in Croatia.* Šumarski list **134**:11-12 (2010), 623 – 631.

I. Balenović, A. Seletković, R. Pernar and A. Jazbec. *Estimation of the mean tree height of forest stands by photogrammetric measurement using digital aerial images of high spatial resolution.* Annals of Forest Research **58**:1 (2015), 125 – 143.

L. Banin, T.R. Feldpausch, O.L. Phillips, T.R. Baker, J. Lloyd, K. Affum-Baffoc, E.J.M.M. Arets, N.J. Berry, M. Bradford, R.J.W. Brienen, S. Davies, M. Drescher, N. Higuchi, D.W. Hilbert, A. Hladik, Y. Iida, K.A. Salim, A.R. Kassim, D.A. King, G. Lopez-Gonzalez, D. Metcalfe, R. Nilus, K.S.H. Peh, J.M. Reitsma, B. Sonké, H. Taedoumg, S. Tan, L. White, H. Wöll and S.L.

Lewis. *What controls tropical forest architecture? Testing environmental structural and floristic drivers.* Global Ecology and Biogeography **21** (2012), 1179 – 1190.

S. Bauwens, H. Bartholomeus, K. Calders and P. Lejeane. *Forest inventory with terrestrial LiDAR: a comparison of static and hand-held mobile laser scanning.* Forests **7**:127 (2016), 1 – 17.

B. Bayram, G. Nemli, T. Ozkan, O.E. Oflaz, B. Kankotan and I. Cetin. *Comparison of laser scanning and photogrammetry and their use for digital recording of cultural monument case study: Byzantine land walls – Istanbul.* ISPRS Annals of the Photogrammetry, Remote Sensing and Spatial Information Sciences **II**:5 (2015), 17 – 24.

A. Berger, T. Gschwantner, R.E. McRoberts and K. Schadauer. *Effects of measurement errors on individual tree stem volume estimates for the Austrian national forest inventory.* Forest Science **60**:1 (2014), 14 – 24.

W. Bitterlich. *Single tree measurement by the Relaskop – a highly efficient tool for forest inventories.* Paper for the 8th World Forestry Congress, Jakarta, Indonesia, 1978.

C.L. Brack and G.P. Richards. *Carbon accounting models for forests in Australia.* Environmental Pollution **116** (2002), 187 – 194.

D.C. Bragg. *The sine method as a more accurate height predictor for hardwoods.* Proceedings of the 15th Central Hardwood Forest Conference (2007), 23 – 32.

D. Brand. *Opportunities presented by the Kyoto protocol in the forest sector.* Commonwealth Forestry Review **77** (1998), 164 – 169.

D.C. Brown. *Decentering distortion of lenses.* Photogrammetric Engineering **32**:3 (1966), 444 – 462.

D.C. Brown. *Close-range camera calibration.* Photogrammetric Engineering **37**:8 (1971), 855 – 866.

I.F. Brown, L.A. Martinelli, W.W. Thomas, M.Z. Moreira, C.A.C. Ferreira and R.A. Victoria. *Uncertainty in the biomass of Amazonian forests – an example from Rondonia, Brazil.* Forest Ecology and Management **75** (1995), 175 – 189.

S. Brown and A.E. Lugo. *The storage and production of organic matter in tropical forests and their role in the global carbon cycle.* Biotropica **14** (1982), 161 – 187.

S. Brown, A.J.R. Gillespie and A.E. Lugo. *Biomass estimation methods for tropical forests with applications to forest inventory data.* Forest Sciences **35** (1989), 881 – 902.

S. Brown. *Estimating biomass and biomass change of tropical forests: a primer.* FAO Forestry Paper **134** (1997), Rome, Italy.

R.K. Brownlie, W.W. Carson, J.G. Firth and C.J. Goulding. *Image-based dendrometry system for standing trees.* New Zealand Journal of Forestry Science **37**:2 (2007), 153 – 168.

D. Bruce. *Evaluating accuracy of tree measurements made with optical instruments.* Forest Science **21**:4 (1975), 421 – 426.

P. Caccetta, S. Collings, K. Hingee, D. McFarlane and X. Wu. *Fine-scale monitoring of complex environments using remotely sensed aerial, satellite, and other spatial data.* In: 2011 International Symposium on Image and Data Fusion (ISIDF), IEEE, 2011.

P. Caccetta, S. Collings, A. Devereux, K. Hingee, D. McFarlane, A. Traylen, X. Wu and Z. Zhou. *Monitoring land surface and cover in urban and peri-urban environments using digital aerial photography.* International Journal of Digital Earth **9**:5 (2016), 457 – 475.

M.G.R. Cannell. *Growing trees to sequester carbon in the UK: answers to some common questions.* Forestry **72** (1999): 237 – 247.

B. Carr. *Using laser technology for forestry and engineering applications.* Compiler **10** (1992), 5 – 16.

B. Carr. *Using the Criterion 400 and Impulse 200 laser instruments to accurately measure trees.* Compiler **14** (1996), 6 – 12.

J.H. Chandler, J.G. Fryer and A. Jack. *Metric capabilities of low-cost digital cameras for close range surface measurement.* The Photogrammetric Record **20** (2005), 12 – 26.

J. Chave, R. Condit, S. Aguilar, A. Hernandez, S. Lao and R. Perez. *Error propagation and scaling for tropical forest biomass estimates.* Philosophical Transactions of the Royal Society B **359** (2004), 409 – 420.

J. Chave, C. Andalo, S. Brown, M. Cairns, J. Chambers, D. Eamus, H. Folster, F. Fromard, N. Higuchi, T. Kira, J. Lescure, B. Nelson, H. Ogawa, H. Puig, B. Riera and T. Yamakura. *Tree allometry and improved estimation of carbon stocks and balance in tropical forests.* Oecologia **145** (2005), 87 – 99.

D.C. Chojnacky, L.S. Heath and J.C. Jenkins. *Updated generalized biomass equations for North American tree species.* Forestry **87** (2014), 129 – 151.

N.A. Clark, R.H. Wynne, D.L. Schmoldt and M. Winn. *An assessment of the utility of a non-metric camera for measuring standing trees.* Computers and Electronics in Agriculture **28** (2000), 151 – 169.

D.A. Coomes, R.B. Allen, N.A. Scott, D. Goulding and P. Beets. *Designing systems to monitor carbon stocks in forests and shrublands.* Forest Ecology and Management **164** (2002), 89 – 108.

S. Cronk. “Automated Methods in Digital Close-Range Photogrammetry”. PhD Dissertation, University of Melbourne, Australia, 2008.

P. Crosby, J.P. Barrett and R. Bocko. *Photo estimates of upper stem diameters.* Journal of Forestry **81**:12 (1983), 795 – 797.

M. Dassot, T. Constant and M. Forunier. *The use of terrestrial LiDAR technology in forest science: application fields, benefits and challenges.* Annals of Forest Science **68** (2011), 959 – 974.

C. Dean. *Calculation of wood volume and stem taper using terrestrial single-image close-range photogrammetry and contemporary software tools.* Silva Fennica **37**:3 (2003), 359 – 380.

R.K. Dixon. *Silvicultural options to conserve and sequester carbon in forest systems: preliminary economic assessment.* Critical Reviews in Environmental Science and Technology **27**:Special (1997), S139 – S149.

D.M. Drew and G.M. Downes. *The use of precision dendrometer in research on daily stem size and wood property variation: a review.* Dendrochronologia **27** (2009), 159 – 172.

J. Ebuy, J.P. Lokombe, Q. Ponette, D. Sonwa and N. Picard. *Allometric equation for predicting aboveground biomass of three tree species.* Journal of Tropical Forest Science **23**:2 (2011), 125 – 132.

C. Elzinga, R.C. Shearer and G. Elzinga. *Observer variation in tree diameter measurements.* Western Journal of Applied Forestry **20**:2 (2005), 134 – 137.

Environmental Systems Research Institute. ArcPad user guide, ESRI, accessed 1 September 2016. http://webhelp.esri.com/arcpad/8.0/userguide/index.htm#capture_devices/using_rangefinder/concept_rangefinderintro.htm

W. Faig. *Calibration of close-range photogrammetric systems: mathematical formulation.* Photogrammetric Engineering and Remote Sensing **31**:12 (1975), 1479 – 1486.

J.G. Falconer. *A method of accurate height measurement for forest trees.* Journal of Forestry **29** (1931), 742 – 746.

O.D. Faugeras, Q.T. Luong and S.J. Maybank. *Camera self-calibration: Theory and experiments.* ECCV Proceedings of the European Conference of Computer Vision (1992), 321 – 334.

A. Fernandez-Sarria, B. Velazquez-Marti, M. Sajdak, L. Martinez and J. Estornell. *Residual biomass calculation from individual tree architecture using terrestrial laser scanner and ground-level measurements.* Computers and Electronics in Agriculture **93** (2013), 90 – 97.

C.S. Fraser. *Multiple focal setting self-calibration of close-range metric cameras.* Photogrammetric Engineering and Remote Sensing **46**:9 (1980), 1161 – 1171.

C.S. Fraser. *On the use of non-metric cameras in analytical non-metric photogrammetry.* International Archives of Photogrammetry and Remote Sensing **24**:5 (1982), 156 – 166.

C.S. Fraser, M.R. Shortis and G. Ganci. *Multi-sensor system self-calibration*. In: Proceedings of SPIE Videometrics IV **2598** (1995), 2 – 18.

C.S. Fraser. *Digital camera self-calibration.* ISPRS International Journal of Photogrammetry and Remote Sensing **52** (1997), 149 – 159.

J.G. Fryer and D.C. Brown. *Lens distortion in close-range photogrammetry.* Photogrammetric Engineering and Remote Sensing **52**:2 (1986), 51 – 58.

M. Forsman, N. Börlin and J. Holmgren. *Estimation of tree stem attributes using terrestrial photogrammetry with a camera rig*. Forests **7** (2016), 61 – 80.

D. Gaffrey, B. Sloboda, M. Fabrika and Š. Šmelko. *Terrestrial single image photogrammetry for measuring standing trees, as applied in the Dobroc virgin forest.* Journal of Forest Science **47** (2001), 75 – 87.

R.M. Gifford. *Carbon contents of above-ground tissues of forest and woodland trees.* National Carbon Accounting System Technical Report **22** (2000). Australian Greenhouse Office, Canberra.

T.G. Gregoire, S.M. Zedaker and N.S. Nicholas. *Modeling relative error in stem basal area estimates.* Canadian Journal of Forest Research **20** (1989), 496 – 502.

G.M.J. Hall, S.K. Wiser, R.B. Allen, P.N. Beets and C.J. Goulding. *Strategies to estimate national forest carbon stocks from inventory data: The 1990 New Zealand baseline.* Global Change Biology **7** (2001), 389 – 403.

N.L. Harris, S. Brown, S.C. Hagen, S.S. Saatchi, S. Petrova, W. Salas, M.C. Hansen, P.V. Potapov and A. Lotsch. *Baseline map of carbon emissions from deforestation in tropical regions.* Science **336** (2012), 1573 – 1576.

T. Hengl and J. Križan. *Analysis of errors in close-range photogrammetry (DLT-method) using simulation.* Geodetski List **74**:3-4 (1997), 181 – 193.

J.G. Henning and P.J. Radtke. *Detailed stem measurements of standing trees from ground-based scanning LiDAR.* Forest Science **52**:1 (2006), 67 – 80.

B. Heske and R.C. Parker. *Collecting and processing forest data with the Tele-Relaskop and the microcomputer.* Proceedings of International Resource Inventory Conference (1983), 714 – 717.

K.L. Hingee. “Ground elevation models and land cover classifiers for decimetre resolution urban monitoring”. Master’s thesis, Curtin University, Perth, 2013.

M. Holopainen, V. Kankare, M. Vastaranta, X. Liang, Y. Lin, M. Vaaja, X. Yu, J. Hyyppä, H. Hyyppä, H. Kaartinen, A. Kukko, T. Tanhuanpää and P. Alho. *Tree mapping using airborne, terrestrial and mobile laser scanning – A case study in a heteogeneous urban forest.* Urban Forestry & Urban Greenin **12**:4 (2013), 546 – 553.

C. Hopkinson, L. Chasmer, C. Young-Pow and P. Treitz. *Assessing forest metrics with a ground-based scanning lidar.* Canadian Journal of Forest Research **34** (2004), 573 – 583.

R.A. Houghton. *Aboveground forest biomass and the global carbon balance.* Global Change Biology **11** (2005), 945 – 958.

T.S. Hsu amd T.C. Wang. *An improvement stereo vision images processing for object distance measurement.* International Journal of Automation and Smart Technology **5**:2 (2015), 85 – 90.

A. Hu, X. Cui, Y. Geng, W.J. Yuan and J. Hou. *Measurement of safe driving distance based on stereo vision.* Proceedings of the 6th International Conference on Image and Graphics (ICIG) (2011), 902 – 907.

A. Hulet, B.A. Roundy, S.L. Petersen, S.C. Bunting, R.R. Jensen and D.B. Roundy. *Utilizing national agriculture imagery program data to estimate tree cover and biomass of Piñon and Juniper woodlands.* Rangeland Ecology and Management **67** (2014), 563 – 572.

J.F. Hullo, P. Grussenmeyer and S. Fares. *Photogrammetry and dense stereo matching approach applied to the documentation of the cultural heritage site of kilwa (Saudi Arabia).* 22nd CIPA Symposium October (2009), Kyoto, Japan.

M.O. Hunter, M. Keller, D. Vitoria and D.C. Morton. *Tree height and tropical forest biomass estimation.* Biogeosciences Discussions **10** (2013), 10491 – 10529.

B. Husch, T.W. Beers and J.A. Kershaw. "Forest Mensuration", 4th Edition, John Wiley, New York, 2003.

W. IJsselsteijn, H. Ridder and J. Vliegen. *Subjective evaluation of stereoscopic images: effects of camera parameters and display duration.* IEEE Transactions on Circuits and Systems for Video Technology ***10***:2 (2000), 225 – 233.

A. Jaakkola, J. Hyyppä, A. Kukko, X. Yu, H. Kaartinen, M. Lehtomäki and Y. Lin. *A low-cost multi-sensoral mobile mapping system and its feasibility for tree measurements.* ISPRS Journal of Photogrammetry and Remote Sensing **65** (2010), 514 – 522.

F.T. Joshua. *UNCTAD's role in greenhouse gas emissions trading.* Commonwealth Forestry Review **77** (1998), 170 – 171.

J. Kalliovirta, J. Laasasenaho and A. Kangas. *Evaluation of the Laser-relascope.* Forest Ecology and Management **204**:3-4 (2005), 181 – 194.

D. Kelbe, P. Romanczyk, J. van Aardt, K. Cawse-Nicholson and K. Krause. *Automatic extraction of tree stem models from single terrestrial lidar scans in structurally heterogeneous forest environments.* SilviLaser (2012), Vancouver, Canada.

H. Kim, C.S. Lin, J. Song and H. Chae. *Distance measurement using a single camera with a rotating mirror.* International Journal of Control, Automation and Systems **3:**4 (2005), 542 – 551.

D.A. King and D.A. Clark. *Allometry of emergent tree species from saplings to above-canopy adults in a Costa Rican rain forest.* Journal of Tropical Ecology **27** (2011), 573 – 579.

A. Kukko, H. Kaartinen, J. Hyyppä and Y. Chen. *Multiplatform mobile laser scanning: usability and performance.* Sensors **12** (2012), 11712 – 11733.

M. Kytö, M. Nuutinen and P. Oittinen. *Method for measuring stereo camera depth accuracy based on stereoscopic vision.* SPIE Electronic Imaging, Three-Dimensional Imaging, Interaction, and Measurement **7864** (2011), 1 – 9.

A. van Laar and A. Akça. "Forest Mensuration". Springer Science & Business Media, the Netherlands, 2007.

M. Lambert and J. Turner. *Commercial forest plantations on saline lands.* CSIRO, Australia (2000).

M. Larjavaara and H.C. Muller-Landau. *Measuring tree height: a quantitative comparison of two common field methods in a moist tropical forest.* Methods in Ecology and Evolution **4** (2013), 793 – 801.

Laser Technology Inc. "Criterion 400 Survey Laser, Operator's Guide". Laser Techonology Inc., Englewood, CO, 1992.

R.K. Lenz and R.Y. Tsai. *Techniques for calibration of the scale factor and image center for high accuracy 3-D machine vision metrology.* IEEE Transactions on Pattern Analysis and Machine Intelligence **10**:5 (1988), 713 – 720.

R. Li and A.R. Weiskittel. *Comparison of model forms for estimating stem taper and volume in the primary conifer species of the Northern American Acadian Region.* Annals of Forest Science **67**:3 (2012), 302.

X. Liang, A. Kukko, H. Kaartinen, J. Hyyppä, X. Yu, A. Jaakkola and Y. Wang. *Possibilities of a personal laser scanning system for forest mapping and ecosystem services.* Sensors **14** (2014a), 1228 – 1248.

X. Liang, A. Jaakkola, Y. Wang, J. Hyyppä, E. Honkavaara, J. Liu and H. Kaartinen. *The use of a hand-held camera for individual tree mapping in forest sample plots.* Remote Sensing **6**:7 (2014b), 6587 – 6603.

D.D. Lichti. "Constrained Finite Element Method Self-Calibration". Master's thesis, University of Calgary, Calgary, Canada.

H.C. Longuet-Higgins. *A computer algorithm for reconstructing a scene from two projections.* Nature **293**:10 (1981), 133 – 135.

J.L. Lovell, D.L.B. Jupp, D.S. Culvenor and N.C. Coops. *Using airborne and ground-based ranging LiDAR to measure canopy structure in Australian forests.* Canadian Journal of Remote Sensing **29**:5 (2003), 607 – 622.

T. Luhmann, S. Robson, S. Kyle and I. Harley. "Close Range Photogrammetry: Principles, Techniques and Applications". Whittles Publishing, UK, 2006.

T. Luhmann, C. Fraser and H.-G. Maas. *Sensor modelling and camera calibration for close-range photogrammetry.* ISPRS Journal of Photogrammetry and Remote Sensing **115** (2016), 37 – 46.

Q.T. Luong and O.D. Faugeras. *Self-calibration of a camera using multiple images.* IEEE Proceedings of the 11th International Conference on Pattern Recognition **1** (1992), 9 – 12.

H.G. Maas, A. Bienart, S. Scheller and E. Keane. *Automatic forest inventory parameter determination from terrestrial laser scanner data.* International Journal of Remote Sensing **29**:5 (2008), 1579 – 1593.

R.E. McArdle. *Relative accuracy of calipers and diameter tape in measuring Douglas fir trees.* Journal of Forestry **26**:3 (1928), 338 – 342.

J.P. Maclaren. *Plantation forestry – its role as a carbon sink: conclusions from calculations based on New Zealand's planted forest estate.* In: Forest

Ecosystems, Forest Management and the Carbon Cycle (M.J. Apps and D.T. Price, Eds.). NATO ASI Series, Springer Verlag, Berlin, Heidelberg, NewYork (1996), 245 – 256.

M.R. McHale, I.C. Burke, M.A. Lefsky, P.J. Peper and E.G. McPherson. *Urban forest biomass estimates: is it important to use allometric relationship developed specifically for urban trees?* Urban Ecosystem **12** (2009), 95 – 113.

H.A.I. Madgwick and T. Satoo. *On estimating the aboveground weights of tree stands.* Ecology **56** (1975), 1446 – 1450.

M.A. Mahammed, A.I. Melhum and F.A Kochery. *Object distance measurement by stereo vision.* International Journal of Science and Applied Information Technology **2:**2 (2013), 5 – 8.

S.D. Makungwa, A. Chittock, D.L. Skole, G.Y. Kanyama-Phiri and I.H. Woodhouse. *Allometry for biomass estimation in jatropha trees planted as boundary hedge in farmers' fields.* Forests **4** (2013), 218 – 233.

Y. Malhi, T.R. Baker, O.L. Phillips, S. Almeida, E. Alvarez, L. Arroyo, J. Chave, C.I. Czimczik, A. Fiore, N. Higuchi et al. *The above-ground coarse wood productivity of 104 neotropical forest plots.* Global Change Biology **10** (2004), 563 – 591.

T. Masuda, E. Ishiyama and H. Tamayama. *Development of "3D measurement system" using images taken with a "FinePix REAL 3D W3" 3D digital camera.* FUJIFILM Research & Development (2011), Saitama, Japan.

R. Mate, T. Johansson, and A. Sitoe. *Biomass equations for tropical forest tree species in Mozambique.* Forests **5** (2014), 535 – 556.

F. Menna, E. Nocerino, F. Remondino and M. Shortis. *Investigation of a consumer-grade digital stereo camera.* Proceedings of Videometrics, Range Imaging and Applications XII, SPIE Optical Metrology **8791** (2013).

E.M. Mikhail, J. Bethel and J.C. McGlone. “Introduction to Modern Photogrammetry”. John Wiley & Sons, New York, 2001.

J.M. Miller. “Estimation of Individual Tree Metrics using Stucture-from-Motion Photogrammetry”. Master’s thesis, University of Canterbury, Christchurch, New Zealand, 2015.

K.D. Montagu, K. Duttmer, C.V.M. Barton and A.L. Cowie. *Developing general allometric relationships for regional estimates of carbon sequestration – an example using Eucalyptus pilularis from seven contrasting sites.* Forest Ecology and Management **204** (2005), 113 – 127.

N. Montès, T. Gauquelin, W. Badri, V. Bertaudiere and E.H. Zaoui. *A non-destructive method for estimating above-ground forest biomass in threatened woodlands.* Forest Ecology and Manage **130** (2000), 37 – 46.

N. Montès. *A non-destructive method to estimate biomass in arid environments: a comment on Flombaum and Sala.* Journal of Arid Environments **73**:6 (2009), 599 – 601.

J. Morgenroth and C. Gomez. *Assessment of tree structure using a 3D image analysis technique – a proof of concept.* Urban Forestry & Urban Greening **13**:1 (2014), 198 – 203.

L.M. Moskal and G. Zheng. *Retrieving forest inventory variables with terrestrial laser scanning (TLS) in urban heterogeneous forest.* Remote Sensing **4** (2012), 1 – 20.

K. Muljowidodo, M.A. Rasyid, N. Sapto and A. Budiyono. *Vision based distance measurement system using single laser pointer design for underwater vehicle.* Indian Journal of Marine Sciences **38** (2009), 324 – 331.

Y.M. Mustafah, R. Noor, H. Hasbi and A.W. Asma. *Stereo vision image processing for real-time object distance and size measurements.* International Conference on Computer and Communication Engineering (ICCCE) (2012), 659 – 663.

P. Muukkonen. *Generalized allometric volume and biomass equations for some tree species in Europe.* European Journal of Forest Research **126** (2007), 157 – 166.

National Forest Inventory. *Australia's state of the forests report 1998.* Bureau of Rural Sciences, Canberra (1998).

G.J. Newnham, J.D. Armston, K. Calders, M.I. Disney, J.L. Lovell, C.B. Schaaf, A.H. Strahler and F.M. Danson. *Terrestrial laser scanning for plot-scale forest measurement.* Current Forestry Reports **1**:4 (2015), 239 – 251.

L.R. Nogueira Junior, V.L. Engel, J.A. Parrotta, A.C. Galvao de Melo and D.S. Re. *Allometric equations for estimating tree biomas in restored mixed-species Atlantic Forest stands.* Biota Neotrop **14**:2 (2014), 1 – 9.

D.J. Nowak, D.E. Crane and J.C. Stevens. *Air pollution removal by urban trees and shrubs in the United States.* Urban Forestry and Urban Greening **4**:3-4 (2006), 115 – 123.

A.P. O'Grady, X. Chen, D. Eamus and L.B. Hutley. *Composition, leaf area index and standing biomass of eucalypt open forests near Darwin in the Northern Territory Australia.* Australian Journal of Botany **48** (2000), 629 – 638.

D.P. Paine and J.D. Kiser. "Aerial photography and image interpretation". 3rd Edition, John Wiley & Sons Inc., Hoboken, New Jersey, 2012.

R.C. Parker and T.G. Matney. *Comparison of optical dendrometers for prediction of standing tree volume.* Southern Journal of Applied Forestry **23**:2 (1998), 100 – 107.

P. Patias and A. Streilein. *Contribution of videogrammetry to the architectural Restitution. Results of the CIPA "O. Wagner Pavillion" test.* ISPRS International Archives of Photogrammetry and Remote Sensing **31**:B5 (1996), 457 – 462.

K.I. Paul, K. Jacobsen, V. Koul, P. Leppert and J. Smith. *Predicting growth and sequestration of carbon by plantations growing in regions of low-rainfall in southern Australia.* Forest Ecology and Management **254** (2008), 205 – 216.

K.I. Paul, S.H. Roxburgh, J.R. England, P. Ritson, T. Hobbs, K. Brooksbank, J. Raison, J.S. Larmour, S. Murphy, J. Norris, C. Neumann, T. Lewis, J. Jonson, J.L. Carter, G. McArthur, C. Barton and B. Rosem. *Development and testing of allometric equations for estimating above-ground biomass of mixed-species environmental plantings.* Forest Ecology and Management **310** (2013), 483 – 494.

K.I. Paul, S. Roxburgh, J. Raison, J. Larmour, J. England, S. Murphy, J. Norris, P. Ritson, K. Brooksbank, T. Hobbs, C. Neumann, T. Lewis, Z. Read, D. Clifford, L. Kmoch, M. Rooney, R. Freudenberger, J. Jonson, A. Peck, R. Giles, J. Bartle, G. McArthur, D. Wildy, A. Lindsay, N. Preece, S. Cunningham, T. Powe, J. Carter, R. Bennett, D. Mendham, R. Sudmeyer, B. Rose, D. Butler, L. Cohen, T. Fairman, R.

Law, B. Finn, M. Brammer, G. Minchin, P. van Oosterzee and A. Lothian. *Improved estimation of biomass accumulation by environmental planting and mallee plantings using FullCAM. Report for the Department of the Environment* (2014). CSIRO Sustainable Agriculture Flagship, Canberra, Australia.

F. Petrokofsky, H. Kanamaru, F. Achard, S.J. Goetz, H. Joosten, P. Holmgren, A. Lehtonen, M.C.S. Menton, A.S. Pullin and M. Wattenbach. *Comparison of methods for measuring and assessing carbon stocks and carbon stock changes in terrestrial carbon pools. How do the accuracy and precision of current methods compare? A systematic review protocol.* Environmental Evidence **1**:6 (2012), 6.

M. Prodan. “Holzmesslehre”. Frankfurt, 1965.

A. Poultouchidou, V. Monnier and L. Birigazzi. *Inventory of allometric equations for estimation of above-ground tree biomass and volume in the Pacific.* UN-REDD Programme, MRV report **17** (2013), Rome, Italy.

K.A. Rahman, M.S. Hossain, M.A. Bhuiyan, Z. Tao, M. Hasanuzzamanm and H. Ueno. *Person to camera distance measurement based on eye-distance.* 3rd International Conference on Multimedia and Ubiquitous Engineering (2009), 137 – 141.

J. Repola. *Biomass equations for birch in Finland.* Silva Fennica **42**:4 (2008), 605 – 624.

M. Rutzinger, A.K. Pratihast, S. Oude Elberink and G. Vosselman. *Detection and modelling of 3D trees from mobile laser scanning data.* The International Archives of the Photogrammetry, Remote Sensing and Spatial Information Sciences **38** (2010), 520 – 525.

J. Ryding, E. Williams, M.J. Smith and M.P. Eichhorn. *Assessing handheld mobile laser scanners for forestry surveys.* Remote Sensing **7** (2015), 1095 – 1111.

N. Saarinen, M. Vastaranta, V. Kankare, T. Tanhuanpää, M. Holopainen, J. Hyyppä and H. Hyyppä. *Urban-tree-attribute update using multisource single-tree inventory.* Forests **5** (2014), 1032 – 1052.

L. Sawadogo, P. Savadogo, D. Tiveau, S.D. Dayamba, D. Zida, Y. Nouvellet, P.C. Oden and S. Guinko. *Allometric prediction of above-ground biomass of eleven woody tree species in the Sudanian savanna-woodland of West Africa.* Journal of Forestry Research **21**:4 (2010), 475 – 481.

F.N. Scatena, W. Silver, T. Siccama, A. Johnson and M.J. Sánchez. *Biomass and nutrient content of the Bisley experimental watersheds, Luquillo experimental*

forest, Puerto Rico, before and after Hurricane Hugo. Biotropica **25**:1 (1989), 1 – 20.

C. Schaaf, I. Paynter, E.J. Saenz, Z. Li, A.H. Strahler, F. Peri, A. Erb, P. Raumonen, J. Muir, G. Howe, K. Hewawasam, J. Martel, E.S. Douglas, S. Chakrabarti, T. Cook, M. Schaefer, G. Newnham, D.L.B. Jupp, J.A. van Aardt, D. Kelbe, P. Romanczyk and J. Faulring. *Using the rapid-scanning, ultra-portable, canopy biomass LiDAR (CBL) alone and in tandem with the full-waveform dual-wavelength Echidna LiDAR (DWEL) to establish forest structure and biomass estimates in a variety of ecosystems.* American Geophysical Union Fall Meeting Abstracts (2014), 1.

T. Schenk. "Digital Photogrammetry Volume I". Department of Civil and Environmental Engineering and Geodetic Science, The Ohio State University, Columbus, 1999.

T. Schenk. "Introduction to Photogrammetry". Department of Civil and Environmental Engineering and Geodetic Science, The Ohio State University, Columbus, 2005.

M.D.C. Schmitt and D.F. Grigal. *Generalized biomass estimation equations for Betula papyrifera Marsh.* Canadian Journal of Forest Research **11** (1981), 837 – 840.

H.T. Schreuder, T.G. Gregoire and G.B. Wood. "Sampling Methods for Multiresource Forest Inventory". John Wiley & Sons, 1993.

P. Snowdon, J. Raison, H. Keith, P. Ritson, P. Grierson, M. Adams, K. Montagu, H.Q. Bi, W. Burrows and D. Eamus. *Protocol for sampling tree and stand biomass.* National Carbon Accounting System Technical Report **31**, Australian Greenhouse Office, 2002.

A. Specht and P.W. West. *Estimation of biomass and sequested carbon on farm forest plantations in northern New South Wales, Australia.* Biomass and Bioenergy **25**:4 (2003), 363 – 379.

R. Staiger and T.A. Wunderlich. *Terrestrisches Laserscanning 2006 – Technische Möglichkeiten und Anwendungen.* Zeischrift für Geodäsie, Geoinformation and Landmanagement **2** (2007), 81 – 86.

A. Strahler, D.L.B. Jupp, C.E. Woodcock, C.B. Schaaf, T. Yao, F. Zhao, X. Yang, J. Lovell, D. Culvenor, G. Newnham, W. Ni-Miester and W. Boykin-Morris. *Retrieval of forest structural parameters using ground-based LiDAR instrument (Echidna).* Canadian Journal of Remote Sensing **34**:2 (2008), 426 – 440.

H. Suganuma, Y. Abe, M. Taniguchi, H. Tanouchi, H. Utsugi, T. Kojima and K. Yamada. *Stand biomass estimation method by canopy coverage for application to remote sensing in an arid area of Western Australia*. Forest Ecology and Management **222** (2006), 75 – 87.

G. Takahashi and R. Matsuoka. *Accuracy of measurement using a pair of stereo images acquired by FinePix without controls.* International Archives of Photogrammetry, Remote Sensing and Spatial Information Sciences XXXVIII (2010), 56.

L. Tang and C. Heipke. *Automatic relative orientation of aerial images.* Photogrammetric Engineering and Remote Sensing **62**:1 (1996), 47 – 55.

M.T. Ter-Mikaelian and M.D. Korzukhin. *Biomass equations for sixty-five North American tree species.* Forest Ecology and Management **97** (1997), 1 – 24.

R.Y. Tsai. *An efficient and accurate camera calibration technique for 3D machine vision.* Proceedings of the IEEE Conference on Computer Vision and Pattern Recognition, Miami, USA (1986), 364 – 374.

United Nations Framework Convention on Climate Change (UNFCCC). Report of the Conference of the Parties on its thirteenth session, held in Bali from 3 – 15 December 2007. Addendum Part Two: Action taken by the Conference of the

Parties 2007 at its thirteenth session. FCCC/CP/2007/6/Add1 distributed 14 March 2008. http://unfccc.int/resource/docs/2007/cop13/eng/06a01.pdf (accessed 17 December 2015)

J. Varjo, H. Henttonen, J. Lappi, J. Heikkonen and J. Juujärvi. *Digital horizontal tree measurements for forest inventory.* Working Papers of the Finnish Forest Research Institure **40** (2006).

M. Vastaranta, T. Melkas, M. Holopainen, H. Kaartinen, J. Hyyppä and H. Hyyppä. *Comparison of different laser-based methods to measure stem diameter.* SilviLaser (2008), 1 – 10.

S.A. Vieira, L.F. Alves, M. Aidar, L.S. Araújo, T. Baker, J.L.F. Batista, M.C. Campos, P.B. Camargo, J. Chave, W.B.C. Delitti, N. Higuchi, E. Honorio, C.A. Joly, M. Keller, L.A. Martinelli, E.A. de Mattos, T. Metzker, O. Phillips, F.A.M. dos Santos, M.T. Shimabukuro, M. Silveira and S.E. Trumbore. *Estimation of biomass and carbon stocks: the case of the Atlantic Forest.* Biota Neotropica **8**:2 (2008), 21 – 29.

R. Vlad. "A Method for the Assessment of the Quality of Stereoscopic 3D Images". PhD dissertation. Signal and Image Processing, Universite de Grenoble, 2013.

R. Wackrow. "Spatial Measurement with Consumer Grade Digital Cameras". PhD dissertation. Department of Civil and Building Engineering, Loughborough University, 2008.

S.A. Weaver, Z. Ucar, P. Bettinger, K. Merry, K. Faw and C.J. Cieszewski. *Assessing the accuracy of tree diameter measurements collected at a distance.* Croatian Journal of Forest Engineering **36**:1 (2015), 73 – 83.

J. Weber. "Holtzmassenermittlung am stehenden Stamm auf grund photographischer Aufnahman". PhD thesis, Gieben, 1902.

P.A. Werner and P.G. Murphy. *Size-specific biomsas allocation and water content of above- and below-ground components of three Eucalyptus species in a northern Australia savanna.* Australian Journal of Botany **49** (2001), 155 – 167.

P.W. West. "Tree and Forest Measurement". Springer-Verlag, Berlin, Heidelberg, 2009.

M. Williams, K. Briggs and D. Martinez. *Evaluation of the Barr Stroud FP15 and Criterion 400 laser dendrometers for measuring upper stem diameters and heights.* Forest Science **45**:1 (1999), 53 – 61.

R.J. Williams, A. Zerihun, K.D. Montagu, M. Hoffman, L.B. Hutley and X. Chen. *Allometry for estimating aboveground tree biomass in tropical and subtropical eucalypt woodlands: towards general predictive equations.* Australian Journal of Botany **55** (2005), 607 – 619.

M.H. Yang, D. Kriegman and N. Ahuja. *Detecting faces in images: a survey.* IEEE Transactions on Pattern Analysis and Machine Intelligence **24**:1 (2002), 34 – 58.

Q. Yu, H. Araujo and H. Wang. *Stereo-vision based real time obstacle detection for urban environments.* In the 11th International Conference on Advanced Robotics, Coimbra, Portugal, 2003.

J.Q. Yuen, T. Fung and A.D. Ziegler. *Review of allometric equations for major land covers in SE Asia: uncertainty and implications for above- and below-ground carbon estimates.* Forest Ecology and Management **360** (2016), 323 – 340.

Z. Zhang. *A flexible new technique for camera calibration.* IEEE Transactions on Pattern Analysis and Machine Intelligence **22**:11 (2000), 1330 – 1334.

D. Zianis, P. Muukkonen, T. Mäkipää and M. Mencuccini. *Biomass and stem volume equations for tree species in Europe.* Silve Fennica Monographs **4** (2005), 1 – 63.

D. Zianis. *Predicting mean aboveground forest biomass and its associated variance.* Forest Ecology and Management **256** (2008), 1400 – 1407.

H.M. Zogg. "Investigations of high precision terrestrial laser scanning with emphasis on the development of a robust close-range 3D laser scanning system". PhD dissertation. Institute of Geodesy and Photogrammetry, Zurich, 2008.